FLEXURAL STRENGTHENING OF REINFORCED CONCRETE BEAMS WITH FABRIC REINFORCED CEMENTITIOUS MORTAR: EFFECT OF REINFORCEMENT RATIOS

by

Trevor Norman Stanley Billows

B.A.Sc., University of British Columbia, Kelowna, 2014

A THESIS SUBMITTED IN PARTIAL FULFILLMENT
OF THE REQUIREMENTS FOR THE DEGREE OF

MASTER OF APPLIED SCIENCE

in

THE COLLEGE OF GRADUATE STUDIES
(Civil Engineering)

THE UNIVERSITY OF BRITISH COLUMBIA
(Okanagan)

December 2016

The undersigned certify that they have read, and recommend to the College of Graduate Studies for acceptance, a thesis entitled:

FLEXURAL STRENGTHENING OF REINFORCED CONCRETE BEAMS WITH FABRIC REINFORCED CEMENTITIOUS MORTAR: EFFECT OF REINFORCEMENT RATIOS

Submitted by: Trevor Billows in partial fulfillment of the requirements of the degree of Master of Applied Science

Dr. Ahmad Rteil, School of Engineering
Supervisor, Professor (please print name and faculty/school above the line)

Dr. Shahria Alam, School of Engineering
Supervisory Committee Member, Professor (please print name and faculty/school in the line above)

Dr. Kasun Hewage, School of Engineering
Supervisory Committee Member, Professor (please print name and faculty/school in the line above)

Dr. Rudolf Seethaler, School of Engineering
University Examiner, Professor (please print name and faculty/school in the line above)

External Examiner, Professor (please print name and university in the line above)

December 16, 2016
(Date Submitted to Grad Studies)

ABSTRACT

The current state of North America's infrastructure system is in dire straits. The cost of repair is estimated at over $3.6 trillion in the United States alone. An innovative and cost-effective method of repair and retrofitting is vital to close what has been referred to as the infrastructure gap. As an alternative to the current methods, fabric reinforced cementitious mortar (FRCM) is proposed to aid the civil engineering industry in removing this gap. Applied to structural members externally, FRCM is characterized by its ability to strengthen and rehabilitate these structures. This study set out to determine the flexural strength improvement of reinforced concrete (RC) beams with different reinforcement ratios, textile layers, fabric materials and anchorage methods. Ten full-scale (200 x 300 x 4000mm) RC beams (2 controls, 8 strengthened) were cast and tested under monotonic four-point bending conditions. Ultimate flexural capacity, pseudo-ductility, energy absorption, stiffness, and failure mode were taken as performance indicators. Results showed all FRCM strengthened beams failed in a similar way to their control counterparts and FRCM did not affect the pre-yielding stiffness or ductility of the strengthened beams. However, FRCM significantly improved the beams' yield load and flexural capacity over the control. Flexural strength improved by up to 81% over the control. Strength improved with an increase in textile layers, and U-shaped strengthened specimens outperformed their soffit-strengthened equivalents.

PREFACE

This thesis is based on original, experimental work completed by the author in the School of Engineering at the Okanagan campus of the University of British Columbia. The author was responsible for completing all literature review, material acquisition, experimental work, data collection and analysis, and thesis writing. Guidance and supervision throughout the thesis work were graciously contributed by Dr. Ahmad Rteil. Major portions of chapter 3 and 4, and a minor portion of chapter 2, have been submitted to a peer-reviewed technical journal for publication. The following is a list of publications based on the thesis:

Billows, T. N. S., & Rteil, A. (2016). Fabric reinforced cementitious mortar (FRCM) strengthened beams in bending. *ACI Structural Journal.* Submitted November 3, 2016.

TABLE OF CONTENTS

LIST OF TABLES

LIST OF FIGURES

LIST OF ACRONYMS

ACI	American Concrete Institute
AR	Alkali-resistant
ASCE	American Society of Civil Engineers
ASTM	American Society for Testing and Materials
EB	Externally bonded
ECC	Engineering cementitious composites
CSA	Canadian Standards Association
DTI	Direct tension indicators
FRC	Fibre reinforced concrete
FRCM	Fabric reinforced cementitious mortar
FRP	Fibre reinforced polymer
LVDT	Linear variable displacement transducer
MBC	Mineral based concrete
NSM	Near surface mounted
PBO	Polyphenylene benzobisoxazole
RC	Reinforced concrete
TRC	Textile reinforced concrete
TRM	Textile reinforced mortar
UHPFRC	Ulta-high performance fibre reinforced concrete

ACKNOWLEDGEMENTS

The amount of effort that goes into completing a work this large, especially an experimental one, is substantial and requires contributions from many. I would be remiss to not acknowledge the efforts and aid of my supervisor Dr. Ahmad Rteil. His approach, mentality and support have been crucial to my completion of this monumental endeavour. I am proud to have worked with him in numerous facets, and prouder to call him my friend.

The completion of the many full-scale components of this project would not have been possible without the financial and technical contribution of some local businesses and people. I am especially grateful to: Okanagan Builders (Desmond O'Brien) for donating wood and concrete, Structural Concrete Repair (Andre Harrichhausen) for donating time in roughening the concrete surface of beams, Crown West Steel Fabricators for partially donating the steel frame construction, and Western Canadian Steel (Corey Ivanitz) for tools to complete the frame construction. I also would like to recognize NSERC and their financial support, without this a Master's degree may never have been attainable.

Some of the most meaningful acknowledgments go to people who personally devoted their time, effort and, in some cases, sweat to the completion of this project. Thank you Alec Smith, Ryan Mandau, Kim Nordstrom, Luis Diaz, Durwin Bossy, and Tim Giesbrecht for your continuous support in the ever-developing Structures Lab at UBC Okanagan, particularly for getting a full-body workout one Friday. I also would like to thank Devin Walline, Tanya Fraser and Ameeta Bhabra for motivating me to get the work done (even on days I probably should have stayed home), and for their hours of contributions.

DEDICATION

There are no more deserving people in this world of this dedication than my parents. This thesis has required substantial devotion of my time, money, and life; however, it is nothing even close to my parents' effort to get me here. Norm and Debbie, you were there for every aspect of my life and I cannot thank you enough for getting me to this point. Every day I continually strive to make you proud of me as a student, and as a person in this world.

CHAPTER 1: INTRODUCTION

1.1 Problem Statement

Reinforced concrete (RC) is one of the most used materials in the world and the singly most used construction material. Due to its numerous advantages, RC constitutes a large percentage of current North American structures and bridges (CAC, 2016; Crow, 2008). Unfortunately, these structures deteriorate due to factors such as reinforcement corrosion, excessive loading, poor design and durability issues (Babaeidarabad, Loreto, & Nanni, 2014; Gil, Escrig, & Bernat, 2014). The deterioration of these structures, along with problems of inadequate design (change of design requirements or increased service loads), have developed into a world-wide problem that has increased the demand for a rehabilitation method (Elsanadedy, Almusallam, Alsayed, & Al-Salloum, 2013).

The severe status of the North American infrastructure has been acknowledged for years; however, it is still met with a shortcoming of resolution. As far back as 2003, Mufti acknowledged this by saying that bridges and roads are "deaf, dumb and blind" due to inadequate maintenance, excessive loading and adverse environmental conditions (pg 1, Mufti, 2003). Numerous reports, documents, and technical papers have been published updating these claims. The American Society of Civil Engineers (ASCE) states the entirety of the American infrastructure improvement requirs $3.6 trillion USD. Of this, an estimated US $76 billion is needed to address structurally obsolete or deficient bridges; this makes up 24.9% of America's bridges. Although recent reports show some investment has been made into bridges, this can be a deceiving report (ACSE, 2013). The nation's nearly 67,000 structurally deficient bridges make up one-third of the total decking area. This illustrates bridges that are being left unvisited are ones significant in size and length.

The ASCE report also states that US $759 billion of the overall cost is required to repair and maintain high-hazard dams, schools, wastewater facilities, and roads (ACSE, 2013).

Canada's infrastructure report card from 2016, on the other hand, breaks down the status of the infrastructure into a scale of very poor, poor, fair, good and very good. Replacement value for infrastructure labelled very poor, poor, and fair in the bridges and building categories totals $45 billion. Further, their structural condition is worsening at the reported investment levels (PSC, 2016). In an alternative technical report on Canada's infrastructure gap, Mackenzie (2013) acknowledges that there has been recent progress and efforts to close the infrastructure gap. However, as shown in Figure 1.1, during the late 1990s the investment dropped to about 1.5% of the GDP. This led to a corresponding underinvestment which has had a drastic cumulative effect. A total estimated public capital of $145 billion in today's value has been shorted (Mackenzie, 2013). These financial numbers are dramatic and a cost-efficient method of repair could be crucial to closing the gap.

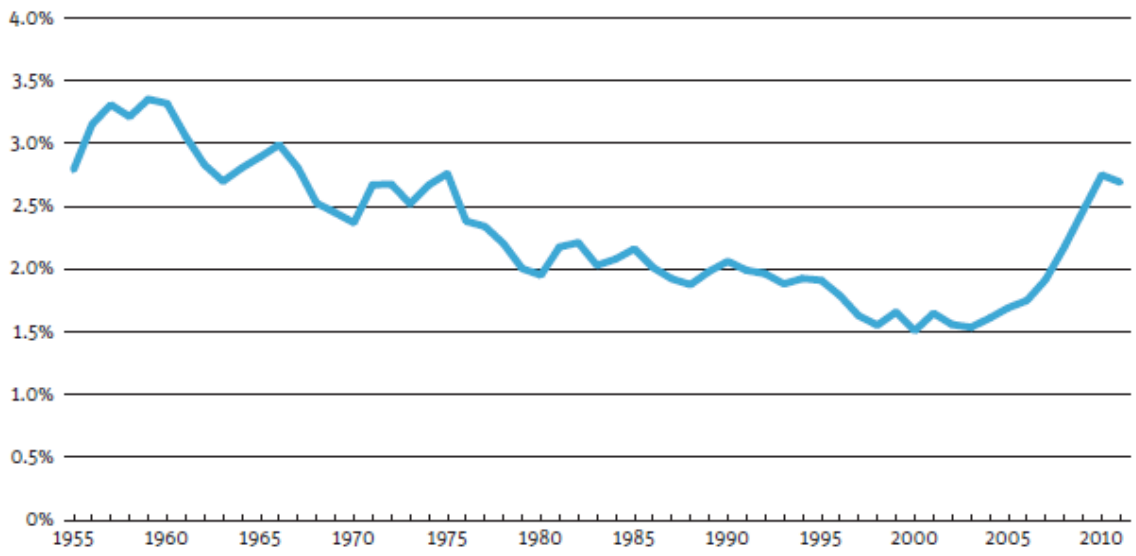

Figure 1.1: Canadian government investment in infrastructure as a percentage of GDP from 1955 to 2011 [(Mackenzie, 2013) with permission through Creative Commons license]

Numerous methods have been applied across the civil engineering industry to strengthen and repair structures such as section enlargement, steel plate addition, posttensioning, and fibre reinforced polymers (FRPs). Over recent decades, FRP in particular has been applied widely due to its many advantages over alternatives and structure replacement (ACI 440.1R, 2007; Awani, Refai, & El-Maaddawy, 2015). One study estimated that utilizing FRP as a repair method on bridges can reduce cost by $1/10^{th}$ or $1/15^{th}$ versus total replacement (GangaRao & Vijay, 2010). However, FRP has disadvantages such as poor performance at elevated temperatures, hazardous application (toxic chemicals), relatively high cost of resin, and incompatibility of resin and substrate, which are mostly associated with the organic resin used. In an attempt to alleviate these drawbacks, the research community began looking into the use of an inorganic binder. This is where research into an innovative new composite, fabric-reinforced cementitious mortar (FRCM), was initialized (ACI 549.4R, 2013; Al-Salloum, Siddiqui, Elsanadedy, Abadel, & Aqel, 2011,

2012; Elsanadedy et al., 2013; Ombres, 2011; C. G. Papanicolaou, Triantafillou, Papathanasiou, & Karlos, 2007b; T. C. Triantafillou & Papanicolaou, 2005).

1.2 Thesis Layout

This thesis is organized into five chapters. Chapter 1 details the motivation behind this research initiative based on the status of the civil engineering industry.

Chapter 2 serves as a source of background information for the reader on the two most relevant and inherently similar strengthening techniques, FRP and FRCM. This chapter includes a thorough literature review of these materials. This is translated into research needs and the objectives of this research study.

The test matrix and the experimental program are outlined in Chapter 3 of this document. Covered in this section is the preamble work of designing and constructing wood formwork to cast the RC beams. Further, to complete the experimental testing, a design and erection of a steel test frame was required and these details are presented. Testing specifications, specimen preparation, material properties, and data acquisition are among other testing details presented in this chapter.

Chapter 4 presents the experimental results of the four-point bending test on 8 FRCM-upgraded RC specimens and 2 control specimens. Performance indicators include failure mode, stiffness, yielding, ultimate flexural strength, and ductility. This chapter also presents trends of the results based on the four input parameters, namely reinforcement ratio, textile material, number of layers and application orientation.

Chapter 5 concludes the document by correlating and summarizing the research findings. Finally, future recommendations for research initiatives are presented which could further establish FRCM as a strong method for civil engineers in structural rehabilitation.

CHAPTER 2: LITERATURE REVIEW AND RESEARCH OBJECTIVES

2.1 Reinforced Concrete Strengthening Methods

The drastic need for effective repair and strengthening methods is evident based on the current state of civil infrastructure (ACSE, 2013; Mackenzie, 2013; Mufti, 2003; PSC, 2016). Based on economic and environmental factors, it is mutually beneficial to maintain and upgrade structures as opposed to reconstructing them (Hag-Elsafi, Lund, & Alampalli, 2001; Silfwerbrand, 2009). A few methods of repair that have been applied with some success include: section enlargement, external posttensioning of members, external bonding of plates (steel or fibre reinforced polymer (FRP)) and applying FRP sheets (ACI 546.1R, 2014; Escrig, Gil, Bernat-Maso, & Puigvert, 2015; Sezen, 2012; Tan, 2016).

Section enlargement is the simplest and most straightforward repair strategy. This method involves placing formwork around an existing section to cast more concrete and steel rebar or other reinforcement. Clearly by increasing the section size of a beam, column or other structural member, the capacity and the stiffness of the member will increase. A key component for this repair is to ensure the section performs monolithically (Júlio & Branco, 2008). Simple in the case of design and homogeneity with base concrete, section enlargement has been an efficient and cost effective alternative. However, in order to efficiently add capacity, RC section enlargement needs to be significant in size; therefore, imposing on clearance allowances and contributing additional load. Further, construction of formwork and placing of reinforcement is a labour intensive task (Sezen, 2012).

External post-tensioning involves stressing high strength bars or tendons to high values to counteract the loading on a structure, and thus can improve its performance. A RC beam for example, would have these tendons placed below the neutral axis to reduce the tensile forces present. Post-tensioning has the potential to be the most efficient option for strengthening as structural performance can be improved drastically. This method is completed with high strength-to-weight ratio materials, in a short period of time, with minimal intrusiveness and without reducing clearance significantly. However, drawbacks associated with this method include lack of corrosion resistance of steel tendons, fire resistance of FRP tendons, high cost of tendons, and potential vandalism (Tan, 2016).

Another commonly used method of repair employs the addition of external plating, usually in the form of FRP or steel. Both options have proven promising by increasing the load capacity, while decreasing the deflection under service loading. Pre-fabricated plates can be bonded or anchored into the concrete substrate enabling transfer of stresses to the strengthening material. When considering steel plates some advantages include application without skilled labour (although heavy materials), low price of available materials, ductile response, and minimal disruption (Aykac et al., 2013). FRP plating requires skilled labour, and loses the ductile response compared to steel plates, however, it has promise due to its high strength-to-weight ratio and can reduce the cost versus a replacement alternative (Hag-Elsafi et al., 2001). Although effective, steel plating repair suffers from potential corrosion, increased weight of the member, heavy strengthening materials, and reduction of structure clearance. Meanwhile, FRP plating reduces ductility, requires skilled workers to handle toxic polymers, and suffers from high temperature susceptibility (Hag-Elsafi et al., 2001).

Each of these methods have associated drawbacks that reduce their desirability including intrusiveness to clear space around structural members, fire resistance, and corrosion protection. Which option to be applied is an engineering decision based on each project's needs and efficient alternatives are valuable to the civil engineering industry (ACI 546.1R, 2014).

2.2 Fibre Reinforced Polymer (FRP)

A composite material named fibre reinforced polymer (FRP) has been implemented substantially as a structural material and in other industries worldwide due to many advantages (ACI 440.1R, 2007; GangaRao & Vijay, 2010; Silfwerbrand, 2009). These materials have been dated back to the 1970s but significant research devotion over recent decades has led to its widespread use, especially in improving a structure's capacity (Aljazaeri & Myers, 2015; Babaeidarabad et al., 2014; D'Ambrisi & Focacci, 2011; Gil et al., 2014; Ombres, 2011; Si Larbi, Agbossou, & Hamelin, 2013). FRP combines high tensile strength fibres with an organic polymer matrix, creating an innovative and diverse composite. The fibres are strong and lightweight. Common materials that have gained the attention of the industry are carbon, aramid, basalt and glass and their properties can vary drastically depending on the type and the manufacturer (ACI 440.1R, 2007; GangaRao & Vijay, 2010; Gil et al., 2014). The other component, the binder that the fibres are impregnated in, is thermosetting organic polymers which usually include epoxy, polyester, vinylester, phenolics, or polyurethane. Once combined together the fibres and polymer act as a single system through a transfer of stresses via the bond interface. Figure 2.1 shows the general stress versus strain diagram for a typical FRP system and steel. It is apparent that the FRP systems consist only of a linear elastic response unlike that of steel where a perfect elasto-plastic

curve is assumed. Table 0.1 through Table 0.4 in Appendix A present further details, examples and material properties of FRP constituents and composites.

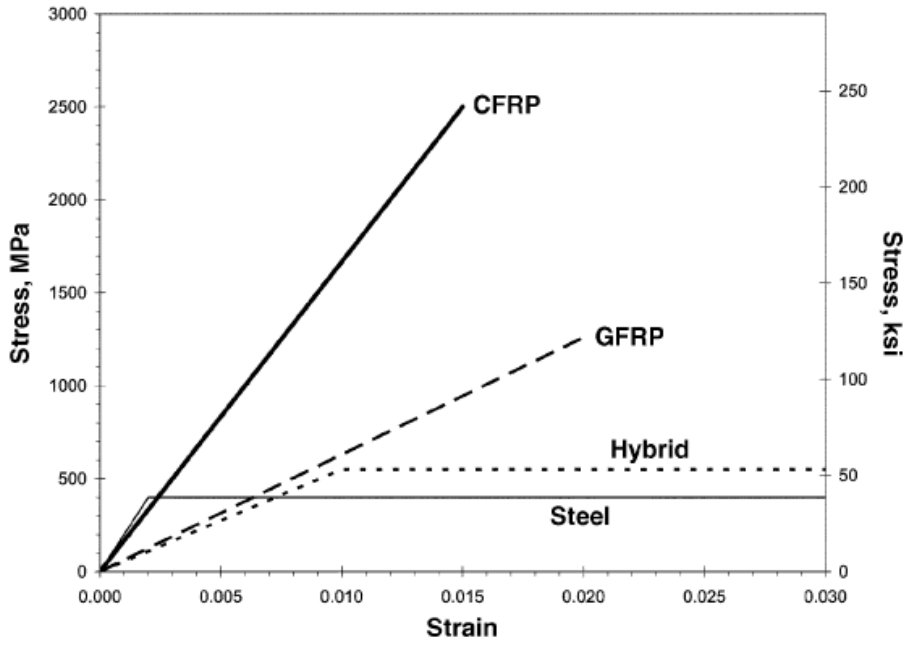

Figure 2.1: The stress-strain relationship of FRP [(ACI 440.1R, 2007) © with permission from ACI]

FRP must have some significant advantages that led to its extensive use across industries. These advantages are very well reported in the technical literature (ACI 440.1R, 2007; Al-Salloum, Almusallam, Elsanadedy, & Iqbal, 2016; Babaeidarabad et al., 2014; Elsanadedy et al., 2013; GangaRao & Vijay, 2010; Korany & Drysdale, 2006; B. Li & Chua, 2009; Ombres & Verre, 2015; C. G. Papanicolaou, Triantafillou, Papathanasiou, & Karlos, 2007a). The first, and possibly the most significant, is FRP's high strength-to-weight ratio. Fibres outlined above are all lightweight with extremely high tensile capacity. This leads directly to other inherent benefits such as easy handling and fast application rate. This reduces construction and potential shut down times. Another advantage is the inherent corrosion resistance of FRP composites, which is of extra interest when comparing to steel products. Rebar corrosion is one of the most impactful processes

when considering the deterioration of RC structures and shortening of its service life. Utilizing FRP as an externally bonded strengthening method provides an external layer that also helps resist corrosion of the RC material below (Gadve, Mukherjee, & Malhotra, 2009). Other research has shown that bond and lap splice strength of internal rebar can be improved with external wrapping and confinement with FRP (Bournas & Triantafillou, 2011; Hamad & Rteil, 2006). Finally, due to the long period that FRP has been researched, design codes have been developed to aid in construction and safety of this composite. In Canada all FRP projects are completed in accordance with CSA S806 design standard for buildings, S6 design standard for bridges and S807 materials specification (CSA S6, 2014; CSA S806, 2012; CSA S807, 2010). Further, there are ACI reports and guides in the United States, and similar codes in Italy, Japan, and Switzerland (ACI 440.1R, 2007; ACI 440.2R, 2008; CNR-DT 200, 2004; FIB TG 9.3, 2001). Numerous research efforts have shown the applicability of FRP in repairing or retrofitting RC or masonry structures in terms of axial capacity, confinement, shear strength, flexural strength, seismic performance and lap splice improvement (ACI 440.1R, 2007; ACI 440.2R, 2008; ACI 546.1R, 2014; Al-Kamaki, Al-Mahaidi, & Bennetts, 2015; Aljazaeri & Myers, 2015; Attari, Amziane, & Chemrouk, 2012; Babaeidarabad et al., 2014; Ebead & Saeed, 2014; El Maaddawy & Sherif, 2009; Gadve et al., 2009; GangaRao & Vijay, 2010; Kassem, Farghaly, & Benmokrane, 2011; B. Li & Chua, 2009; Mostofinejad & Mahmoudabadi, 2010; Mufti, 2003).

Despite the strong attributes and industry wide application, FRP has some significantly noted drawbacks widely covered in the literature. Namely, poor behaviour at temperatures above the polymer's glass transition temperature, relatively high cost of resin, hazardous to manual workers (chemicals used), non-applicability on wet surfaces or at low temperatures, lack of vapour permeability, incompatibility of resin and substrate, UV degradation of epoxy polymer, difficulties

assessing post-earthquake damages behind the FRP, and poor recyclability (Al-Salloum et al., 2011, 2012; Alhaddad, Siddiqui, Abadel, Alsayed, & Al-Salloum, 2012; Babaeidarabad et al., 2014; Bournas, Triantafillou, Zygouris, & Stavropoulos, 2009; D'Ambrisi & Focacci, 2011; Elsanadedy et al., 2013; Ombres, 2011; C. G. Papanicolaou et al., 2007a; Yin, Sheng, Ph, Wang, & Li, 2014). Figure 2.2 illustrates one of these substantial downfalls, FRP's performance under high temperatures. For a FRP strengthened specimen subjected to 80°C for one hour, the strength nearly matches that of the original unstrengthened specimen (Ruredil, 2008). In other words, the FRP has been rendered fully ineffective, which is a worrisome property. Other research noted further that, at only 40°C, FRP confined specimen could lose 20% of its expected strength; a temperature that occur during a day in some climates (Trapko, 2013). When inspecting the list, it is evident that most drawbacks of a FRP system can be attributed to the organic matrix employed. The civil engineering industry has been looking for a novel solution to meet the structural upgrading deficit but with a more efficient method. FRP also suffers from a brittle debonding failure, usually intermediately, that leads to detaching of strengthening materials which reduces the strength consideration (ACI 440.2R, 2008; D'Ambrisi & Focacci, 2011; Si Larbi et al., 2013).

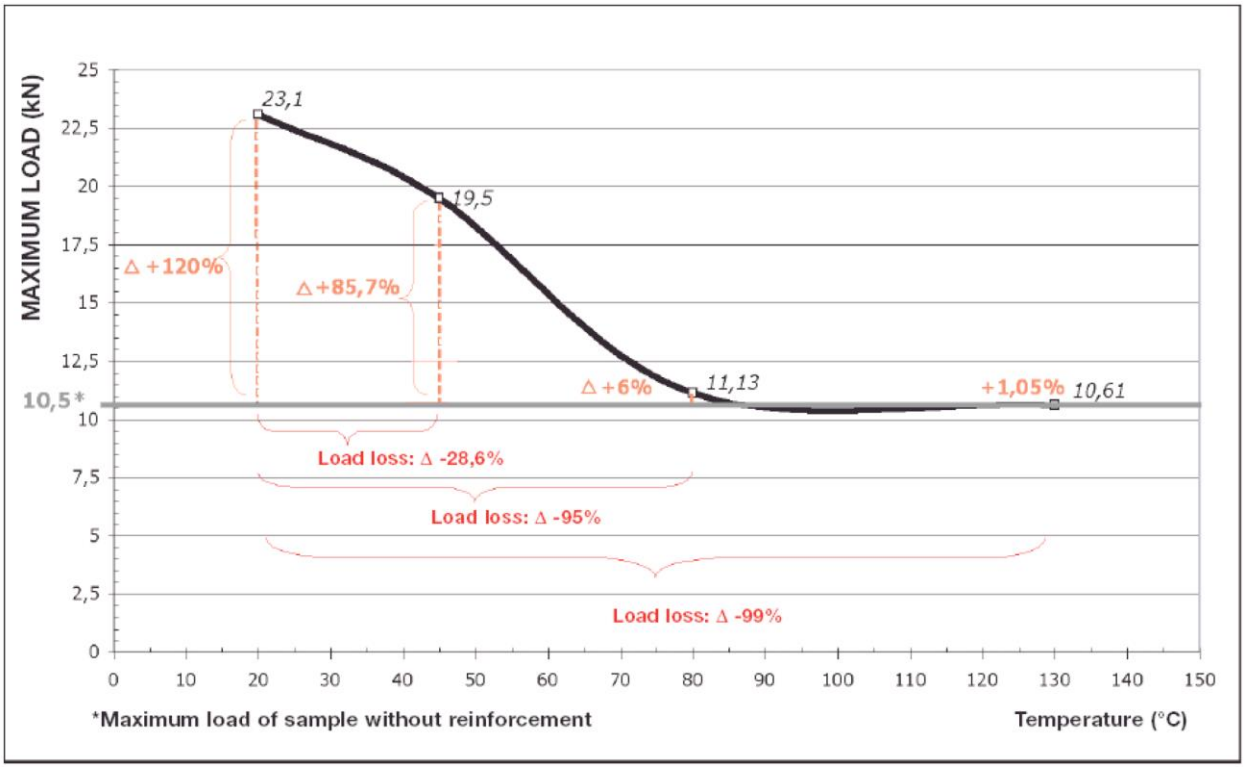

Figure 2.2: Performance of FRP system under high temperature exposure [(Ruredil, 2008) © with permission from author]

2.3 Fabric Reinforced Cementitious Mortar (FRCM)

Fabric reinforced cementitious mortar (FRCM), also known as textile reinforced mortar (TRM), has been proposed as an alternative to FRP systems in the strengthening of RC components. This material has gained the interest of the research community, especially in Europe. Although research into FRCM began in the 1980's, the development was slow until the late 1990's and only starting in 2002 has the research community put considerable effort into FRCM (ACI 549.4R, 2013; Bournas et al., 2009; Colajanni, Fossetti, & MacAluso, 2014; C. G. Papanicolaou et al., 2007a). Applied to structures in an extremely similar fashion as FRP (hence the comparisons), FRCM reduces or removes many disadvantages of FRP by replacing the polymer matrix with an inorganic cementitious binder. However, in first attempts when replacing the resin,

the cement counterpart lacks the ability to impregnate continuous fibre sheets (Figure 2.3a) that the resin holds (Al-Salloum et al., 2011, 2012; Elsanadedy et al., 2013; Ombres, 2011; C. G. Papanicolaou et al., 2007b; T. C. Triantafillou & Papanicolaou, 2005). This led to the replacement of sheets with open mesh textiles or fabrics (Figure 2.3b). Thus allowing for a mechanical interlock to form, drastically improving the bond between the cementitious adhesive and the composite (ACI 549.4R, 2013).

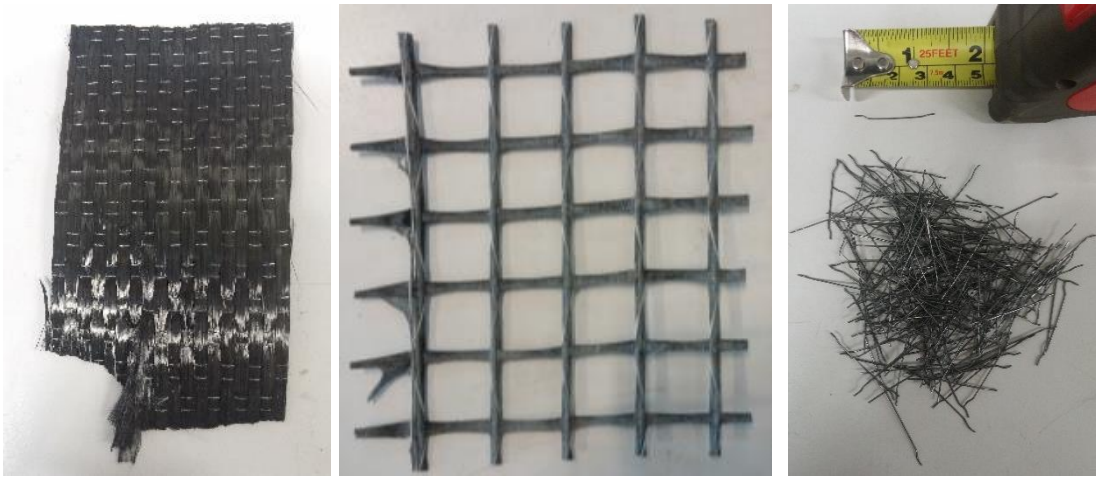

Figure 2.3: Different types of reinforcement, a) carbon fibre sheet, b) carbon fabric or textile, and c) dispersed steel fibres

FRCM has been referred to under many different titles throughout the research industry, which could lead to confusion if not straightened out. Figure 2.4 shows a chart with a few of the related materials inside of the blanket of brittle matrix composite. These composites are targets of much successful research and contributing to the confusion is the use of both classifications in both new construction and in the repair and upgrade of existing structures (Bandelt & Billington, 2015; Q. Li, Gao, Xu, Peng, & Fu, 2016). A very key distinction is that between long, continuous fibres in sheets (Figure 2.3a) or fabrics (Figure 2.3b) and short, discrete, dispersed fibres (Figure 2.3c). A few materials that fall into the latter category are engineered cementitious composites (ECC), fibre

reinforced concrete (FRC) and ultra-high performance fibre reinforced concrete (UHPFRC). The aforementioned short fibres in this grouping are added to the concrete mix and have short lengths of only 6 mm to 76 mm and small diameters. The term aspect ratio is often used and defined as the fibre length to diameter ratio. Typical values of dispersed fibre aspect ratio range from 20 to 100 and an example is shown in Figure 2.3c (ACI 544.1R, 2002; ACI 544.5R, 2010). These materials are often referred to as fibre-reinforced cementitious composites which can be a source of misperception compared to FRCM (Zhu, Zhang, Yao, Guan, & Yang, 2016). However, the long, continuous, and dry fibres of FRCM separates it as the aspect ratio is essentially infinite (micron diameters versus meter lengths). Depending on the region, the term FRCM seems to be most widely used across the current literature (ACI 549.4R, 2013; Alecci et al., 2016; Aljazaeri & Myers, 2015; Awani, El-Maaddawy, & Refai, 2015; Babaeidarabad et al., 2014; Carozzi, Colombi, Fava, & Poggi, 2016; Colajanni et al., 2014; D'Antino, Sneed, Carloni, & Pellegrino, 2016; ICC Evaluation Service, 2013; Jung, Hong, & Han, 2015; Michels, Zwicky, Scherer, Harmanci, & Motavalli, 2014; Ombres, 2011; Pohoryles et al., 2016; Trapko, 2013). Although FRCM has become common, textile reinforced mortar (TRM) was initially used frequently and other variations of the base terms have been used elsewhere in the literature (Al-Salloum et al., 2016; Bernat-Maso, Gil, & Roca, 2015; Bournas et al., 2009; D'Ambrisi & Focacci, 2011; Elsanadedy et al., 2013; Escrig et al., 2015; Gil et al., 2014; Gopinath, Murthy, Iyer, & Prabha, 2014; Ramaglia, Lignola, Balsamo, Prota, & Manfredi, 2015). Textile reinforced concrete (TRC) is a term that is used widely but tends to specify application of fabric as a new construction method as opposed to strengthening of an existing structure (RILEM Technical Committee 201, 2006; Si Larbi et al., 2013; Williams Portal, Lundgren, Wallbaum, & Malaga, 2014; Xu, Shen, & Wang, 2016; Yin et al., 2014).

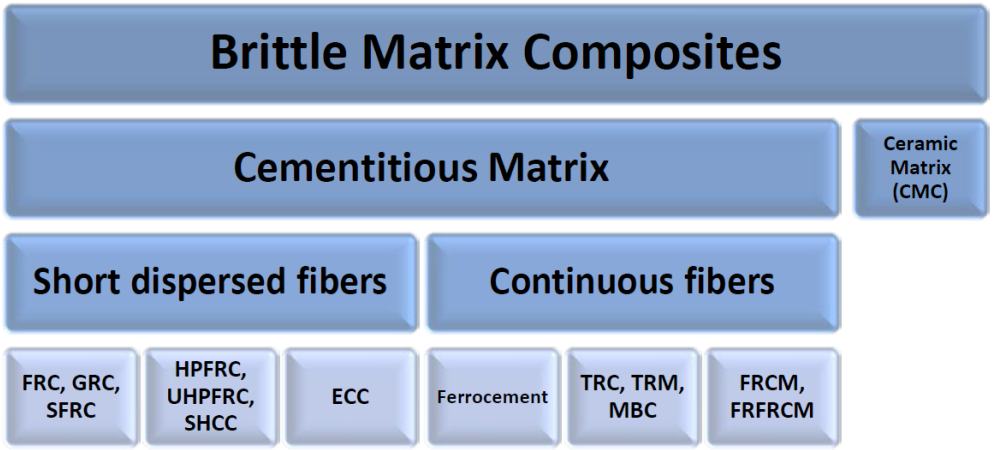

Figure 2.4: Different names of materials within brittle matrix composites [(Diana Arboleda, 2014) © with permission from author]

2.3.1 Fabrics and Textiles

As mentioned earlier, FRCM is inherently similar to FRP and is sometimes referred to as the "twin brother" (Nanni, 2014). However, the two most intrinsic differences are replacement of sheets and resins, with textiles and mortar, respectively. Described as continuous, dry woven meshes disposed along two orthogonal directions, the textile or fabric is bonded to concrete surfaces with a cementitious based mortar as the matrix. Some strands use small amounts of epoxy as a coating to improve durability or manufacturing, however, it does not impregnate the fibres hence the term dry fabric (ACI 549.4R, 2013; Babaeidarabad et al., 2014; D'Ambrisi & Focacci, 2011; Elsanadedy et al., 2013; ICC Evaluation Service, 2013; Loreto, Leardini, Arboleda, & Nanni, 2013; Ombres, 2011). The textiles implemented are high performance fabrics and can vary widely in pattern as well as mechanical properties depending on the application. Typical materials considered are carbon, basalt, glass, aramid and polyphenylene benzobisoxazole (PBO) that are known for having high strength-to-weight ratio, reduced manufacturing costs, improved fatigue and corrosion resistance and applicability due its composite nature (Yao et al., 2016). Special

consideration must be taken when using glass due to the alkaline environment of the cement matrix. Therefore, glass must be designated as alkali-resistant (AR) for utilization in FRCM (Michels et al., 2014). Four fabrics used in literature are shown in Figure 2.5.

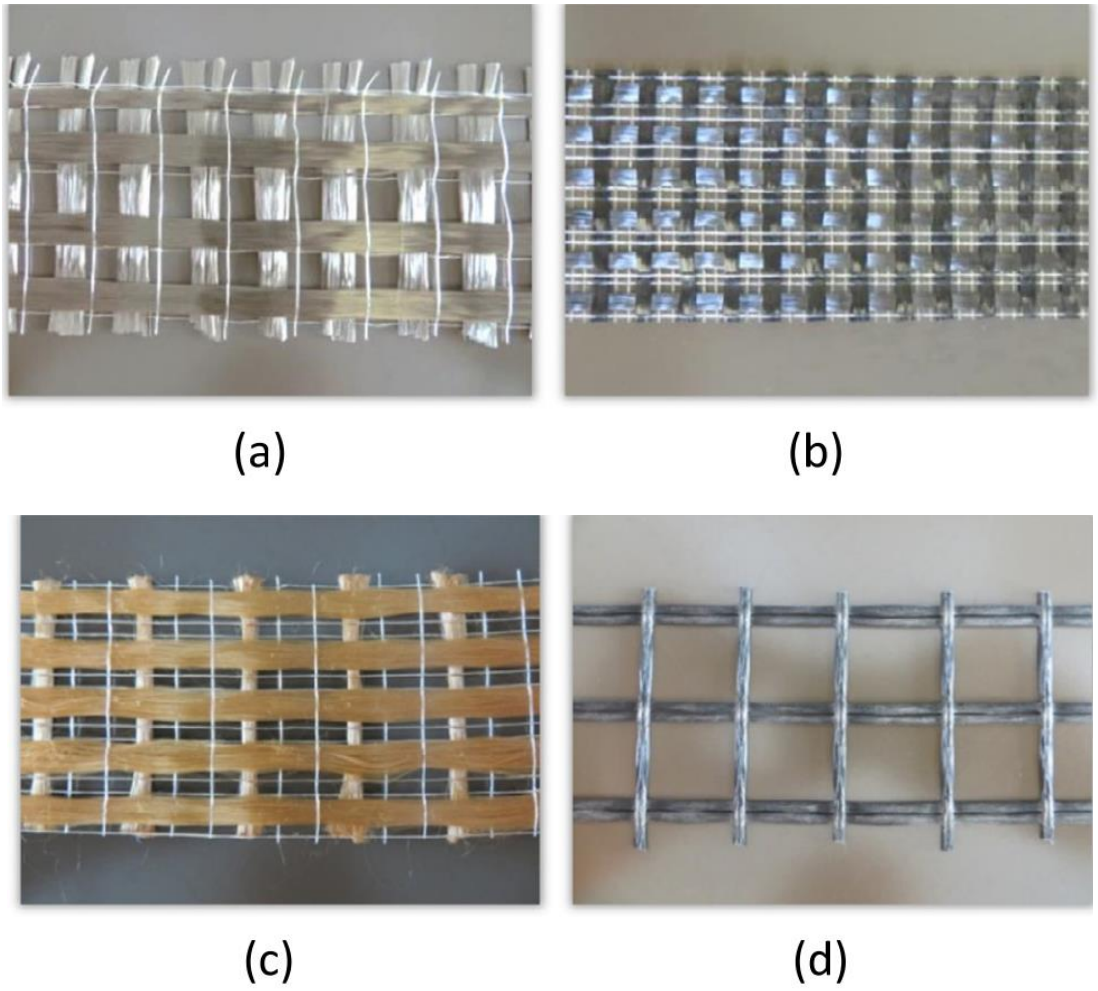

Figure 2.5: Fabric materials used in FRCM a) basalt, b) carbon, c) PBO, and d) glass [(Escrig et al., 2015) © with permission from publisher]

Within these material types the important properties such as tensile strength, stiffness and elongation can vary. Furthermore, the spacing, grid pattern and thickness can change on application and design. Spacing of fabric in the orthogonal directions, referred to as weft, tends to be less than 25 mm (1 inch) and with a coverage area of around 30% (ACI 2013; ICC Evaluation Service, 2013). Thicknesses typically range from 0.025 to 10.2 mm can be found in widths from 25 to 3050 mm. Figure 2.6 presents five different materials and spacing arrangements. Meanwhile, additional types are given in Appendix B (Appendix B: FRCM Material Properties

Table 0.5 and Table 0.6).

	Carbon fiber	Basalt fiber	Bitumen-coated E-glass fiber	Bitumen-coated polyester fiber	Polypropylene net
	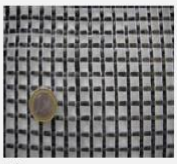	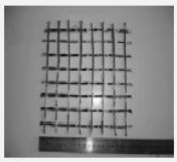		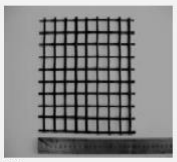	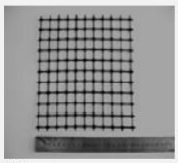
G.S.	10 mm	25 mm	25 mm	22 mm	19 mm
N.G.S.	6 mm	23 mm	23 mm	18 mm	16 mm
W	168 g/m^2	192 g/m^2	290 g/m^2	600 g/m^2	265 g/m^2
t	0.047 mm	0.07 mm	0.47 mm	0.84 mm	1.14 mm
f_t	157 kN/m	66 kN/m	54 kN/m	≈10 kN/m (at 5% elongation)	≈10 kN/m (at 5% elongation)
ε_u	1.5%	3.15%	2.9%	>5%	>5%
E_f	225 GPa	89 GPa	70 GPa	≈2 GPa	≈2 GPa

G.S.: grid spacing (mid-roving to mid-roving); *N.G.S.*: net grid spacing; *W*: weight; *t*: thickness of each layer (nominal values based on the equivalent smeared distribution of fibers for carbon and basalt fiber textiles and measured values for the rest); f_t: tensile strength of the grid per running m; ε_u: rupture strain of the fibers; E_f: fibers' modulus of elasticity. Mechanical properties are the same in both directions.

Figure 2.6: Typical textile layout and properties [(C. Papanicolaou, Triantafillou, & Lekka, 2011) © with permission from publisher]

There are three main methods of constructing the fabrics or textiles utilized in FRCM, namely, stitched (non-woven or knitted), weaving, and breading (ACI 549.4R, 2013; Hollaway & Head, 2001; Mobasher, 2011). Figure 2.7 illustrates a few examples of manufacturing methods of textiles. Woven fabrics (Figure 2.7a) have rovings crossed over and under fibres in the other direction in a different pattern depending on the weave pattern. Fabrics constructed by stitching

have optimized strength properties because of the fibre architecture. Finally, braided fabrics consist of an engineered system that is optimized for load distribution by the way yarns are intertwined and interlocked (ACI 440.1R, 2007).

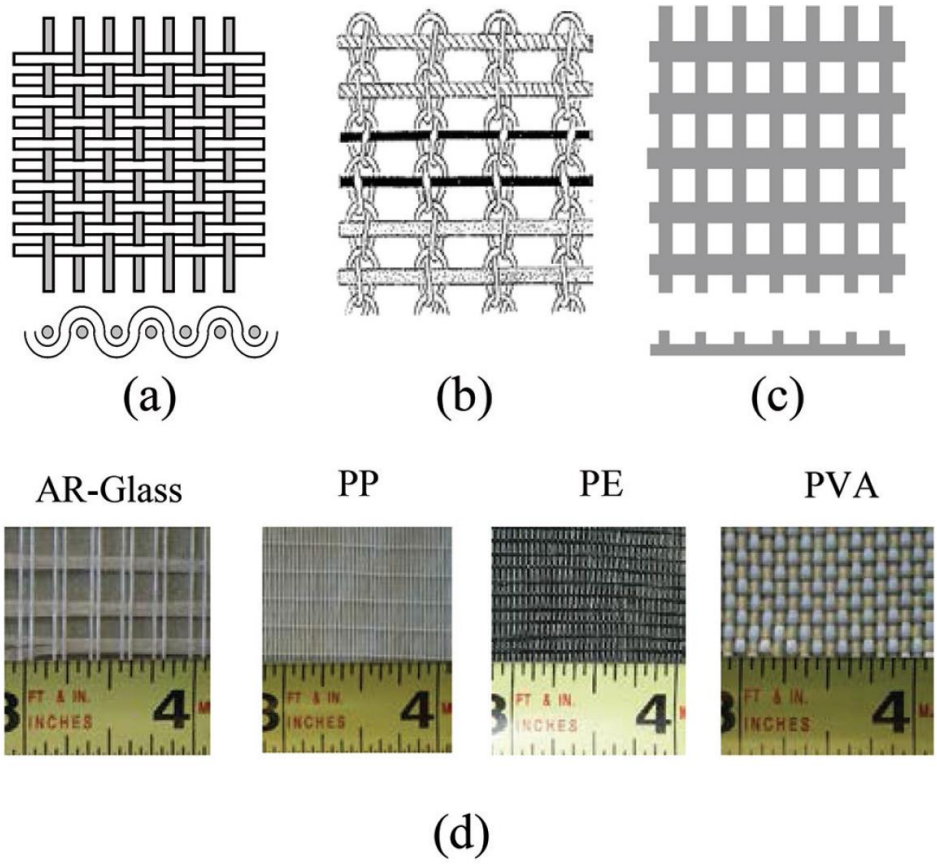

Figure 2.7: Typical fabric manufacturing methods and available fabrics a) woven, b) knitted, c) bonded and d) four available types – AR glass, polypropylene (PP), polyethylene (PE), and poly-vinyl alcohol (PVA) [(ACI 549.4R, 2013) © with permission from ACI]

2.3.2 Mortars

The mortar utilized for FRCM is important since it acts to transfer the applied load to the strong textile it has impregnated and adequately bond to the substrate. There are some general requirements for the mortar matrix, namely, it should be non-shrinkable, highly workable (ability to apply using a trowel), high viscosity (applicable on vertical or overhead surfaces), low rate of

workability loss (for each layer applied successively) and sufficient shear strength to avoid premature debonding (Ruredil, 2008). The matrix is grout systems based on Portland cement or lime, which has low dosage of short fibres and additives such as up to 5 percent of dry polymer. These polymers serve the function of improving the bond, providing proper workability, setting time and mechanical properties (ACI 549.4R, 2013; D. Arboleda, Carozzi, Nanni, & Poggi, 2015). The selection of mortar is vital to the performance of the FRCM system due to the fact that matrix performance cannot necessarily be predicted based on classical mechanical properties such as compressive and tensile strength, and modulus of elasticity. The bond between fabric and mortar, and between mortar and substrate, is what determines the performance quality of the matrix not necessarily mechanical properties. Mortar can be optimized based on the fabric being used through changes to its composites such as high fineness cement, adhesion promoter, additives, inorganic nanoparticles, micro aggregates, polycarboxylic, and fly ash (ACI 549.4R, 2013; D'Ambrisi & Focacci, 2011). Table 0.7 in Appendix B presents a mortar mixes that comply with ASTM C387 for high strength mortars (ASTM, 2015c).

2.3.3 Composite Properties

FRCM is recommended to be marketed and employed as a bundled system to optimize the bond and, therefore, the performance of the system (ACI 549.4R, 2013; D'Ambrisi & Focacci, 2011). Many studies have reported on the tensile response of FRCM specimen as this correlates to the response of the overall structure in many upgrading situations. The ICC Evaluation Service has published a document (AC434 Annex A) that outlines the acceptance criteria for this type of tensile testing (ICC Evaluation Service, 2013). Details include casting a single or multiple layers of FRCM samples in large wood forms, dimensions and gripping techniques. The response of the

FRCM system is a function of the two materials the FRCM is a composite of as well as the test gripping method.

The stress-strain response is characterized as being non-linear and three regions are formed (Figure 2.8). The first region, up to cracking of the mortar, corresponds to uncracked linear behaviour. This region is defined by a high stiffness, uncracked modulus of elasticity, due to the cementitious matrix. This region can be referred to as State I in Figure 2.8. The transition point, or sometimes called bend over point, refers to the mortar first cracking at the end of this first linear stage and has an associated stress and strain value. At this point, cracks begin to form across the specimen and a region of reduced stiffness occurs. As cracks continue to form and propagate, the stress-strain curve shows spiking as cracks suddenly form (State IIa in Figure 2.8). This region has the least stiffness of the noted regions. Crack spacing and width are a function of the stress, bonding action between fabric and matrix, reinforcement properties, and concrete failure strain (RILEM Technical Committee 201, 2006). At the end of this region, the crack pattern stabilizes and no new cracks form. A third region (State IIb in Figure 2.8) is defined and continues until failure which has filaments strained to full strength or slippage failure. This should lead to a response parallel to that of the fabric only under tension. However, analyzing Figure 2.8 and the textile line (linear elastic), it is apparent that these have slightly different stiffnesses, with the FRCM being less stiff. The only explanation is that a small volume of the fibres must have ruptured during the cracking phase leading to the lower extensional stiffness (RILEM Technical Committee 201, 2006). Further, the horizontal offset between the FRCM and textile response is referred to as tension stiffening. The ultimate strength and ultimate strain of the FRCM composite is defined at the end of this region (State IIb). These are critical values for the design and performance. Research

has shown that the composite has a strength of less than 50% of the filament strength due to the bonding failure (RILEM Technical Committee 201, 2006)

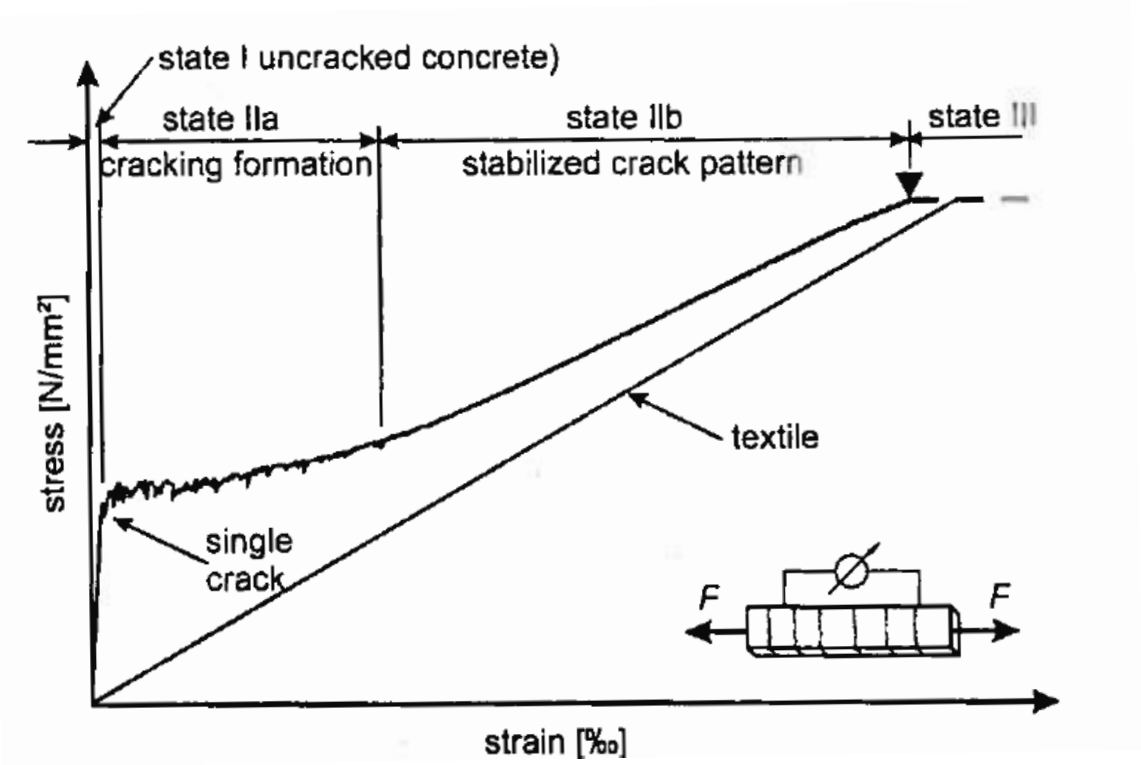

Figure 2.8: Stress strain response of FRCM specimen in tension [(RILEM Technical Committee 201, 2006) © with permission from publisher]

Two gripping methods for testing of FRCM coupons in tension have been explored recently, namely clevis and clamping (ACI 549.4R, 2013; D. Arboleda et al., 2015; Babaeidarabad et al., 2014; De Santis & de Felice, 2015; Ebead, Shrestha, Afzal, Refai, & Nanni, 2015). Clevis style gripping involves epoxying aluminum plates to each end of the external face of the FRCM coupons. These plates extend beyond the end of the specimen with holes that align allowing for a clevis to be gripped and tensile force applied. The clamping method involves externally reinforcing the clamping region with a layer of FRP then clamping the specimen directly. The former fails due to fabric slippage and, therefore, reaches lower ultimate strengths. Meanwhile, due to the

compressive forces added, slippage is delayed or removed in clamping style leading to better strength results. Figure 2.9 illustrates the effect on the stress-strain response with idealized responses for each gripping method. Clevis gripping leads to less well defined cracking region and, therefore, is modelled as a bi-linear response. Alternatively, clamping shows the third phase associated with cracking, and therefore, is modelled as tri-linear. In some literature, despite the cracking formation region, a bi-linear assumption is used that ignores the cracking phase (ACI 549.4R, 2013). Based on a few pieces of literature typical ranges for the stiffness for each region and the ultimate strength and strain values are presented in Table 2.1 (D. Arboleda et al., 2015; Babaeidarabad et al., 2014; De Santis & de Felice, 2015; Ebead et al., 2015).

Table 2.1: Summary of properties of typical tensile testing from literature

Material	E1 (GPa)	E2 (GPa)	E3 (GPa)	Ultimate Strength (MPa)	Ultimate Strain (%)
PBO	1180 - 1805	76	120 - 220	1550 - 3320	1.4 - 1.8
Carbon	460 - 1575	68	50 - 186	970 - 1500	0.74 - 1.8
Glass	260 - 1310	16 - 71	55 - 110	870 - 1980	0.69 - 1.92
Steel	290 - 1060	56 - 120	170 - 190	2800 - 3030	1.65 - 2.2

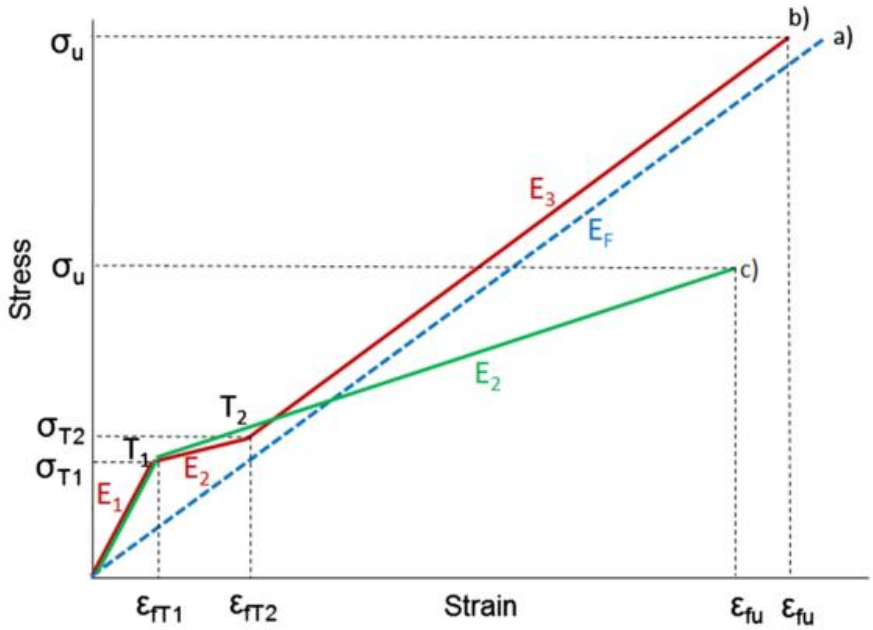

Figure 2.9: Stress strain curve in tension of a) textile only, b) FRCM with clamp grips, and c) FRCM with clevis style grips [(D. Arboleda et al., 2015) © with permission from ASCE]

2.3.4 Uses

Due to the novelty of the FRCM as a solution in the civil engineering industry, the extent of its application is quite limited. Depending on which portion of the cementitious matrix composites considered, the uses can vary. Applications such as integrated formworks (stay-in-place), external facades, structure members, new construction and strengthening of existing structures have all been explored. TRC for example, has been used in Europe extensively for new construction of cladding, industrially-manufactured products, thin walled construction, panel materials and sandwich structures. Its potential as a new construction material has led to promising results in life cycle assessments versus standard reinforcement materials (ACI 549.4R, 2013; Williams Portal et al., 2014; Xu et al., 2016). The field gaining most interest and particular to FRCM is as an externally bonded material to existing structures, both for RC and masonry structures, for strengthening and retrofitting. Figure 2.10 illustrates FRCM being applied by the hand lay-up method for external strengthening. A few noted field examples include soffit strengthening of brick

railroad bridge in Italy, tunnel lining in Greece, concrete support base of trestle bridge in New York, confine concrete support base in an industrial plant in Midwest US with high temperatures, bridge piers in Russia, masonry chimney in France, school building retrofit in Greece, and church dome in Greece (ACI 549.4R, 2013).

Figure 2.10: Application of FRCM to a RC beam as an external strengthening method

2.3.5 Advantages

There are numerous advantages to utilizing FRCM as an upgrading method that alleviates some drawbacks associated with the current use of FRP. These motivating advantages include: better compatibility with constituent materials, ease of installation with concrete tools, non-toxic matrix, improved porosity, improved high temperature performance and ease of reversibility (ACI 549.4R,

2013; D'Antino, Sneed, Carloni, & Pellegrino, 2015; Yin et al., 2014). Aljazeri added enhanced impact tolerance to this list, while Larbi expanded the ease of installation to include application with shotcrete (Aljazaeri & Myers, 2015; Si Larbi et al., 2013). The compatibility with substrate and porosity are inherent benefits of using a cement based matrix similar to that of the concrete. Porosity is vital when considering repair of masonry structures where FRP has noted problems, as well as changing the look of historical structures. The non-toxic cementitious matrix improves the working conditions and allows for cleaning of concrete tools as compared to disposable polymer ones. Figure 2.11 demonstrates one of the most exciting characteristic: FRCM's ability to strengthen concrete members at high temperatures (Colombo, Colombo, Magri, Zani, & di Prisco, 2011). At a temperature as high as 550°C, the FRCM was still efficient at strengthening in compression (173%) over the control member (CLS), which has drastically lost strength itself (Ruredil, 2008). This is in comparison to the FRP mentioned before (Figure 2.2) where at a temperature of only 80°C, the FRP was rendered completely useless. Trapko found only a 5-10% loss of FRCM strengthening at this same 80°C temperature (Trapko, 2013).

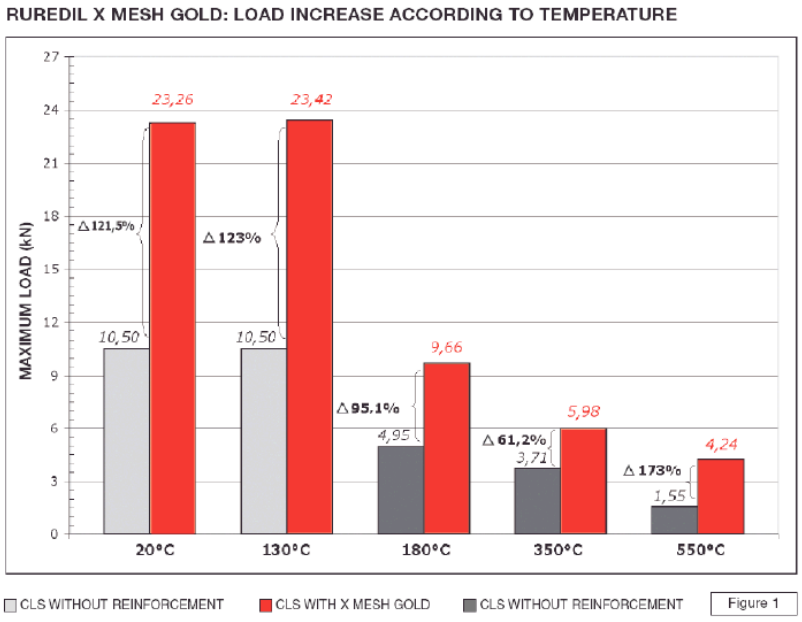

Figure 2.11: Performance of FRCM upgraded beams under increased temperatures [(Ruredil, 2008) © with permission from author]

2.3.6 Limitations

Although there are numerous benefits that result from using FRCM, it is worth noting any anticipated disadvantages. In some preliminary cases, FRCM appears slightly less effective than FRP at increasing the strength capacity. However, this could be made up with sufficient layers of FRCM, which based on the rovings of the textile, results in the material stiffness often being similar to that of FRP (Al-Salloum et al., 2011). The next disadvantage just relates to the pure novelty of the composite. The material is still said to be in its infancy and the results into FRCMs performance are still very limited thus far. Therefore, research has not yet paved a path for any sort of design codes, simply a guide that was recently published based on the limited data available (ACI 549.4R, 2013; D'Antino et al., 2015; Pellegrino & D'Antino, 2013; Pohoryles et al., 2016). This extends to the lack of skilled contractors to use the novel product. Furthermore, the research

that does exist is focused mostly in Europe and there has yet to be significant results produced in North America especially in Canada.

2.3.7 Flexural Strengthening of Reinforced Concrete (RC) Beams

Preliminary results of FRCM as a strengthening method are promising thus far. Shear strengthening of beams and columns have been explored with success (Al-Salloum et al., 2012; Awani, El-Maaddawy, et al., 2015; Ombres, 2015; T. C. Triantafillou & Papanicolaou, 2005). Axial tensile testing has been conducted to measure the properties of FRCM systems and axial compression research has seen the confinement effect (Al-Salloum et al., 2016; D. Arboleda et al., 2015; Loreto et al., 2013; Ombres & Verre, 2015; Trapko, 2014; T. C. Triantafillou & Papanicolaou, 2005). Further testing has shown the benefits to masonry structures and the seismic improvement capability for RC and masonry structures (Al-Salloum et al., 2011; Alecci et al., 2016; Alhaddad et al., 2012; Bernat-Maso et al., 2015; Ramaglia et al., 2015; T. Triantafillou & Papanicolaou, 2013). RC beams are strengthened in flexure by externally adding layers of FRCM to the tension area of a beam which also has seen success. Typical experimental testing involves three- or four-point bending test. Parameters that decide the strengthening effect of a RC with FRCM beam include: concrete compressive strength, beam dimensions, steel reinforcement ratio (tension and compression), steel yield strength, textile area, textile tensile strength, textile stiffness, mortar tensile strength, mortar stiffness and failure mode. RC beams have shown to have strength improvement up to 120%, and although a reduced ductility due to the fabric stiffness was noted, energy dissipation has improved by up to 36% (Aljazaeri & Myers, 2015; Jung et al., 2015). The sections below outline the research reported on the effect of FRCM on the flexural performance of RC beams.

2.3.7.1 Beam Properties

The base beam properties such as dimensions, steel reinforcement ratio and concrete strength can have significant impact on the flexural strength of a FRCM upgraded beam. Beam dimensions are typically rectangular with base sizes ranging from 100 to 400mm and heights from 150 to 305mm, with one research group looking at precast prestressed T-beams. Typical lengths fall in the small to medium scale range from 1000 to 3000mm (D'Ambrisi & Focacci, 2011; Gil et al., 2014; Gopinath et al., 2014; Ombres, 2011). The concrete compressive strength is a commonly varied parameter when looking at upgrading with FRCM with strengths ranging from 22 to 67.5 MPa explored (Ebead et al., 2015; Ombres, 2011). Typical results show that when comparing concrete strengths, the higher the compressive strength the less efficient the FRCM strengthening system serves to be (Yin et al., 2014). Depending on the number of layers of textile, Babaeidarabad et al. (2014) had a strength improvement of up to 92% with lower strength concrete (29.1 MPa) and only a 73% improvement at a higher strength concrete (42.9 MPa).

2.3.7.2 Upgrading Materials

Both separately, and as a system, the FRCM materials and their application will have a direct impact on the output upgraded strength. Textile materials used are commonly PBO, carbon, glass, basalt, and steel. PBO is used as the high strength option with its tensile strengths above 5,000 MPa and modulus of elasticity around 270 GPa. Basalt is typically the lower bound sustainable option with values of 623 MPa and 32 GPa for tensile strength and modulus of elasticity, respectively. D'Ambrisi & Foccaci (2011) compared PBO and carbon FRCM (CFRCM) with CFRP. PBO had 75% of the fibre area and 83% of the axial stiffness of FRP, however, both improved the flexural strength by the same value of 30% compared to the control. For the same

textile ratio, PBO outperformed CFRCM by 67%. The trend of increasing layers leading to increased flexural strength, however, with less efficiency after each additional layer is a prevalent trend in the literature (Babaeidarabad et al., 2014; D'Ambrisi & Focacci, 2011; Ombres, 2011; Yin et al., 2014).

The mortar matrix, as discussed, serves the two purposes of bonding the FRCM system to the substrate and the transfer of stresses. It is this bond ability that is shown to outweigh typical mechanical properties of mortars such as compressive strength, tensile strength and stiffness. Due to mortars and fabrics being implemented as a system from a supplier, the mortar details are not commonly listed. One case of it being outlined is shown in Table 2.2 where a self-designed fine grained concrete was used. Alternatively research from Gil et al. (2014) looked at four different cementitious matrices while only listing a product name and slight description. D'Ambrisi & Foccaci (2011) compared two mortar products from Ruredil, M50 and M750, without listing the mix values. However, they concluded that M750, which was designed for an improved bond with PBO, outperformed the M50 mortar. Beams with the same arrangement but with M750 mortar yielded 26% higher flexural strength despite having 8% lower mechanical properties.

Table 2.2: A fine grained concrete used as the mortar matrix [(Yin et al., 2014) © with permission from ASCE]

Component	Content (kg/m^3)
Portland cement PII52.5R	475
Fly ash	168
Silica fume	35
Water	262
Fine sand	460
Coarse sand	920
Super plasticizer	9.1

Another important consideration is the anchorage method of the FRCM system to RC beams. Three methods have been applied in the literature, namely U-shaped along the length, soffit face only, or soffit face with U-wraps at the ends only. Most research tends to prefer applying to soffit face only. Gil et al. (2014) found adequate bond for their research on precast prestressed sections. However, both U-shaped options were able to change failure mode from end debonding to fibre slip inside the matrix (D'Ambrisi & Focacci, 2011; Elsanadedy et al., 2013). Although potentially associated with the additional fibres in tension on the side of the beams, D'Ambrisi & Focacci (2011) also found an 18% strength improvement of complete U-wrapped sections as compared to the end anchors only.

2.3.7.3 Upgraded Beam Response

In order to correctly predict and design the strength gain, significant interest must be paid to the upgraded beam's response and eventual failure mode. The FRCM strengthened RC beam response is best summarized as tri-linear with each section having decreased stiffness (Figure 2.12). The first stage represents the uncracked concrete and mortar stage before the modulus of rupture of concrete. After cracking, the second stage is characterized by cracked behavior before steel reinforcement yields. Finally, stage three is post yielding with an increased stiffness compared to unstrengthen RC beams that is a function of the FRCM applied (Babaeidarabad et al., 2014; Ombres, 2011; Si Larbi et al., 2013). Babaeidarabad et al. expands that applying FRCM also increases both the yield point and clearly the ultimate strength.

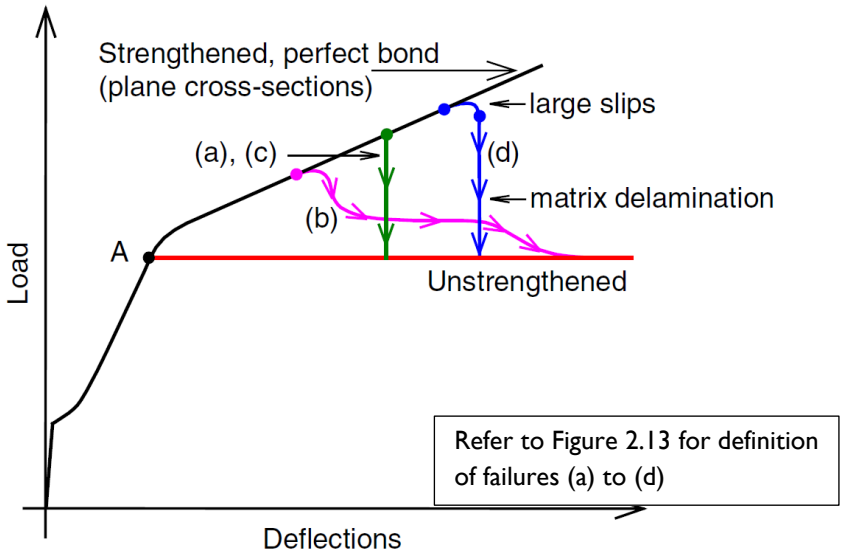

Figure 2.12: Visual representation of the typical tri-linear response of a FRCM upgraded beam depending on failure mode [(D'Ambrisi & Focacci, 2011) © with permission from ASCE]

Numerous studies acknowledge that the strengthening is dependent on the controlling failure mode. The common failures have been summarized by the authors and codes into the following: 1) concrete crushing in compression before tension steel yielding, 2) yielding of steel in tension followed by concrete crushing, 3) shear or tension delamination of the concrete cover, 4) debonding of the FRCM from the concrete substrate, 5) interlaminar debonding and 6) slipping of fibre mesh within the matrix (ACI 549.4R, 2013; D'Ambrisi & Focacci, 2011; ICC Evaluation Service, 2013; Jung et al., 2015; Ombres, 2011). The first two are failure modes that are characteristic of RC beams, leaving the last four of interest in FRCM strengthened RC beams. These failure modes are grouped under the term debonding. Debonding, or loss of strengthening action, is the most common and brittle failure and it is the main reason for strengthening limitations applied by design guides. Figure 2.13 visually represents these failure types. Although classified as a brittle failure, debonding in some cases can show pseudo-ductility. This is usually associated with the fabric slippage failure which adds ductility (Ombres, 2015). Unfortunately, the bond is a

complex interaction that depends on numerous factors such as mechanical interlock, matrix penetration and substrate/matrix interaction (D'Ambrisi & Focacci, 2011). The trend of loss of strengthening action has been reported commonly in the literature. Typically under-reinforced RC beams with low textile ratio have a slippage failure, while those with a higher ratio yield system detaching (Aljazaeri & Myers, 2015; Babaeidarabad et al., 2014; D'Ambrisi & Focacci, 2011; Elsanadedy et al., 2013; Gil et al., 2014; Jung et al., 2015; Ombres, 2011). A rarely reported, yet desirable, seventh failure mode is that of the textile rupture. With adequate bond strength, the rupture of the applied fabric gives full utilization of the material strength. However, only one study in the research has noted this failure mode thus far (Gil et al., 2014)

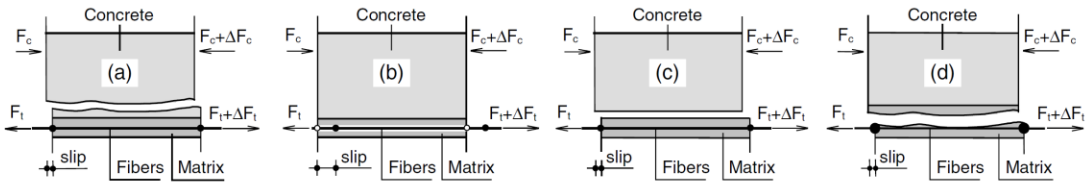

Figure 2.13: Illustration of the four failure modes in a FRCM upgraded beam: a) detaching of FRCM with portion of substrate concrete, b) debonding of fibres from matrix with large internal slip, c) detaching of FRCM/substrate interface and d) fracture within matrix layer [(D'Ambrisi & Focacci, 2011) © with permission from ASCE]

2.4 Research Needs

The previous background information shows that there is promise with FRCM as a RC upgrading material, however, further research is required. Although some data and field applications were reported, the very limited depth of validation is acknowledged in the literature (D'Antino et al., 2015; Pellegrino & D'Antino, 2013; Pohoryles et al., 2016). More promising research results are vital to expanding the introduction of this material in the civil engineering industry. This is especially the case when noting the location of research completed thus far. The

majority of research has been completed in Europe in places like Italy (Babaeidarabad et al., 2014; Carozzi et al., 2016; Colajanni et al., 2014; D'Ambrisi & Focacci, 2011; D'Antino et al., 2016; Ombres, 2011; Pellegrino & D'Antino, 2013; Ramaglia et al., 2015), Spain (Escrig et al., 2015; Gil et al., 2014), France (Si Larbi et al., 2013), Switzerland (Michels et al., 2014), UK (Pohoryles et al., 2016) and Greece (Bournas et al., 2009). A small number of papers have been submitted from places like USA, China, India, UAE and Qatar (Aljazaeri & Myers, 2015; Awani, El-Maaddawy, et al., 2015; D'Antino et al., 2015; Ebead et al., 2015; Gopinath et al., 2014; Xu et al., 2016; Yin et al., 2014). Very limited research has been completed in North America let alone in Canada. Thus far, to the best of the author's knowledge, there are no reported experimental results of flexural strengthening from Canada. This shows a need for local results completed using Canadian construction methods and materials. Without these results the development of Canadian design guides and codes is difficult. These documents are instrumental to the acceptance of a new material and lead to the use by the local engineering industry. Further, all flexural tests completed used small or medium scale beams; therefore, there is a need for larger scale specimen in the research repertoire. Another need is for an effectively anchorage method of the FRCM system. Currently nearly all flexural tests failed by some sort of bond failure, with only one reporting rupture (Gil et al., 2014). Flexural results that yield rupturing of the fabric could be instrumental to full utilization of the applied material. Therefore, there is a need to explore anchorage methods that lead to this result.

2.5 Objectives of the Current Investigation

The current research initiative set out to experimentally evaluate the flexural performance of externally bonded FRCM on RC beams in four-point bending. There are numerous significant

factors that can affect this result; the following are the investigated factors explored in this experimental program:

- Track the improvement on flexural strength using multiple layers of FRCM
- Explore steel reinforcement ratio effect on the strength gain of FRCM improved beams
- Analyze the effect of the application orientation (U-shaped or soffit) of two types of carbon FRCM systems (uni-directional or bi-directional) on the anchorage of the FRCM system and failure mode

The performance indicators include failure mode, beam stiffness, yielding, ultimate flexural strength, and ductility.

CHAPTER 3: EXPERIMENTAL METHODOLOGY

This chapter outlines the details of the experimental testing program that determined the validity of FRCM systems in flexural upgrading.

3.1 Test Matrix

A total of 10 beams (2 control and 8 FRCM strengthened) were cast and tested to analyze the bending performance of RC beams when varying four parameters: reinforcement ratio (0.8 and 2.0%), FRCM application orientation (U-wrapped and soffit), fabric type (uni-directional and bi-directional) and textile reinforcement ratio (1 and 3 layers). Table 3.1 lists each of the 10 beams tested with a Beam ID in the format X_Y_LZ_RW. Where X refers to the upgrading fabric ("Uni" for uni-directional carbon fabric or "Bi" for bi-directional carbon fabric), Y refers to the application orientation ("U" for U-shaped wrap or "S" for soffit only application), prefix L represents number of layers and Z is the number of layers (1 or 3 layers) and prefix R represents reinforcement ratio and W is the reinforcement ratio (8 for 0.8% reinforcement or 20 for 2.0% reinforcement). The two control beams were simply named CON_R8 and CON_R20 to specify the different reinforcement ratios.

Table 3.1: Test matrix

Group	Beam ID	Reinforcement Ratio (%)	Fabric Type	Fabric Orientation	Number of Layers
R8	CON_R8	0.8	-	-	-
	Bi_U_L1_R8	0.8	Bi-directional	U-shaped	1
	Uni_S_L1_R8	0.8	Uni-directional	Soffit	1
	Uni_U_L1_R8	0.8	Uni-directional	U-shaped	1
	Uni_U_L3_R8	0.8	Uni-directional	U-shaped	3
R20	CON_R20	2	-	-	-
	Bi_U_L1_R20	2	Bi-directional	U-shaped	1
	Uni_S_L1_R20	2	Uni-directional	Soffit	1
	Uni_U_L1_R20	2	Uni-directional	U-shaped	1
	Uni_U_L3_R20	2	Uni-directional	U-shaped	3

3.2 Test Specimens

The test specimens for this experimental program were designed to replicate full-scale beams in an existing structure that would require upgrading. Relatively low strength concrete was used and a beam cross section of 200 by 300 mm with a cast length of 4000 mm was taken. The beams were tested in four-point bending with a span of 3800 mm between the two supports. Point loads were applied spaced 1250 mm apart to create a constant moment region through this region.

Steel stirrups were bent from 10M rebar and placed at 150 mm spacing to ensure substantial shear resistance and, therefore, shear failure would not occur. Longitudinal tension reinforcement consisted of two 15M or 25M bars to achieve the desired reinforcement ratios of 0.8% and 2.0%. Two 6 mm smooth bars were used in the compression side to stabilize the rebar cage and, therefore, no strength contribution was considered. Concrete cover was 30 mm on all sides, leading to an effective depth of approximately 250 mm for the two reinforcement ratios. Figure 3.1 has the details of the RC beams including the FRCM system for upgraded beams.

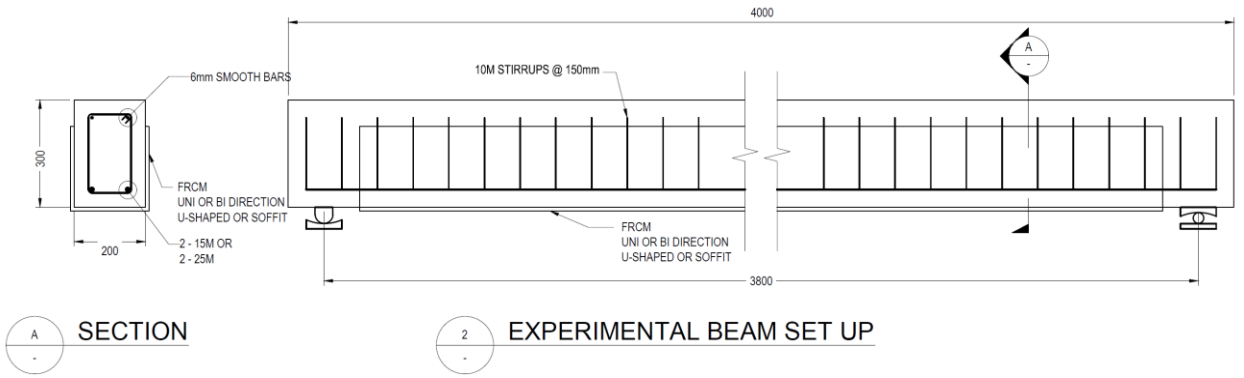

Figure 3.1: Longitudinal and cross-sectional details of the beam specimens

3.3 Formwork Construction

In order to cast the full scale RC beams, concrete formwork was required. The design for the formwork was created with the ability of multiple uses and with varying size of members. Removable post-tensioned wall panels were used to meet this criterion as well as for easy cleaning after use. Each formwork base had a capacity to form four beams, and three formwork sets were constructed for a total capacity of 12 beams. The cross-section is constant at 200 mm x 300 mm. However, the end panels can be placed anywhere along the length and, therefore, a beam of any length up to 4200 mm can be cast. The design implemented threaded rods running through plywood wall panels reinforced with 2x4's that could be tightened firm for casting, and released for cleaning and storage. Wood was selected as the material for construction due to its lower initial cost, constructability and strength. Figure 3.2 shows a plan view and cross-section of the as built formwork. Details of the formwork construction are described in Appendix C.

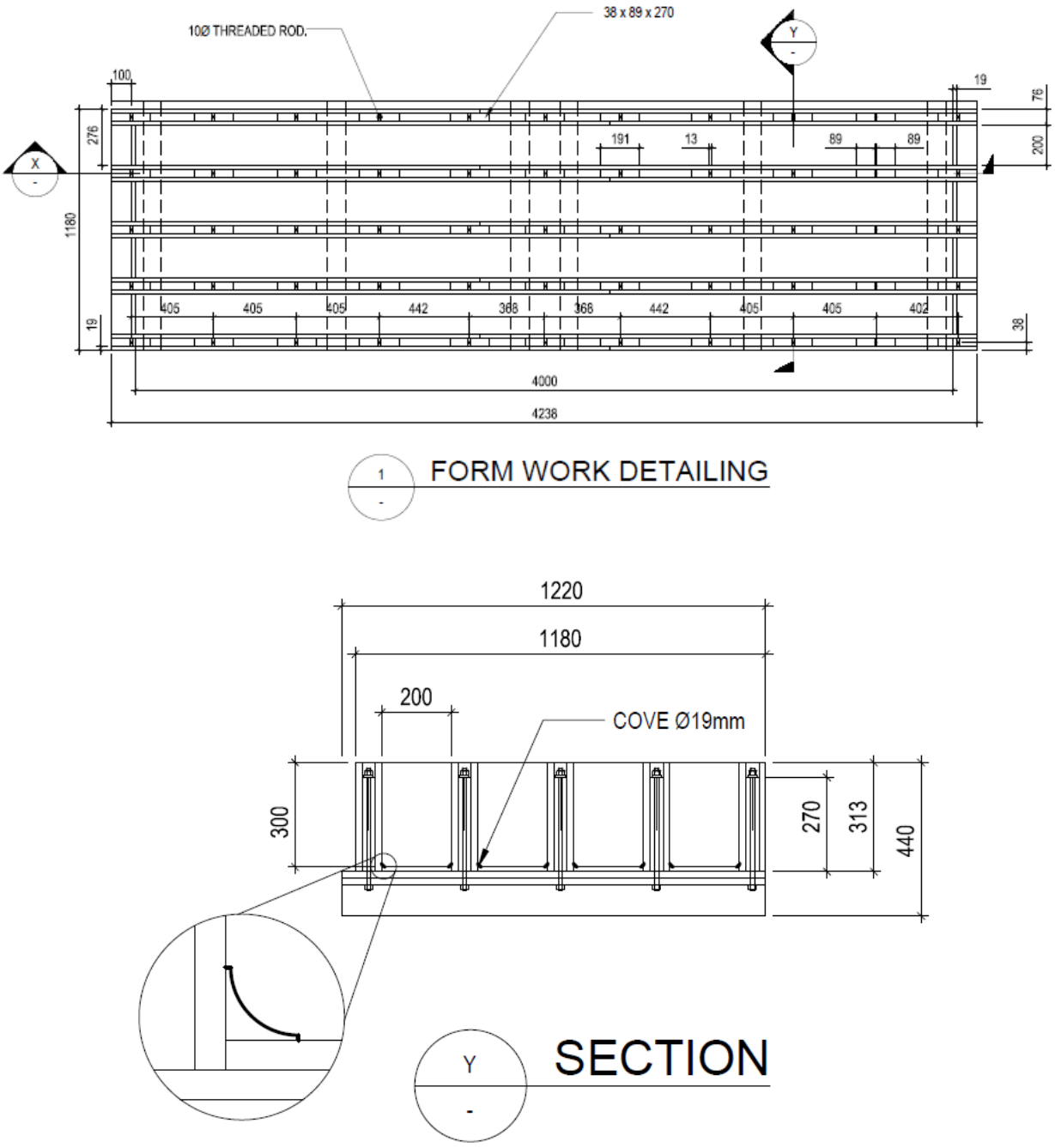

Figure 3.2: Details of the as built reusable concrete formwork

3.4 Steel Test Frame Construction

In order to properly test the RC beams, a test frame needed to be constructed in the newly built UBC Okanagan Structures Lab. Although this test matrix only calls for monotonic loads of less than the available 250kN actuator capacity, the design and construction process of the frame considered future testing. This included a higher load capacity, cyclic load application, mobility of the frame, and variability in the size of specimen such as testing slabs. The test frame was designed as portal frame with bolted connections. Column sections were W310x86 with 34 mm holes spaced at 100 mm over the top half of the column height, on both flange faces (Figure 3.3). Two C-sections (MC460x77.2) crossheads, with aligning bolt holes, were used to support the top of the actuator. Steel plate was welded into a U-shaped bracket with holes to allow connection to the base of the actuator (Figure 3.3). Bolts and nuts used were 1.25 inch grade A490M as per ASTM F3125M (ASTM, 2015b). All contact faces between steel elements were sandblasted to establish a roughened surface. This created a Class B surface for a slip-critical connection (CSA S16, 2014). Finally, the column base plates were post-tensioned to the floor to anchor the frame. Figure 3.3 shows the completed steel frame while detailed description of the design and construction of the steel frame is presented in Appendix D.

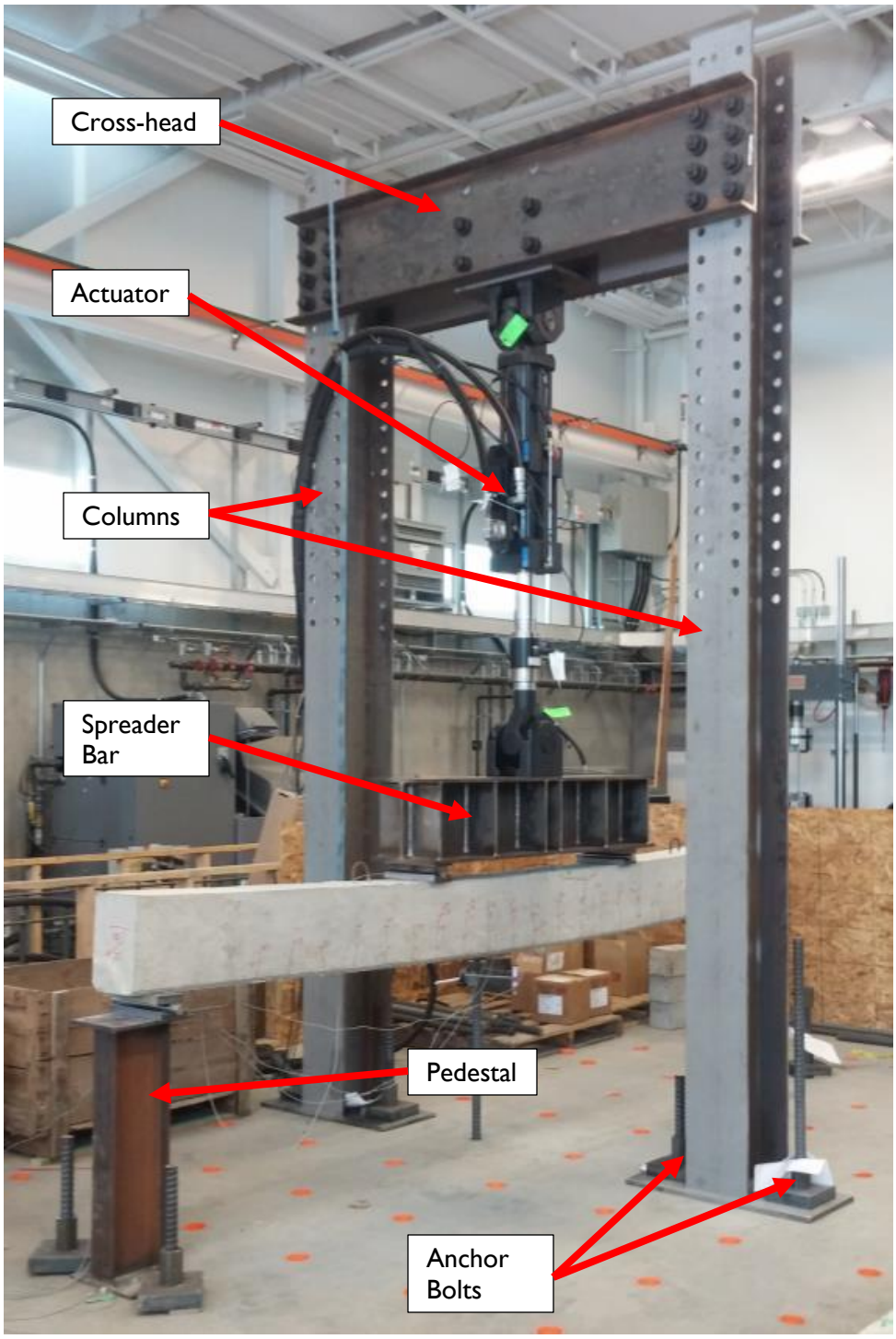

Figure 3.3: Steel test frame for four-point bending tests

3.5 Specimen Preparation

The following subsections breakdown the fabrication of the FRCM strengthened RC beams.

3.5.1 Casting

A total of 10 beams were cast using ready mix concrete in three wood formwork sets. The exposed faces of the painted wood formwork were greased with oil to enable easy removal of specimen from the formwork. Cove moulding with a diameter of 19mm was placed longitudinally in both bottom corners of the beam, which aided with removal and created a rounded corner for FRCM application. Steel rebar cages were supported by plastic concrete chairs at the bottom and hung from the formwork walls with rebar wire. Concrete was delivered in a mixing truck and poured directly into the forms. Once the forms were half full and the steel cages were supported by the concrete, the hanging supports were clipped and the wood hangers were removed to allow for beam finishing. Care was taken to ensure that wires connected to the rebar strain gauges exited the concrete in an appropriate location and were not damaged during casting. All beams were consolidated using a hand-held vibrator to ensure proper placing and consolidation. Excess concrete was removed from the surface, the surface was floated and then finished smoothly. Steel carry hooks were placed in the beam outside the points of loading to allow for the beam's removal from the formwork and transportation. Figure 3.4 show the stages of concrete casting. Numerous standard test cylinders and beams were cast to determine the concrete's compressive, tensile and flexural strength as per CSA A23.2 requirements (CSA A23.1/A23.2, 2014). All beams were left in the forms for 2 days with plastic sheet covering before being removed and placed on quarter support spaced dunnage. Beams were cured under wet burlap and plastic sheets for an additional 5 days following the removal from the forms.

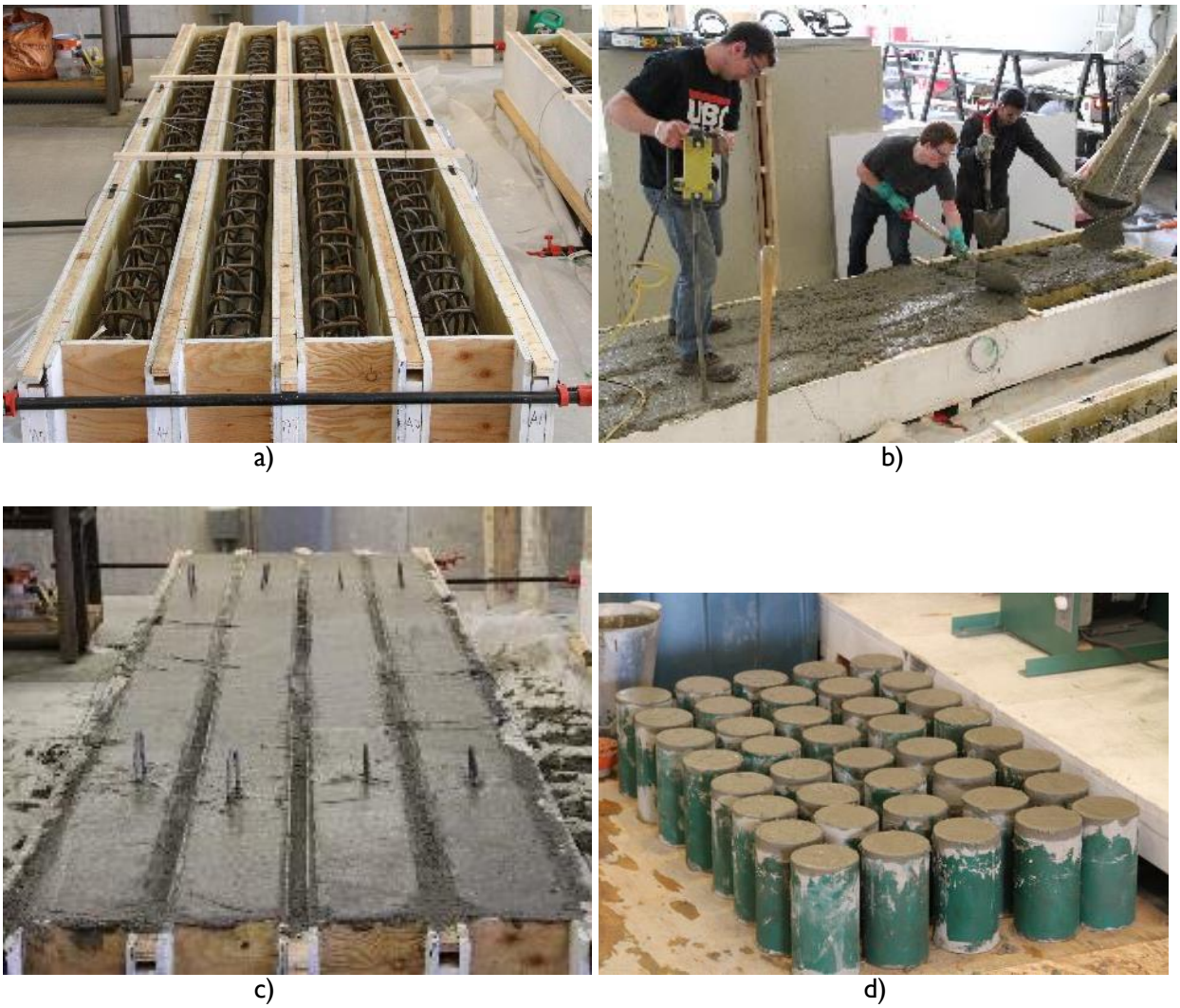

Figure 3.4: Beam casting a) formwork with rebar cages, b) consolidation of concrete in forms, c) concrete beams with carry hooks placed after casting, and d) cylinders cast for testing

3.5.2 Surface Preparation

After 60 days, the beams were moved outside, rotated and reorganized to allow for easy surface roughening. A shotblasting unit was utilized to roughen the concrete surface for bonding. The unit, a Blastrac 1-8DEC230V, fired steel shot of S-280 size at both the sides and the bottom surface of the concrete beams that were to have FRCM applied. The process created a roughened surface equivalent to a concrete surface profile (CSP) of 5-6 on the scale of 10 (ICRI, 2013). Due to the

edges of the cove moulding, small ledges were cast in the concrete on each side of the curved face. Therefore after roughening, a diamond face concrete grinding bit was used with a hand angle grinder to create a roughened but continuous rounded surface removing any potential stress concentrations at the corners. Figure 3.5 shows the effect of the roughening processes and shot used. Specimen were left outside the laboratory after the roughening process before testing.

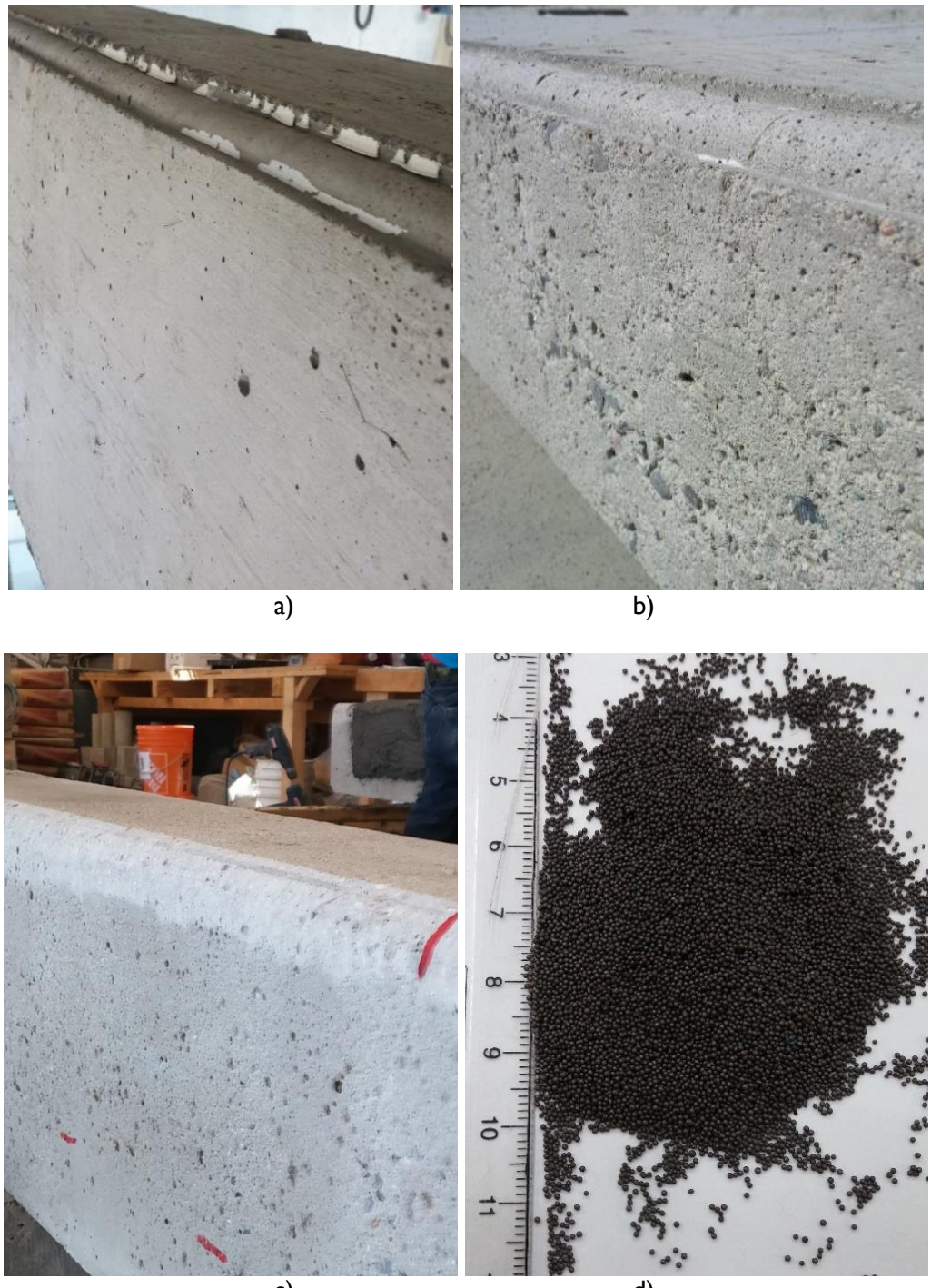

Figure 3.5: Concrete beam a) before shotblasting, b) after shotblasting, and c) during grinding of curved edge, and d) the shot steel used for roughening

3.5.3 FRCM Application

The FRCM was applied by the hand lay-up method with trowels as per the typical procedure followed elsewhere (ACI 549.4R, 2013; Babaeidarabad et al., 2014; D'Ambrisi & Focacci, 2011; Ebead et al., 2015; Jung et al., 2015). Firstly, beams were placed upside down on supports to simplify the application process as shown in Figure 3.6a. Research has shown that there is a region between dry and free moisture that optimizes the bond between cementitious material and concrete substrate (Silfwerbrand, 2009). Therefore, in order to ensure a clean, sound surface for bonding, the beam surfaces were washed and scrubbed with a bristle brush starting 24 hours before mortar application. This removed any dirt, debris or fine silt that had accumulated on the surface. The process also served to moisten the concrete substrate before applying the mortar. Beams were again sprayed with water multiple times before the FRCM application to ensure a damp concrete substrate. Before mixing the mortar, fabric pieces were cut to size depending on the application orientation. Fabric for U-shaped orientation had dimensions of 600 x 3600mm and the soffit fabric was 150 x 3600mm in size. This ensured FRCM stopped before support locations and wrapped up two-thirds of the beam's side in U-shaped orientation. The cementitious mortar matrix was mixed with hand drill mortar mixers in standard 5 gallon plastic buckets with a water dosage of 3.7 L per 24.9 kg bag of mortar. The dosage was increased slightly from the originally recommended value by Simpson Strong Tie (2.7 L) to allow for more workability and better bond. The application procedure followed was: first, a layer of cementitious mortar with thickness of 5 mm was applied to the concrete surface. Next, the fabric was placed over the surface and pressed into the mortar such that mortar extruded through the openings between the rovings (Figure 3.6b). For only one layer another 5 mm layer of mortar was applied over the fabric and trowelled finished. Tape was used to isolate a roving at midspan in the warp direction to allow for strain gauge application after

casting as shown in Figure 3.7a. In the case of multiple layers this process was repeated, with the final layer of mortar being trowelled to a finished surface. Mortar was cured for 4 hours before wet burlap and plastic sheets were placed over the mortar (Figure 3.7b). FRCM was cured for 5 days under wet burlap and plastic sheets before being removed and cured at ambient laboratory conditions for at least 28 days before testing.

a) b)

Figure 3.6: Concrete beams placed upside down for FRCM application showing; a) markings of the extent of mortar application and b) fabric pressed into mortar layer

a) b)

Figure 3.7: Concrete beams showing a) rovings isolated for strain gauges, and b) curing under burlap and plastic sheets in laboratory conditions after mortar application

3.6 Materials

The concrete utilized was intended to have a compressive strength of 30 MPa to replicate that of an existing structure that is in need of repair. A ready mix truck provided the concrete and the mix proportions are listed in Table 3.2 The fresh properties of concrete tested as per CSA A23.2-5C/ASTM C143 and A23.2-4C/ASTM C231 were slump and air content which were 145 mm and 2.7% respectively (ASTM, 2014, 2015d; CSA A23.1/A23.2, 2014).

Table 3.2: Concrete mix values

Material	**Amount**	
Cement	260	kg/m^3
Coarse Aggregate (20mm)	1030	kg/m^3
Fine Aggregate	765	kg/m^3
Water	155	kg/m^3
Fly Ash	60	kg/m^3
Superplasticizer	180	mL/100kg cement

Standard concrete cylinders of dimensions 100 mm in diameter and 200 mm in length were cast, and tested at 7, 28, and 56 days as per CSA A23.2-9C and ASTM C39 (ASTM, 2012; CSA A23.1/A23.2, 2014) with an average compressive strength of 14.5, 21.4 and 22.4 MPa respectively. The flexural strength of the concrete was 2.0 MPa as per CSA A23.2-8C and ASTM C78 (ASTM, 2010; CSA A23.1/A23.2, 2014). The average tensile strength of the concrete was 2.5 MPa in accordance with CSA A23.2-13C and ASTM C496 (ASTM, 2011; CSA A23.1/A23.2, 2014).

All steel used for reinforcement was mild steel with specified yield strength of 400MPa. True yield values supplied by the manufacturer were 450, 440 and 458 MPa for 10M, 15M and 25M bars respectively. Meanwhile, ultimate tensile strength values were 705, 640 and 663 MPa for 10M, 15M and 25M bars respectively.

Six standard 50 mm cubes were cast and tested at 1, 3, 7, 28 and 56 days of curing to determine the cementitious mortar's compressive strength in accordance with CSA A3004-C2 and ASTM C109 and the values were 16.0, 31.5, 40.1, 50.4 and 54.4 MPa respectively (ASTM, 2012; CSA A3000, 2013). Two different sourced fabrics were chosen for strengthening. Both consist of carbon in warp or strong direction. However, where one has carbon in both directions, the other has glass fibres in the weft direction. Therefore, one fabric type has a strong direction while the other is symmetrical and are named uni- and bi-directional accordingly. The details of these two fabrics as provided by the manufacturer are shown in Figure 3.8 and Table 3.3.

Figure 3.8: Geometry of fabrics used: a) uni-directional carbon, b) bi-directional carbon

Table 3.3: Fabric properties

	Uni-directional Carbon	**Bi-directional Carbon**
Warp Spacing	15mm	20mm
Weft Spacing	30mm	20mm
Equivalent Dry Fabric Thickness	0.157mm	0.044mm
Density	280 g/m^2	80 g/m^2
Ultimate Tensile Strength	450 kN/m	138 kN/m
Axial Stiffness by width unit	30,000 kN/m	9200 kN/m
Area by width unit	162 mm^2/m	46 mm^2/m

3.7 Test Setup and Instrumentation

RC beams were tested in four-point bending using the constructed steel frame. Two point loads (P), 1250 mm apart, were applied to the top of the RC beams using a spreader bar attached to a 250 kN actuator (MTS model 244.31). This load, P (Figure 3.9a), is the reported value in the results section and used to define load carrying capacity. The span length was taken as 3800 mm and steel pedestals were used to support beams at this distance. Figure 3.9 schematically illustrates the beam layout for testing. MTS software was used to write a program that ramped the actuator to failure with the ability to pause testing to record crack patterns and dimensions. LabView software was used with a National Instrument (NI) cDAQ-9178 DAQ system to record and tabulate data from the load cell, strain gauges, and linear variable displacement transducer (LVDT). A NI-9215 and 9237 module were used in the system for acquiring data while a NI-6008 module was utilized to sync the MTS and DAQ with a trigger system. Data recorded included actuator load, actuator displacement, strain and midspan deflection. The test was carried out under displacement control at a constant rate of 2 mm/min and data was recorded at a frequency of 10 Hz.

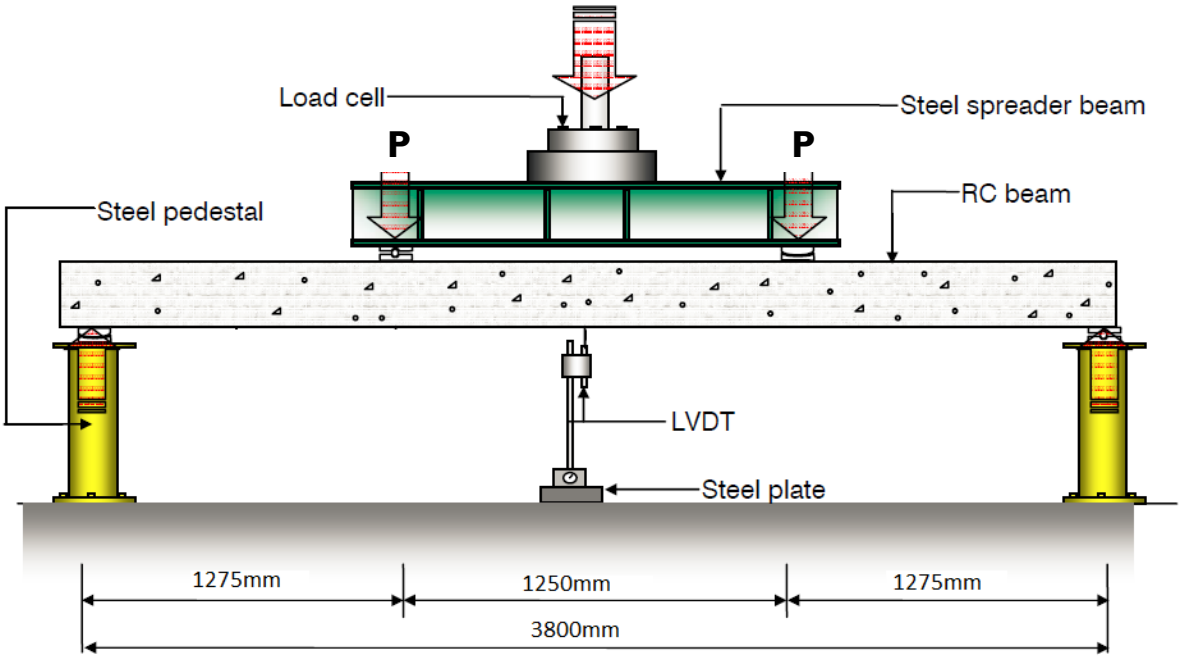

a)

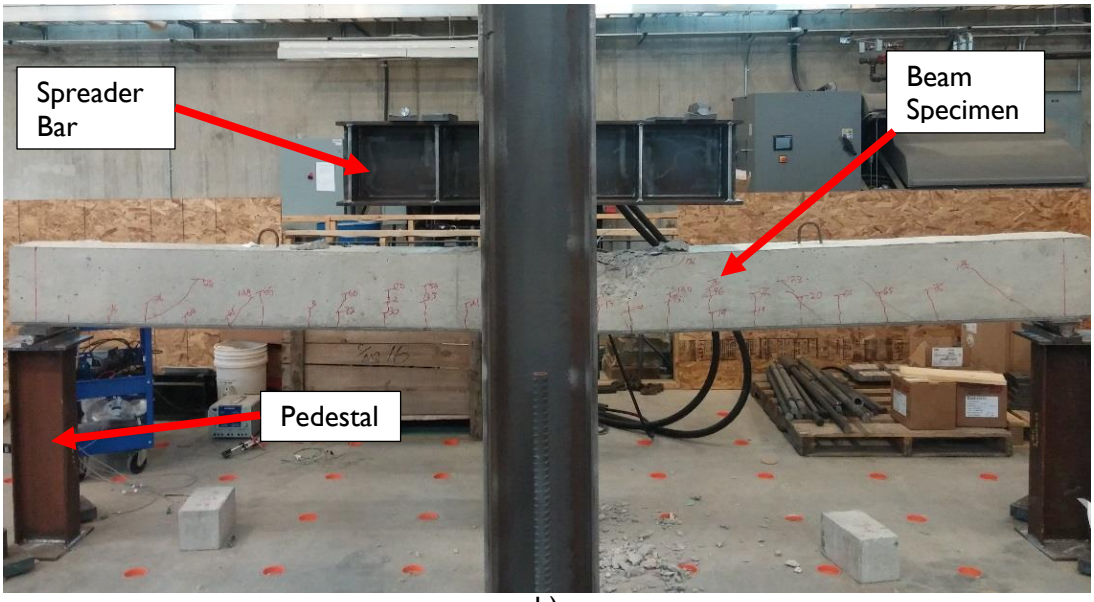

b)

Figure 3.9: Four point bending test set up a) schematically, b) experimentally

Strain gauges were applied in numerous locations in order to monitor beam performance. The surface, depending on either concrete, steel or fabric, was prepared properly for best results as per Micro-Measurements recommendations (Micro-Measurements, 2014, 2015). This usually included sanding to smooth the surface and then cleaning with acetone to provide a uniform surface for application. In the case of the concrete and the fabric surfaces, due to their permeability, a layer of epoxy was applied to seal the surface. A KYOWA strain gauge (type KC-70-120-A1-11) with 70 mm length was applied at midspan to the compression concrete surface (Figure 3.10). Meanwhile, a 5 mm KYOWA strain gauge (type KFG-5-120-C1-11) was applied to the longitudinal rebar at midspan and under one load point (Figure 3.10). For FRCM strengthened beams, the same 5 mm gauge type was applied to the exposed fabric roving at midspan that was left during FRCM application (Figure 3.10). For gauges applied on all three surfaces, a coating of wax was applied to the strain gauge and connecting terminal to seal and protect the gauges from either the concrete or exposed conditions such as dust.

Figure 3.10: Strain gauges applied on a) steel rebar, b) concrete compression surface, and c) exposed fabric roving

CHAPTER 4: EXPERIMENTAL RESULTS AND DISCUSSION

4.1 General

The test matrix presented in the previous chapter (Table 3.1) was set out to experimentally determine the flexural performance and improvement of fabric-reinforced cementitious mortar (FRCM) reinforced concrete (RC) beams. Beams with dimensions of 200 x 300 x 4000 mm were tested in four-point bending at UBC Okanagan's Structures Lab. The tested parameters were the steel reinforcement ratio (0.8% or 2.0%), the fabric used (uni-directional carbon or bi-directional carbon), application orientation (soffit only or U-wrapped) and number of layers (1 or 3). The performance indicators include failure mode, beam stiffness, yielding, ultimate flexural strength, and ductility.

Yielding of tension reinforcement was taken when strain gauges read true yield strain values or 2200 and 2290 microstrain for 15M and 25M bars, respectively. Beam yield was defined when the stiffness of the beam changed on the load-deflection diagram. Beam failure was defined as the ultimate load capacity before a load drop of 20% which was usually associated with concrete crushing and fabric rupture. All tests were carried out beyond this failure to gain data about the post failure response. After full completion of a test, the beam was removed from the test set up and inspected. This allowed for verification of failure and potential FRCM debonding. A hammer was tapped along the length of the beam to qualitatively detect any areas of mortar separating from the concrete face. In the area of a major flexural crack, a hammer was used to remove and break away some mortar exposing the fabric. This allowed for inspection of fabric for rupture.

Concrete required for this study was designed and planned to be of strength of 30 MPa and reinforcement ratios were selected based on this value. However, the delivered concrete from a local ready mix plant had an actual 28 days compressive strength of 21.4 MPa. This had a significant impact on the true balanced reinforcement ratios for the two group of beams. The balanced reinforcement ratio, ρ_b, was calculated to be 3.43% based on 30 MPa compressive strength and 400 MPa steel yield strength. At this value, the beams' reinforcement ratio would have been 23% and 58% of ρ_b for 15M and 25M, respectively. However, when accounting for the lower than intended strength concrete and the actual yield strength values of the steel, the beams' balanced reinforcement ratio dropped to 2.24% and 2.12% for 15M and 25M reinforced beams, respectively. This resulted in actual reinforcement ratios that were 36% and 94% of that of the balanced. The intention was to have one of the reinforcement ratios close to the balanced ratio to determine if adding FRCM would change the failure mode. However, for Group R20 beams the reinforcement ratio (94% of ρ_b) was much closer than intended. In the following discussions, the beams were often split between the two reinforcement ratios as their flexure response differs. However, some common trends between the different ratios were noted.

Strain gauges were applied on each upgraded beam in four locations: 1) steel rebar at midspan, 2) steel rebar under point load, 3) concrete compression face at midspan, and 4) exposed fabric roving at midspan. The two steel gauges were used to track any irregularity in strain readings in the beam and verify a beam yielding response. Of all ten beams, half of the beams had the midspan gauge reach the yield value first and half had the support gauge reach the yield first. At yield values the average difference between the two strain gauges of all 10 beams was only 7% or 158 microstrain. Therefore, midspan steel strain was used in all cases to define when steel bars had yielded. Data after yield from the steel strain gauges became unusable. The strain gauges placed

on the compression concrete surface of each beam were to monitor concrete strain up to crushing. All concrete strain gauges performed well up until concrete crushing. In most cases the portion of concrete that the gauge was applied to detached after crushing, and therefore, the gauge was rendered useless. Finally, a gauge was placed on the fabric via an exposed roving during mortar casting. This was used to monitor the strain and detect the failure (rupture or slippage). All gauges functioned properly past at least steel yielding. Of all 8 upgraded beams, only 2 (Uni_U_L1_R8 and Uni_U_L1_R20) had cracks run through the strain gauge location, thus losing strain readings but showing there was no noticeable impact of leaving the roving exposed. Beam Bi_U_L1_R8 had the strain gauge stop reading properly immediately after the beam yielded. Strain plots with each of concrete, steel and fabric for each individual beam can be found in Appendix F.

4.2 Beam Behaviour and Failure Modes

4.2.1 Cracking

The beam behaviour and failure mode are two of the most important comparison factors as they govern the ultimate strength and ductility for a RC beam. Expected cracking load based on the modulus of rupture for both control specimens was 6.5 kN. Beams were moved to facilitate surface roughening and fabric application and the handling led to cracking before experimental testing. Therefore, most beams did not show typical pre-cracking stiffness associated with RC beams. As the load was applied on the beam, flexural cracks began to open on the tension side throughout the constant moment region. After these initial cracks and with further loading, some cracks would open outside of the point loads. The crack distribution can be classified based on the amount of mortar and the fabric applied as well as the reinforcement ratio.

Both controls and FRCM soffit beams (Beams CON_R8, CON_R20, Uni_S_L1_R8, and Uni_S_L1_R20), showed surface cracking around the expected cracking load of 6.5 kN. All four beams with one U-layer of FRCM reinforcement (Beams Uni_U_L1_R8, Bi_U_L1_R8, Bi_U_L1_R20 and Uni_U_L1_R20) typically showed less cracking and most notably at a much later load value. The first crack noted for these beams was on average at 14.2 kN (118% increase compared to the control) and cracks showing through the mortar seemed to be less evident than that of the controls and FRCM soffit only beams. Finally, the two beams strengthened with 3 layers of fabric and, therefore, approximately 20 mm of mortar showed limited cracking. Based on general observations, cracks were marked at a higher load and fewer cracks appeared. In fact, Beam Uni_U_L3_R20 did not have noted cracks appear through the mortar surface before the concrete crushed in compression. Figure 4.1 presents crack patterns at failure of all tested beams. When comparing the two reinforcement ratios, Group R8 beams had cracks that propagated further up the beam compared to that of the Group R20 specimens. This is due to the lower reinforcement ratio and, therefore, having a smaller compression block. Further evidence of the larger compression block with Group R20 specimens was apparent when looking at the area of concrete crushing. Group R20 had a substantially larger area of crushed concrete compared to Group R8, evident by the exposure of internal reinforcement.

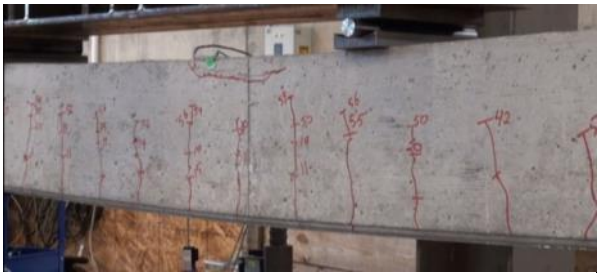

a) CON_R8

b) CON _R20

c) Bi_U_L1_R8

d) Bi_U_L1 _R20

e) Uni_S_L1_R8

f) Uni_S_L1_R20

g) Uni_U_L1_R8

h) Uni_U_L1_R20

i) Uni_U_L3_R8

j) Uni_U_L3_R20

Figure 4.1: Crack patterns at failure for all tested beams (loads shown are the actuator load, or 2P)

4.2.2 Failure Mode

All beams in Group R8 failed in a ductile manner with steel yielding first before concrete crushing in compression (Table 4.1). The control specimen (CON_R8) failed by steel yielding followed by concrete crushing as in a typical tension-controlled failure. This is evident by the load deflection response and the post-yielding ductility. The steel reinforcement ratio was 0.8% as compared to the balanced ratio (ρ_b) of 2.24%, corresponding to 36% of ρ_b. Fabric upgraded specimens all failed in the same manner of steel yielding followed by concrete crushing which was upon further loading followed by fabric rupture. Rupturing was associated with an increase in deformation and flexural cracks widening further. There was no evidence of debonding or fabric slippage in any tested beam. This is opposite to the trend reported in the technical literature (Babaeidarabad et al., 2014; D'Ambrisi & Focacci, 2011; Ebead & Saeed, 2014; Ombres, 2011). Figure 4.2 shows the dry fibres frayed, and therefore ruptured, after being removed from the test set up. The three beams in Group R8 with the larger fabric areas (Beams Uni_S_L1_R8, Uni_U_L1_R8 and Uni_U_L3_R8) all had textile rupture in a somewhat sudden manner. A crack opened quickly causing a jolt and small, instantaneous jump in midspan deflection. This corresponded with a large load carrying capacity drop. Except for Beam Uni_U_L1_R8 (which had gauge failure), the strain gauge on the fabric confirmed this with a large drop in strain reading (Figure 4.3). As evident from the gauge reading, one beam (Beam Uni_S_L1_R8) had the fabric ruptured simultaneously with the concrete crushed. Meanwhile, Beam Uni_U_L3_R8, had the ruptured shortly after the concrete crushed. Beam Bi_U_L1_R8 had the fabric ruptured in a more gradual manner as flexural cracks opened further with larger deflections.

a) Bi_U_L1_R8

b) Uni_S_L1_R8

c) Uni_U_L1_R8

d) Uni_U_L3_R8

Figure 4.2: Tension surface of R8 group after test end and with some mortar removed to show rupture of the fabric

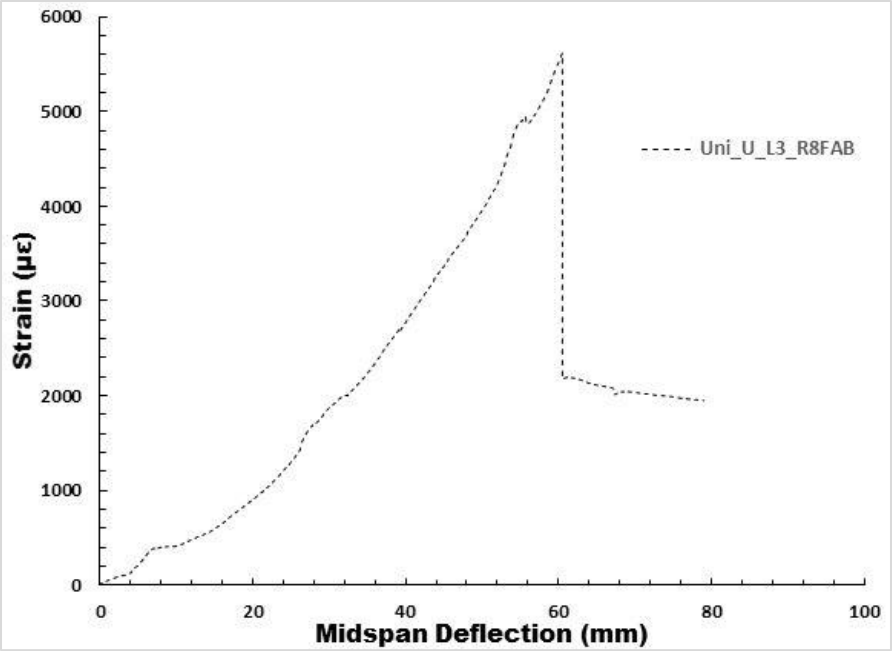

Figure 4.3: Fabric strain versus midspan deflection for Beam Uni_U_L3_R8

In comparison, Group R20 specimens were much closer to the balanced reinforcement ratio (94% of ρ_b) due to the concrete being delivered under strength. All specimens in this category failed in a near balanced failure. Strain gauges read that steel had yielded, and beams just began to display non-linear behaviour when the concrete crushed. Similar to Group R8, all upgraded specimens were then followed by fabric rupture associated with flexural crack opening. Figure 4.4 shows the fabric rupture region after test end and with some mortar removed. An interesting point to note based on response and strain gauge readings, is that with the addition of a large amount of fabric (three layers) the failure did not seem to change to that of fully over-reinforced. In contrast to Group R8, three beams (Beams Bi_U_L1_R20, Uni_S_L1_R20, and Uni_U_L1_R20) had fabric rupture gradually as deflection increased post-concrete crushing. This was evident by inspection of the fibres, and the fact that no sudden strain drop was noted. One beam, with the largest fabric area (Beam Uni_U_L3_R20), was the exception to this in the R20 group. After

concrete had crushed and load capacity was steadily decreasing with further deflection, fabric ruptured suddenly causing large flexural cracks to open and a large load drop in capacity. This sudden rupture was confirmed by a large strain drop in the fabric strain gauge on the outermost layer of the fabric (Figure 4.5).

a) Bi_U_L1_R20

b) Uni_S_L1_R20

c) Uni_U_L1_R20

d) Uni_U_L3_R20

Figure 4.4: Tension surface of R20 group after test end and with some mortar removed to show rupture of fabric

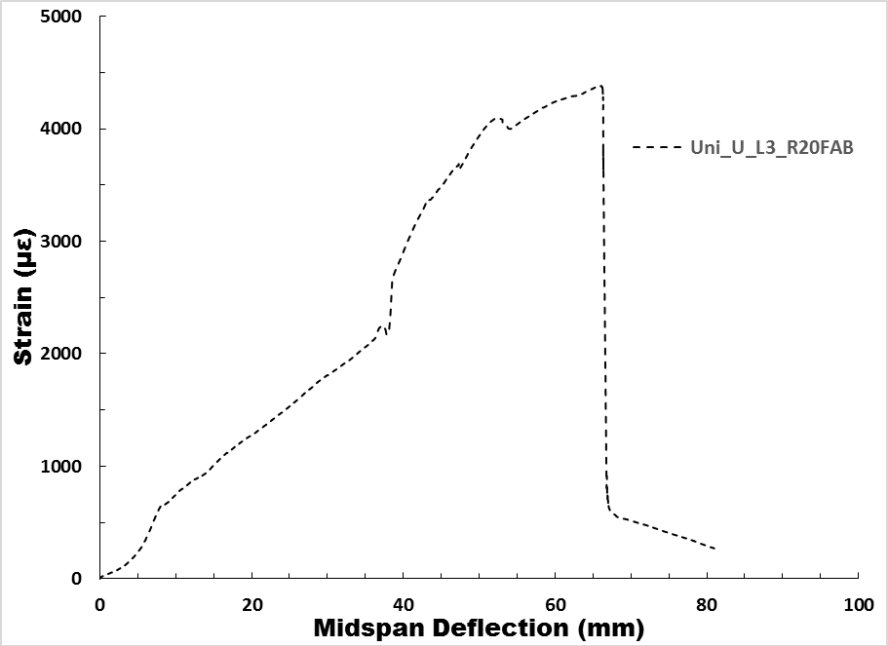

Figure 4.5: Fabric strain versus midspan deflection for Beam Uni_U_L3_R20

4.2.3 Concrete Strain

Concrete strain gauges in all beams were able to successfully record at failure when concrete crushed. Table 4.1 presents the maximum strain value reached in the concrete. When comparing values to their relative control, beams upgraded with FRCM tended to have an increased maximum strain reached in the concrete (Table 4.1) except for Beam Bi_U_L1_R8. The other 7 had a substantial gain averaging an increase of 26.3%. This is contrary to the findings of one recent article where the control beams had the largest strains reached before crushing (Ebead et al., 2015). The increase was expected since the beams reached a higher load carrying capacity due to the addition of high strength tensile fabric compared to the control specimens. This leads to higher forces and higher strains in the concrete in the upgraded specimens than the control specimens. Figure 4.6 and Figure 4.7 present the concrete strain curves for Groups R8 and R20, respectively.

Table 4.1: Failure mode and concrete strain

Specimen ID	First Cracking Load (kN)	Maximum Compressive Strain (με)	Percent Change vs Control	Failure Mode*
CON_R8	5.5	1810	-	BY, then CC
Bi_U_L1_R8	16	1556	-14.1%	BY, CC, then GR
Uni_S_L1_R8	8.5	1944	7.4%	BY, CC with SR
Uni_U_L1_R8	18	2816	55.6%	BY, CC, then SR
Uni_U_L3_R8	41	2534	40.0%	BY, CC, then SR
CON_R20	6.5	1934	-	BY with CC
Bi_U_L1_R20	22.5	2310	19.4%	BY with CC, then GR
Uni_S_L1_R20	17.5	2248	16.2%	BY with CC, then GR
Uni_U_L1_R20	22.5	2018	4.3%	BY with CC, then GR
Uni_U_L3_R20	80	2727	41.0%	BY with CC, then SR

*BY – Beam yield, CC – concrete crushing, SR – sudden fabric rupture, and GR – gradual fabric rupture

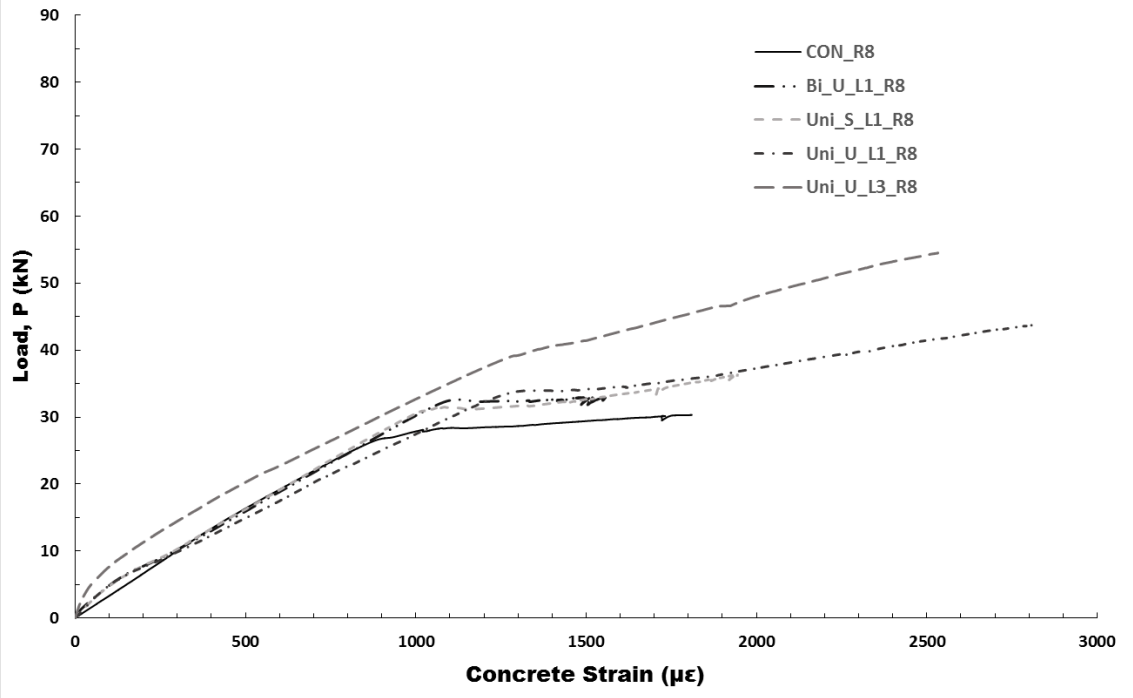

Figure 4.6: Load versus concrete strain curve for Group R8 specimens

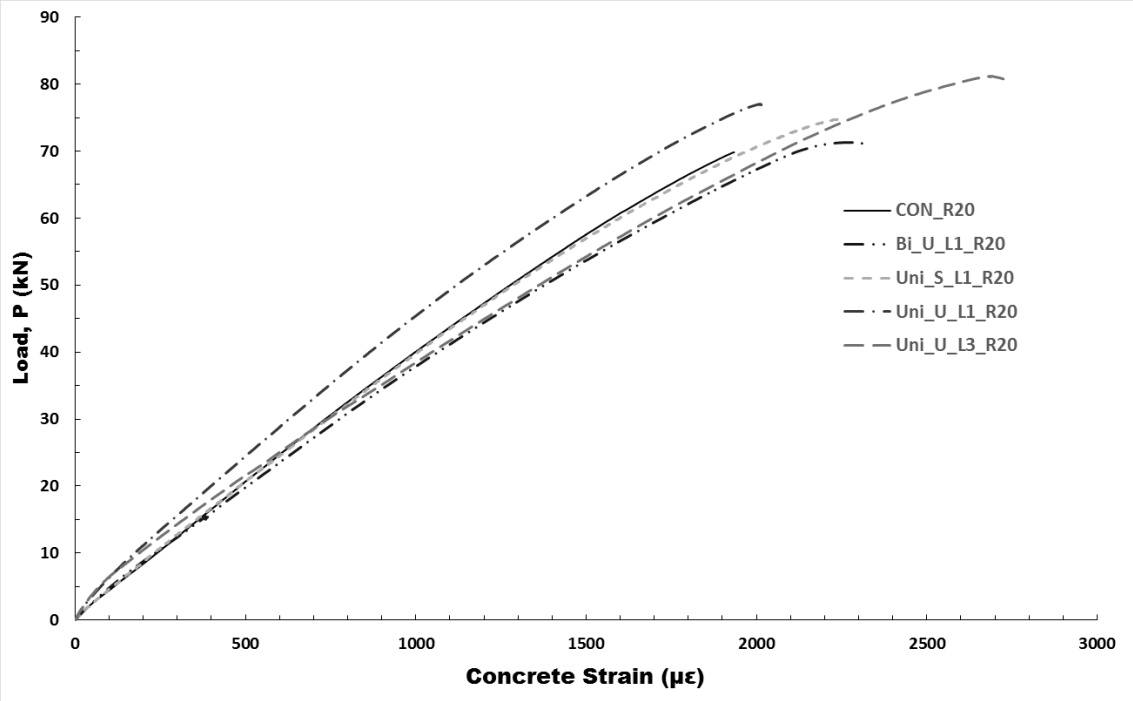

Figure 4.7: Load versus concrete strain curve for Group R20 specimens

4.3 Load-Deflection Response

The R8 control beam (Beam CON_R8) performed in a typical ductile manner when analyzing the load deflection curve. Once steel yielded, the beam maintained its load carrying capacity while continued deformation occurred, illustrated by the load plateau or plastic response (Figure 4.8). This carried on until concrete began to crush which was defined as the beam failure. Testing was taken farther to determine the post-failure response. The beam maintained a slightly lower load carrying capacity until further area of concrete crushed away causing further load drop. Three specimens with FRCM applied had very similar response to one another, namely Beams Uni_S_L1_R8, Uni_U_L1_R8 and Uni_U_L3_R8. Each of these beams had similar pre-yielding stiffness as shown in the load-deflection response in Figure 4.8. The post-yielding response was characterized by another region of linear increase in capacity. This region's stiffness is a function

of the area of the textile applied with the three layer specimen (Uni_U_L3_R8) having the largest stiffness and the largest flexural capacity. Concrete crushing followed by textile rupture led to a large drop in the load carrying capacity, which is evident from the sudden drop in Figure 4.8. These three specimens then mimicked the capacity and response of the control specimen after failure. The one bi-directional upgraded specimen (Beam Bi_U_L1_R8) had a slightly different response. After yielding the load carrying capacity plateaued as compared to a third linearly increasing phase with the other three beams. This is attributed to the small area of textile not having substantial enough stiffness to increase the capacity further. As shown in Figure 4.8, the FRCM did increase the load of this beam at which the capacity plateaued. Appendix E has the load-deflection curves for separate beams.

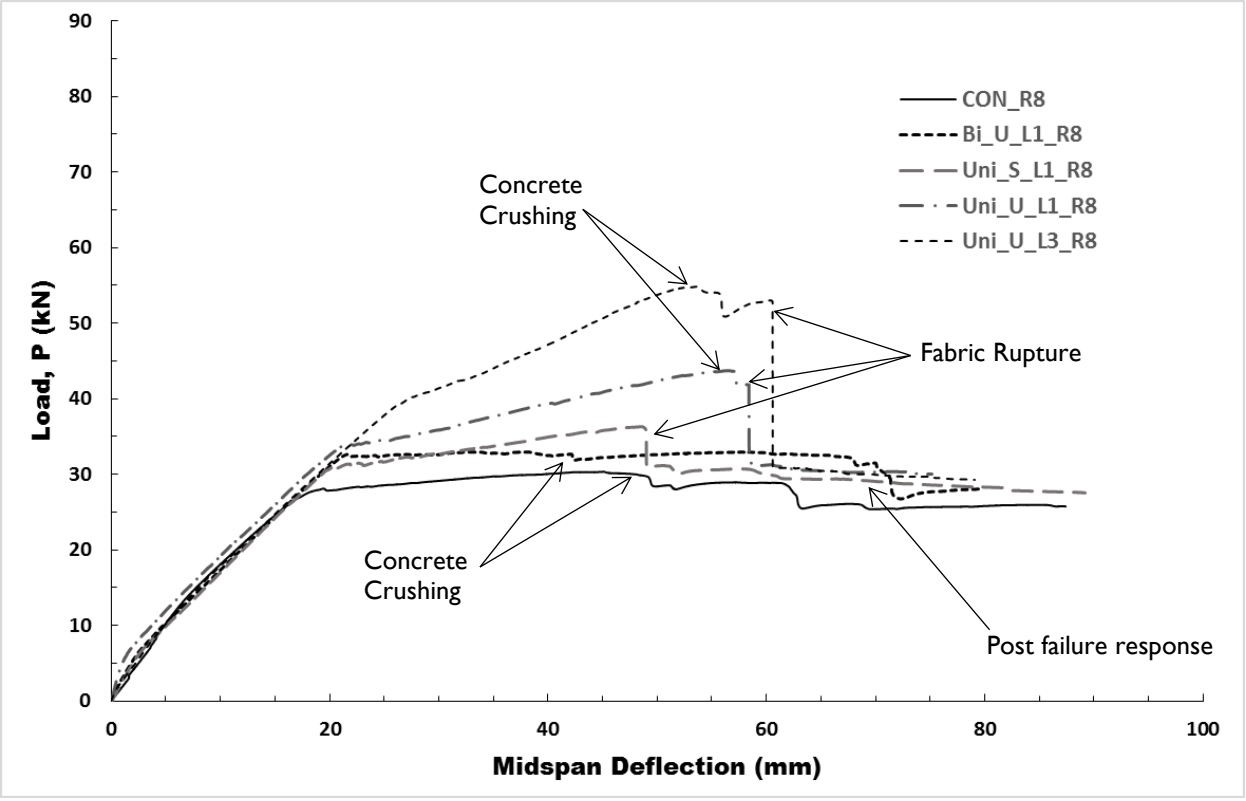

Figure 4.8: Load versus deflection response of Group R8

Group R20 specimens all had a very similar load-deflection response up to and after failure. The control beam performed as expected for a beam with a reinforcement ratio so close to that of the balanced reinforcement ratio (94% of ρ_b). Strain gauges on the rebar reinforcement indicated that steel had surpassed the true yield value; however, the load-deflection response did not quite reach a ductile performance before concrete crushed causing a load drop. The design compressive concrete strength of 30 MPa would have led to a much larger margin in reinforcement ratio, thus, a more ductile behaviour. The control beam (CON_R20) increased in load carrying capacity until concrete crushed causing a sudden drop in strength (Figure 4.9). No ductile response, or load plateau formed like Beam CON_R8. All FRCM upgraded specimens had very similar responses to that of the control, but with an increased peak load reached. Unlike Group R8, the concrete crushed before the load-deflection response changed to a post-yield response. Once concrete crushed, a large area of concrete was rendered unused and the load carrying capacity of all beams dropped suddenly followed by a somewhat linear decreasing capacity. This is an unfavourable, brittle response due to the near balanced performance of all beams. As tests were carried on past the defined failure, further concrete crushing in the compression zone occurred and the textile fibres ruptured gradually with flexural cracks widening further. Analyzing beam Uni_U_L3_R20's response in Figure 4.9, a few anomalies to this post-failure response can be noted. After concrete crushing, there was a region of maintained load carrying capacity before further concrete crushing that caused further gradual load drop. Also, for this beam a large, sudden load drop was noted which was associated with a sudden fibre rupture. Appendix E has the load-deflection curves for separate beams.

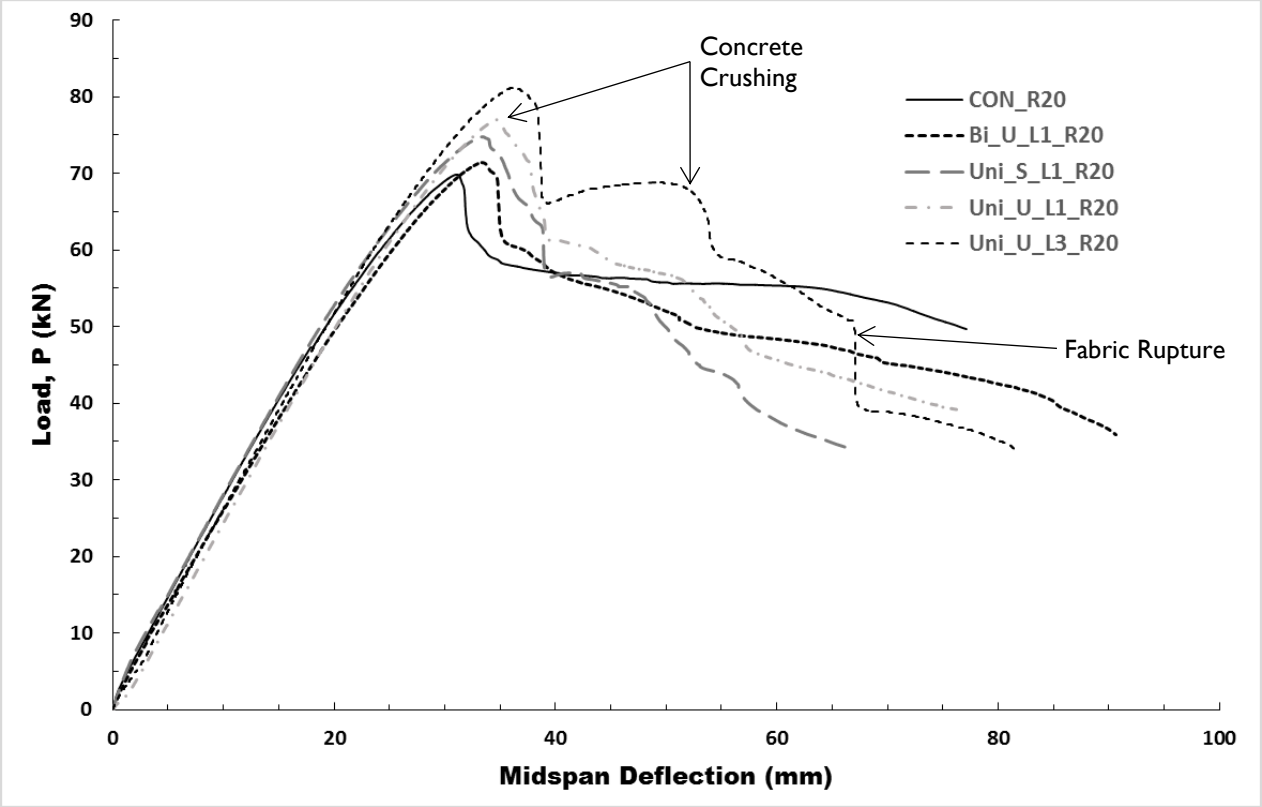

Figure 4.9: Load versus deflection response of the Group R20

4.4 Stiffness Response

Analyzing the slope of the load deflection curve in the region between cracking and yielding can determine the pre-yielding stiffness of a beam. To quantify this, the stiffness during the pre-yielding phase was calculated for each beam for comparison. From the load-deflection data, seven sets of data points over the span of pre-yielding region were taken and used to calculate stiffness. These seven stiffness values were then averaged to determine a single stiffness value. The pre-yielding region is bound by concrete cracking before and steel yielding after. To ensure that non-linearity near the transition zone was not considered, points within a minimum of 15% of cracking and yielding were not included in the calculation. The bar chart in Figure 4.10 shows this stiffness relative to each of the control beams (Beams CON_R8 and CON_R20). Analyzing the figure, the

stiffness ranged between 6 percent below and 3 percent above the control beams' values. Therefore, it can be concluded that the addition of FRCM does not impact a beam's pre-yielding stiffness. When visually analyzing the slope of the load-deflection curves, this conclusion is evident for both Groups (Figure 4.8 and Figure 4.9). This was confirmed by the response of the fabric strain gauges prior to yielding. Four beams were reading a strain slightly higher than that in the rebar, while another four had a lower strain value. The beam strain plots are shown in Appendix F. Adding FRCM to the tension face is expected, as is the case for FRP, to increase the pre-yielding stiffness of the beam response compared to that of the respective control beam (Attari et al., 2012). However, analyzing the load-deflection curves from the reported literature on FRCM strengthened beams, typically the pre-yielding stiffness does not change like that of FRP, something that most literature does not comment on (Babaeidarabad et al., 2014; D'Ambrisi & Focacci, 2011; Ebead et al., 2015; Elsanadedy et al., 2013; Gil et al., 2014; Loreto et al., 2013; Ombres, 2011). The result of this test matrix on pre-yielding stiffness agrees with this outcome. This can be explained by the fact that small fabric area, and more importantly small axial stiffness, was used compared to that of the steel reinforcement. The axial stiffness values are calculated as the area multiplied by the modulus of elasticity and are given in Table 4.2. Inspection yields that the fabric axial stiffness is a small fraction of that of the steel reinforcement. Therefore, the FRCM's contribution is minimal and does not result in a stiffness increase. Only in one case (Beam Uni_U_L3_R8) which was strengthened with three layers, is the value somewhat considerable at 28.1%. However, as evident in the flexural capacity, the addition of each subsequent layer does not yield equal efficiency. Therefore, the highest value of 28.1% is an inflated value compared to the true effective axial stiffness. Another reason for the stiffness not increasing is the mortar of FRCM cracks whereas the epoxy matrix in FRP does not.

Table 4.2: Comparison of axial stiffness values

Specimen ID	Steel Axial Stiffness (kN)	Fabric Axial Stiffness (kN)	Percentage of Steel Stiffness
Bi_U_L1_R8	80,000	2,300	2.9%
Uni_S_L1_R8	80,000	4,500	5.6%
Uni_U_L1_R8	80,000	7,500	9.4%
Uni_U_L3_R8	80,000	22,500	28.1%
Bi_U_L1_R20	200,000	2,300	1.2%
Uni_S_L1_R20	200,000	4,500	2.3%
Uni_U_L1_R20	200,000	7,500	3.8%
Uni_U_L3_R20	200,000	22,500	11.3%

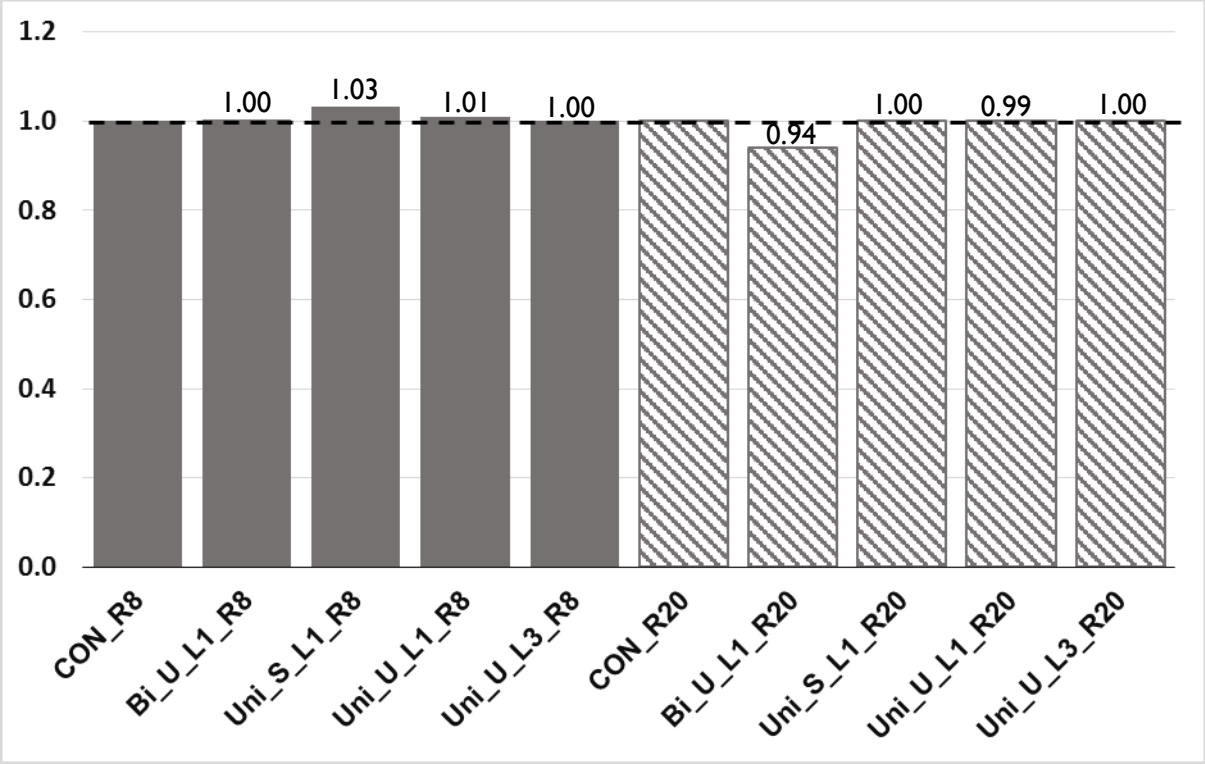

Figure 4.10: Bar chart of relative beam stiffness to control value of the pre-yielding phase

Another region of the load deflection curve where beam stiffness can be analyzed is in the post-yielding region for strengthened beams. In this region three beams in Group R8 showed linear strength gain up to concrete crushing, namely Beams Uni_S_L1, Uni_U_L1 and Uni_U_L3. Analyzing the load deflection curves of these beams, it is evident that the post-yielding stiffness increased in each of these specimens (Figure 4.8). Stiffness in this region was calculated from the load-deflection data in the same manner discussed for the pre-yielding stiffness. Having the lowest stiffness was Beam Uni_S_L1 which was used as the benchmark to compare the other two beams against. The stiffness of Beam Uni_U_L1 was approximately 1.5 times that of its soffit counterpart. Meanwhile, the three-layer specimen (Beam Uni_U_L3) had its stiffness value triple compared to that of the soffit only beam (Beam Uni_S_L1) and 2.0 times that of the one-layer specimen (Beam Uni_U_L1). This trend is related to the increase in the area of the fabric in tension of each respective beam; with an increase in area comes an increase in post-yielding stiffness. This is a trend that is supported in the literature for FRCM and FRP strengthened beams (Attari et al., 2012; Babaeidarabad et al., 2014; D'Ambrisi & Focacci, 2011; Ebead et al., 2015; Elsanadedy et al., 2013; Loreto et al., 2013).

4.5 Yield Load and the Corresponding Deflection

4.5.1 Steel Yielding from Strain Gauge

Strain gauges were placed on the rebar to determine when the steel yielded. Table 4.3 shows the load and deflection values when the strain gauge reached the yield value for the respective steel (15M or 25M). As outlined previously, the stiffness of the beam up to yield was not impacted by the addition of the FRCM. This is verified by the result of these strain gauge readings. Inspecting the yield point (load and deflection) of the upgraded beams compared to the controls, it is apparent

that the FRCM did not have an effect on when gauges indicated yield. One beam (Uni_U_L3_R8), however, had a significant increase in the point of steel yielding (32% for load, 33.7% for deflection).

Table 4.3: Comparison of yield value in strain gauge placed at midspan

Specimen ID	Steel Strain (με)	Load, P (kN)	Percent difference	Midspan Deflection (mm)	Percent difference
CON_R8	2200.9	27.4	- -	17.8	- -
Bi_U_L1_R8	2200.8	27.4	0%	17.1	-4.0%
Uni_S_L1_R8	2200.0	26.8	-2.2%	16.9	-5.1%
Uni_U_L1_R8	2200.6	26.1	-4.8%	15.1	-11.8%
Uni_U_L3_R8	2200.5	36.2	32%	23.8	33.7%
CON_R20	2290.1	63.9	- -	26.4	- -
Bi_U_L1_R20	2290.1	63.4	-0.8%	27.1	2.6%
Uni_S_L1_R20	2290.5	59.0	-7.7%	23.0	-12.9%
Uni_U_L1_R20	2290.4	65.6	2.6%	27.2	3.0%
Uni_U_L3_R20	2290.1	64.5	1.0%	25.6	-3.1%

4.5.2 Beam Yielding

Steel yielding is associated with the transition to the ductile portion of RC beam response. In the case of the control beams, this corresponds to load plateauing, while for FRCM upgraded specimens it corresponds to the transition to a region of continued load carrying capacity but at a lower rate. This point can be defined as the beam yielding and can be determined from the load-deflection curve. This was verified by the fact that strain gauges were reading past yielding values when the beam's response showed yielding. Therefore, based on this definition Group R20 specimens did not have a defined yield value and no associated ductility. This is apparent from the load-deflection response shown in Figure 4.9. When analyzing the yield response for R8 group

specimens, the control specimen yielded at a load value of 28.1 kN and midspan deflection of 19.6 mm as shown in Table 4.4. All upgraded specimens had yield occur at a higher load value and a larger midspan deflection compared to that of the control specimen, indicating an increased beam yielding. This test matrix had Group R8 upgraded beams yield at an average 22% higher load and a 14% higher deflection compare to the control. Figure 4.11 presents the relative increase of yield load and yield deflection for each beam in Group R8 with the control beam as the reference. This is a conclusion that is observed in the literature on load-deflection diagrams (Babaeidarabad et al., 2014; Gil et al., 2014; Loreto et al., 2013; Ombres, 2011). As mentioned earlier, FRCM did not contribute when the steel was in the linear-elastic region. This is due to the axial stiffness of the steel being much higher than that of the FRCM added. However, once the steel bars yielded, the FRCM started engaging in resisting the load applied. Thus, compared to the control beam, the FRCM strengthened beams was able to resist a higher load before its response deviated from linearity. Therefore, it is evident that the fabric was able to delay beam yielding and then dictate the post-yielding linear strength gain.

Table 4.4: Strength and ductility results

Specimen ID	Yield Load, P (kN)	Deflection at Yield, δ_y (mm)	Ultimate Load, P (kN)	Deflection at Ultimate, δ_u (mm)	Strength Gain (%)	Pseudo-ductility, δ_u/δ_y	Relative to Control (%)
CON_R8	28.1	19.6	30.3	45	- -	2.30	--
Bi_U_L1_R8	32.6	21.5	32.9	38.1	8.6%	1.78	77%
Uni_S_L1_R8	30.9	20.1	36.3	48.5	19.8%	2.41	105%
Uni_U_L1_R8	33.9	21.3	43.7	57.1	44.2%	2.68	117%
Uni_U_L3_R8	39.2	26.4	54.8	53.8	80.9%	2.04	89%
CON_R20			69.8	31.1	- -		
Bi_U_L1_R20			71.3	33.3	2.1%		
Uni_S_L1_R20			74.7	33.4	7.0%		
Uni_U_L1_R20			77	34.7	10.3%		
Uni_U_L3_R20			81.2	36.3	16.3%		

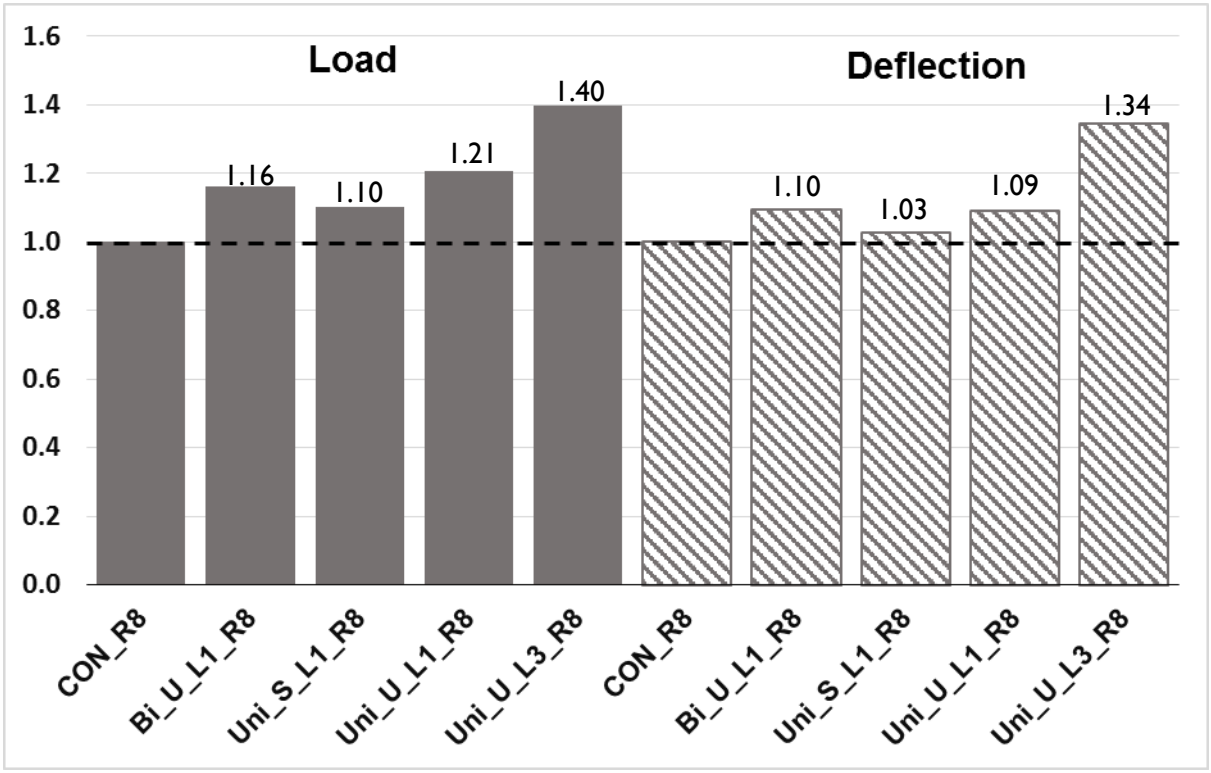

Figure 4.11: Relative increase of yield load and yield deflection for Group R8

4.6 Flexural Capacity

The flexural strength of a beam is one of the most important design values and comparison points. The control specimens (Beams CON_R8 and CON_R20) failed at an ultimate load of 30.3 kN and 69.8 kN respectively. All FRCM upgraded specimen showed some increase in flexural capacity over these benchmarks (Table 4.4). Group R8 specimens saw load increases to 32.9, 36.3, 43.7 and 54.8 kN, while R20 specimen increased to 71.3, 74.7, 77 and 81.2 kN for Beams Bi_U_L1, Uni_S_L1, Uni_U_L1 and Uni_U_L3 respectively. This translates to improvement up to 80.9% for Group R8 and a maximum gain of 16.3% for Group R20 (Figure 4.12). This aligns with the upper bound for strength improvements in flexural reported in the literature which ranges from 44% to 120% (Aljazaeri & Myers, 2015; Babaeidarabad et al., 2014; Carozzi et al., 2016; D'Ambrisi & Focacci, 2011; Ebead et al., 2015; Jung et al., 2015; Ombres, 2011; Si Larbi et al., 2013; Yin et al., 2014). The flexural strength gain is due to the addition of strong fibres on the tension region of the beam. In the control beam, the steel rebar yields giving a load carrying plateau. However, in the case of strengthened beams, after steel yields the linear elastic FRCM picked up the load until the concrete failed in compression. As discussed earlier, the stiffness of this region increased with addition of the fabric and, therefore, the strength gain increased as well. Group R8 had larger strength gains than compared to its Group R20 counterpart. This is attributed to the lower reinforcement ratio, and therefore, a smaller concrete area in compression before adding FRCM. A smaller initial compression area allows more concrete area to be stressed before concrete crushing, and therefore, larger flexural improvements. Comparing deflection values (Table 4.4), Group R8 upgraded specimens tended to reach ultimate at a later deflection value compared to that of the control. Group R20 FRCM specimens' ultimate deflections also increased, however, by a much smaller margin.

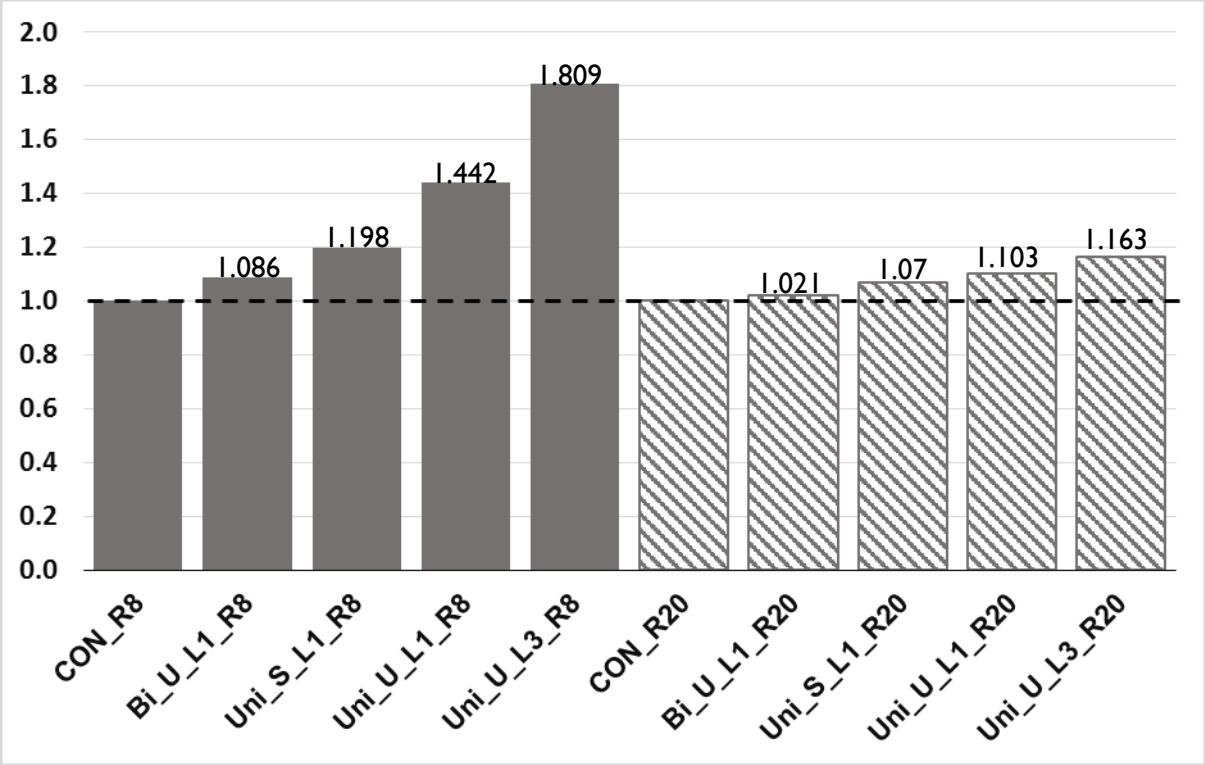

Figure 4.12: Flexural strength improvement over the control beams

4.7 Ductility Analysis

Ductility is a very important property of RC beams and one that can be compared based on this experimental test set up especially. One half of the beams, Group R20, failed in a near balanced failure which inherently does not show much ductility. Although strain gauges read that yielding of the steel rebar did occur, there was no beam yield defined and, therefore, this group will not be included in this discussion. As for Group R8 specimens with a defined yield location, some ductility comparisons can be made. Although the beam yield was delayed, a term pseudo-ducility, sometimes ductility index or displacement ductility, is often defined to compare beams as the ratio of the ultimate deflection to the yield deflection (Aljazaeri & Myers, 2015; Babaeidarabad et al., 2014; Ebead & Saeed, 2014; Ombres, 2011). This value is important because, as Babaeidarabad et al. states, the higher the pseudo-ductility the better a beam can redistribute moment, and have

larger global deformation and energy dissipation (Babaeidarabad et al., 2014). Comparing this value for the R8 specimens versus the control, two specimens showed an increase in pseudo-ductility (Beams Uni_S_L1 and Uni_U_L1) while two specimens (Beams Bi_U_L1 and Uni_U_L3) experienced a decrease (Figure 4.13 and Table 4.4). With an average pseudo-ductility value of 97% that of the control beam, it is apparent that no significant change in this value is detected. This result is drastically different than what is reported in the literature where pseudo-ductility typically decreased substantially (Aljazaeri & Myers, 2015; Babaeidarabad et al., 2014; Ebead & Saeed, 2014; Elsanadedy et al., 2013; Loreto et al., 2013). Ombres, however, had one of three beam groups show an increase in pseudo-ductility (Ombres, 2011). These pieces of literature all had failure by debonding and, therefore, led to less ductility associated with the response compared to this study. Attari et al. (2012) confirms that with FRP the pseudo-ductility reduces as well, ranging from 35% to 89% of the control value.

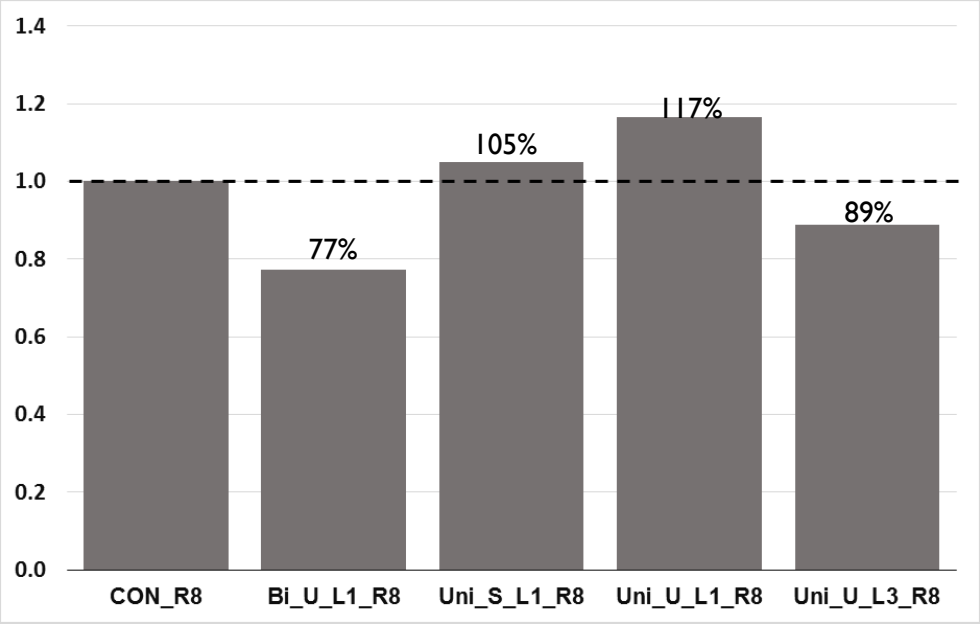

Figure 4.13: Pseduo-ductility relative to the control beam for Group R8

Another metric used to compare beams in terms of ductility is the energy absorption, or sometimes energy dissipation. This is defined as the area under the load-deflection curve (Aljazaeri & Myers, 2015; Ebead et al., 2015; Gopinath et al., 2014). Energy absorption in this research was calculated as the area under the curve until the failure point, which is the load and deflection at ultimate. Beams in Group R8 had values ranging from 921 kN-mm to 1650 kN-mm, whereas Group R20 had absorption values ranging from 1,084 kN-mm to 1,433 kN-mm. An energy index was taken as the ratio of a FRCM strengthened beam energy absorption to that of the respective control beam. Figure 4.14 presents the relative energy index in a bar chart. From inspection, all but one beam (Beam Bi_U_L1_R8) had an increase in energy absorption, where the largest increase was 79% over the control (Beam Uni_U_L3_R8). This is consistent with two pieces of literature on FRCM in flexural. Gopinath et al. (2014) had an increase in the energy in the one beam tested and Aljazaeri & Myers (2015) showed improvement ranging from 3% to 36%. Alternatively, Ebead et al. (2015) found that energy dissipation was reduced by up to as much as 54%. Combining this result with pseudo-ductility, it was apparent that ductility has not been impacted by FRCM strengthening, however, further research is recommended.

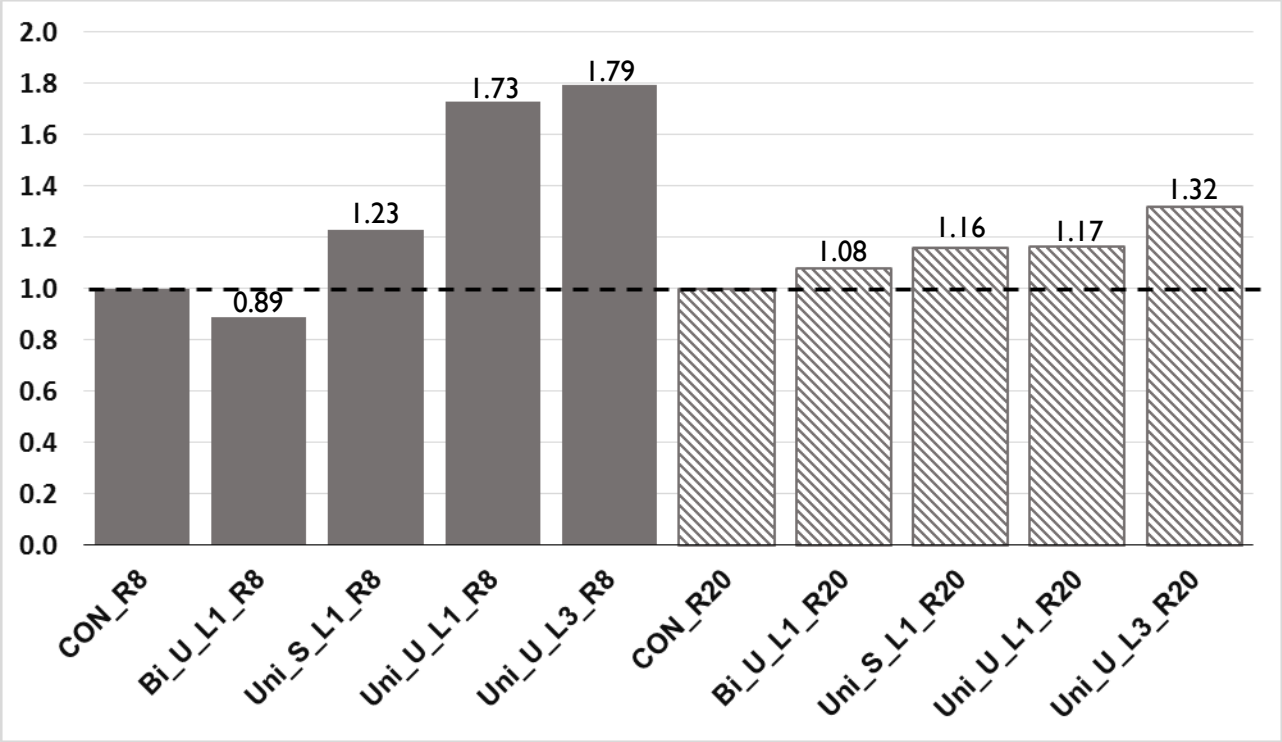

Figure 4.14: Comparison of relative energy absorption

4.8 Results Analysis

4.8.1 Effect of Reinforcement Ratio

The steel reinforcement ratio of a RC beam has a drastic effect on the load carrying capacity. Increasing the ratio from 0.8% (2 - 15M rebars) to 2.0% (2 - 25M rebars), or a 150% increase in steel area, changed the control load capacity from 30.3 to 69.9 kN (130% increase). Other typical control beam comparisons are acknowledged such as increased yield load (133%), increase pre-yielding beam stiffness (86%), and different failure modes and associated ductility (under-reinforced versus balanced). The last of these, the failure mode, becomes very prevalent in this test matrix due to the delivery of understrength concrete. The two reinforcement ratios were chosen relative to an expected 30 MPa and associated 3.43% balanced reinforcement ratio. Due to the true strength at 28 days of 21.4 MPa the balanced ratio dropped to 2.24 and 2.12% for 15M and 25M

respectively. Although a nearer balanced ratio was intended to outline potential failure mode changes from under to over-reinforced, the margin was not intended to be this slim. Despite this fact, conclusions can still be drawn. All R8 specimens failed in a typical under-reinforced manner, and all R20 specimens failed in a near balanced failure with strain gauges reading yield followed shortly by concrete crushing. However, the addition of fabric did not change the failure to that of over-reinforced despite a tiny margin.

The natural divide when drawing conclusions in this test matrix is between the two reinforcement ratios, however, some discussion across the two ratios is needed. When comparing the FRCM upgraded beams based on reinforcement ratio a few important points can be drawn. Beams in Group R8 increased in flexural capacity from 8.6% to 80.9% while in Group R20 strength only increased between 2.1% and 16.3%. Figure 4.15 illustrates each upgraded beam of the same fabric arrangement but at different reinforcement ratio versus the control specimen. The direct comparison at the two ratios for Beams Bi_U_L1, Uni_S_L1, Uni_U_L1, and Uni_U_L3 shows flexural strength improvements of 4.1, 2.8, 4.3 and 5.0 times for Group R8 over their counterparts in Group R20. This gives an average of 4 times more strength improvement for Group R8 specimens than the corresponding beam in Group R20. This shows that the efficiency of FRCM upgrading is substantially greater for beams with a lower reinforcement ratio.

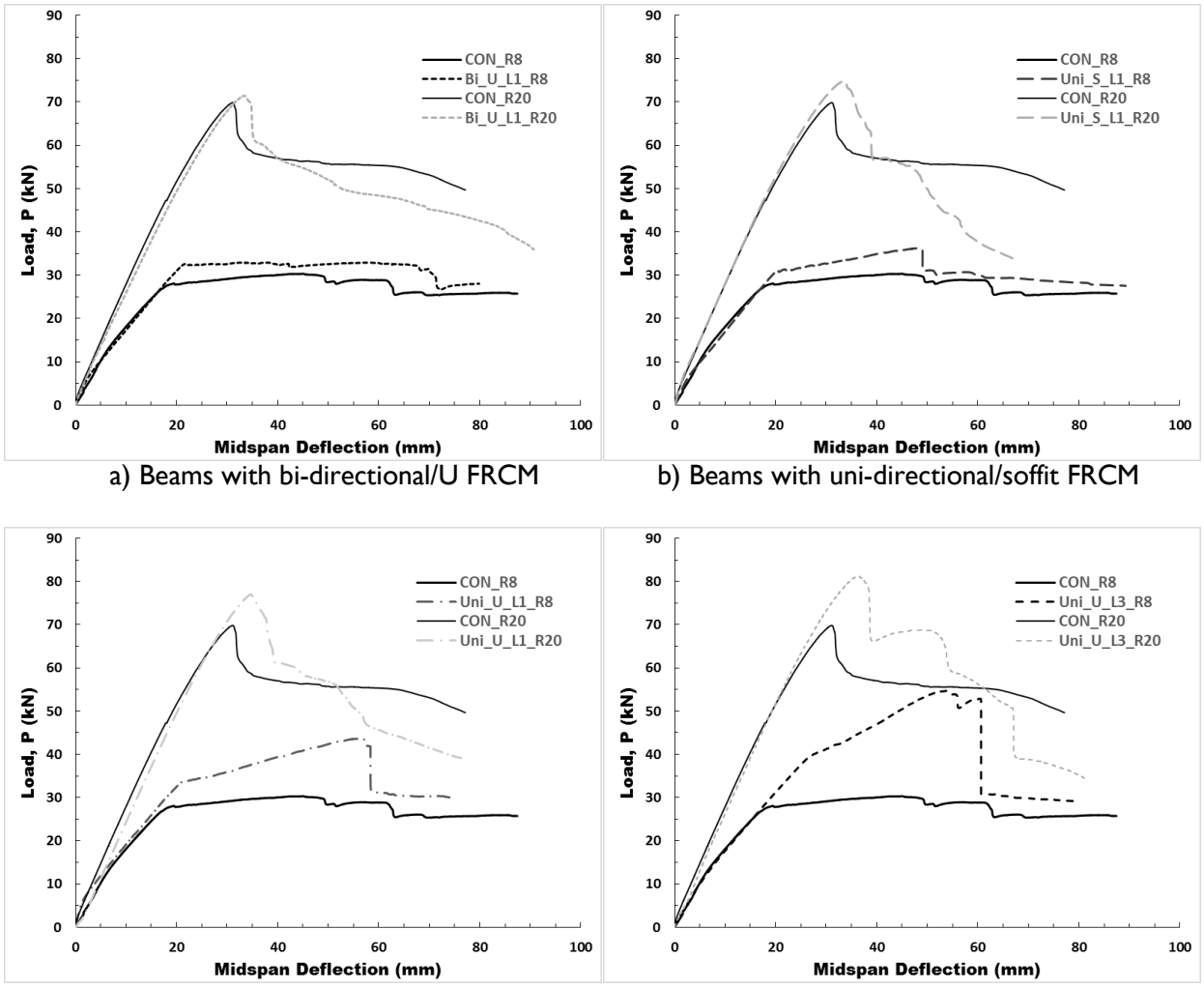

Figure 4.15: Comparison of load deflection response for the two different reinforcement ratios by specimen type

4.8.2 Effect of Textile Material

Two textile materials were tested for their flexural performance as a FRCM system; a bi-directional and uni-directional carbon fabric. The bi-directional fabric, which had carbon in the weft direction as opposed to glass in uni-directional fabric, was explored with the intention of reducing bond failure. Stronger carbon fibres in the weft direction were expected to help anchor the fibres in the longitudinal direction. However, the uni-directional orientation did not show debonding failure and was much more efficient in terms of flexural capacity than the bi-directional

material. The uni-directional specimens, Beams Uni_U_L1_R8 and Uni_U_L1_R20, had strength improvements of 44.2% and 10.3% compared to their control. Meanwhile, the two bi-directional counterparts had improvements of only 8.6% and 2.1%, respectively. This means that the uni-directional material was on average 5 times more efficient than the bi-directional material. Figure 4.16 presents two load-deflection diagrams to directly compare the two textile materials used. Although the longitudinal area of the uni-directional fabric is approximately 3.5 times that of the bi-directional, this does not directly correlate to the average 5 times increase in the capacity across the specimens. Also, when analyzing the load-deflection curve for Group R8 bi-directional specimen (Beam Bi_U_L1_R8), the post-yielding response did not show a linear strength gain after steel yielding like the others. With such a small fibre area, the additional reinforcement was not substantial enough to impact the post-yielding stiffness and strength gain. This, along with the small average strength improvement, may garner a minimum amount of fabric to be used.

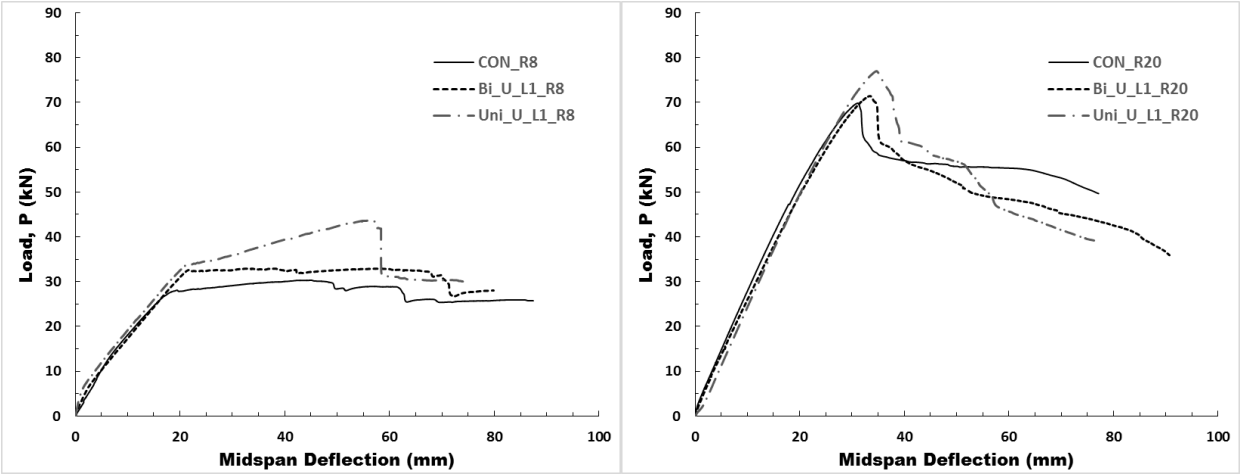

Figure 4.16: Comparison of load deflection response of the two fabric materials used at each reinforcement ratio

4.8.3 Effect of Number of Layers

By adding more layers of strong-in-tension fabric to the tension surface of a beam it is inherent that strength would improve. This theory was confirmed based on this test matrix as both three layer specimens outperformed their one-layer counterpart. For Group R8, the strength improvement increased from 43.7 kN for one layer to 54.8 kN for three layers or 83% increase. Meanwhile, in Group R20 the same arrangements changed the strength from 77 kN to 81.2 kN or 58% increase. However, the increase in the area of the textile in each case had been increased by 200% and, therefore, the improvement is not directly proportional. It is apparent that as the number of layers increased, the strength increased but with less efficiency with each layer. Figure 4.17 illustrates this trend which is evident when comparing to the projected rate line based on the first layer of strengthening. This matches the typically noted trend in literature of increasing strength gain with increasing number of layers but at a lower rate with each additional layer (Babaeidarabad et al., 2014; D'Ambrisi & Focacci, 2011; Ebead et al., 2015; Gopinath et al., 2014; Ombres, 2011). With further research, an upper bound for number of layers of fabric could be established where no further strength gain is achieved with an additional layer.

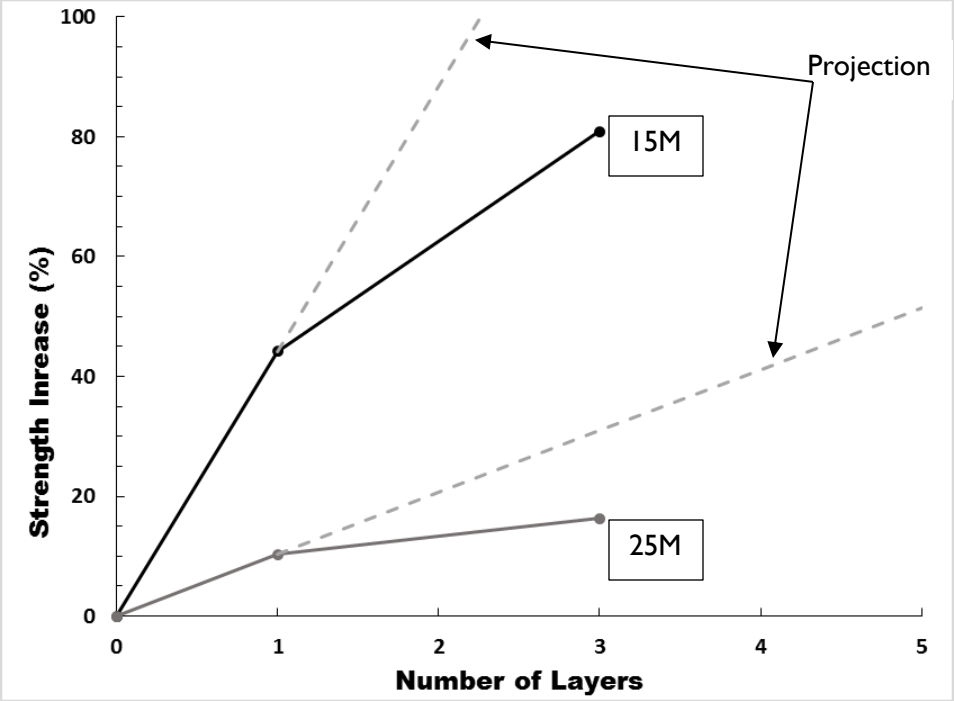

Figure 4.17: Strength increase as a function of number of layers of FRCM

The three layer arrangement was intended to determine if a large enough area could cause a failure mode change from under-reinforced to over-reinforced, a potentially disastrous effect. However, at both groups tested R8 and R20 the failure mode matched that of the one layer beams. Additional layers did not affect the pre-yielding stiffness of the beams as all FRCM upgraded beams showed no stiffness effect as shown in Figure 4.18. When analyzing the yield point, further layers proved to delay beam yield in Group R8. The load and deflection of the three-layer specimen (Beam Uni_U_L3_R8) were higher than that of the one-layer arrangement (Beam Uni_U_L1_R8). The former yielded at 39.2 kN and 26.4 mm while the one-layer yielded at 33.9 kN and 21.3 mm (16% and 24% increases respectively). The additional layers did also have an effect on the post-yielding response for Group R8, in particular the stiffness. When considering the slopes in this region, the stiffness of the three layer specimen was double that of the one layer (Figure 4.18).

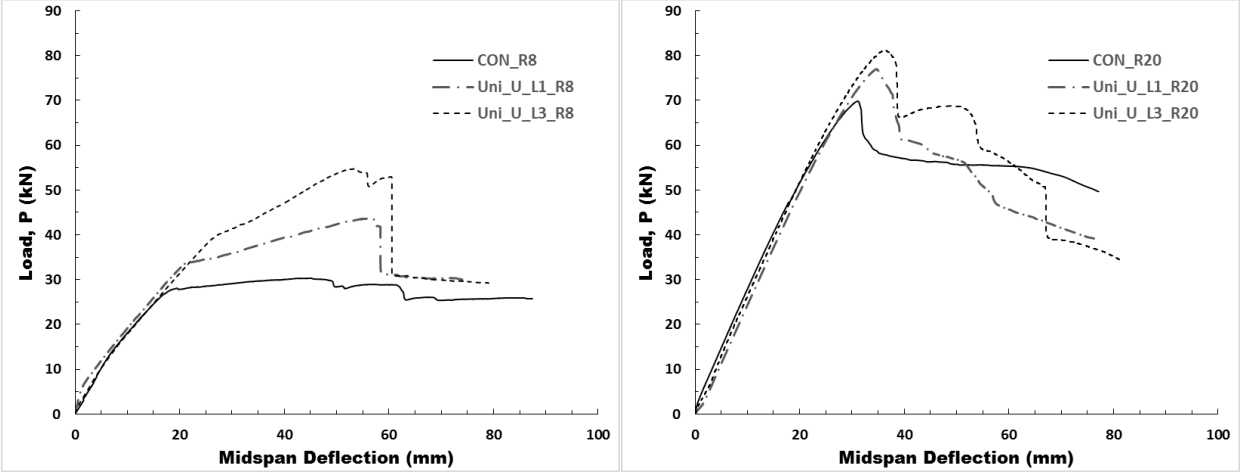

Figure 4.18: Comparison of load deflection response of the two denomination of layers used at each reinforcement ratio

4.8.4 Effect of Application Orientation

Applying the fabric to the soffit only, and as a U-wrapped extending two thirds up the sides of the beam were the two configuration methods explored. Based on the literature, it was a common occurrence to have debonding as a failure mode and this was why a U-shaped application was considered (D'Ambrisi & Focacci, 2011; Ebead & Saeed, 2014; Ombres, 2011). However, even with the soffit only, debonding did not occur in any of the FRCM specimens; all beams failed in steel yielding followed by concrete crushing and then fabric rupture. Group R8 soffit and U-wrapped specimens garnered a strength improvement over the control of 19.8% and 44.2%, respectively. Meanwhile, the R20 alternatives gained 7.0% and 10.3% respectively. Figure 4.19 shows load-deflection curves comparing the two application methods. Both the soffit only application and the U-wrap orientation failed with fabric rupture, therefore, the additional strength is due to the additional area of fabric applied on the tension side. As with the increase in layers, the yield point of the R8 specimen was delayed in the beam with more area of fabric (U-wrapped). Similarly, the U-wrapped specimen had an increase in post-yielding stiffness compared to its lesser

area alternative. In the case of R8 specimens, the U-wrapped specimens had a post-yielding stiffness 51% higher than that of the soffit only application.

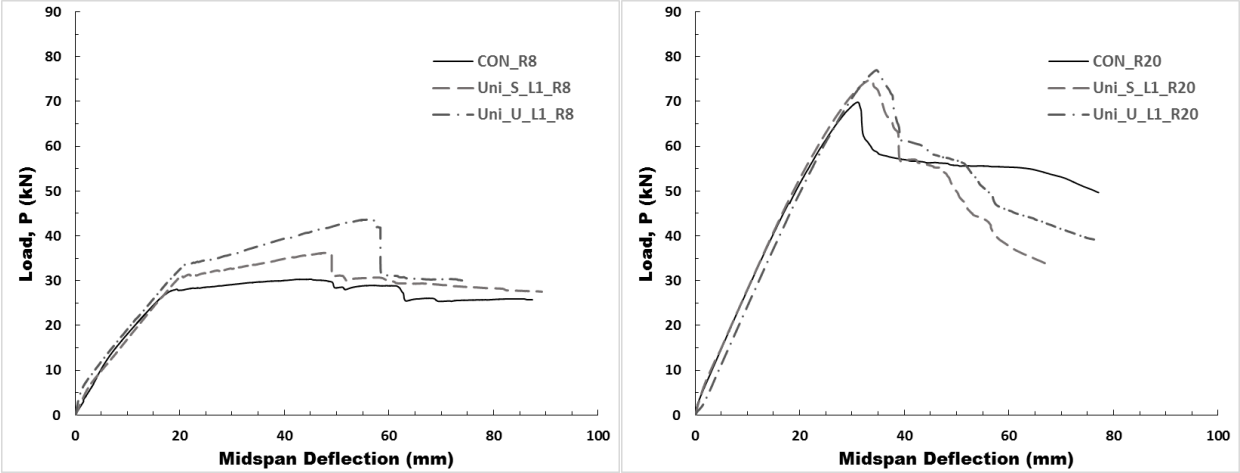

Figure 4.19: Comparison of load deflection response of two application orientations at each reinforcement

CHAPTER 5: CONCLUSIONS AND FUTURE RECOMMENDATIONS

5.1 Summary and Conclusions

This study intended to determine the flexural performance of RC beams strengthened with FRCM. Ten full-scale beams (200 x 300 x 4000 mm) were cast and tested under monotonic four-point bending conditions. The experimental parameters explored included steel reinforcement ratio, fabric type, application orientation and number of layers. Flexural performance indicators recorded and observed were concrete cracking, load carrying capacity, ultimate deflection, yielding, failure mode, and ductility. The following presents the conclusions that can be drawn from this test matrix:

- All beams failed by steel yielding, followed by concrete crushing, followed by fabric rupture. Group R20 beams failed in a very close to balanced manner where steel strain gauges indicated yielding but no beam ductility was present. For all upgraded specimens, debonding was not found as a failure mode. Despite a near balanced failure in Group R20, the addition of FRCM did not change the failure to that of over-reinforced.
- Pre-yielding stiffness of all beams was deemed to be the same. The addition of FRCM to the tension face did not increase the beam's stiffness before yield.
- Group R20 beams did not have a defined beam yield due to the reinforcement ratio being very close to that of a balanced ratio (2.0% versus 2.12%).
- Upgraded beams in Group R8 showed a delayed beam yield in terms of both load and deflection compared to the control (22% and 14% higher on average respectively).

- Post-yielding stiffness for Group R8 was increased with an increased amount of fabric area applied.
- Flexural strength improvements ranged from 2% to 82% over the respective unstrengthen control beam depending on the strengthening arrangement.
- Group R8 beams showed flexural capacity gains of 4 times more than the corresponding beam in Group R20. Beams with lower initial load carrying capacity yield higher strength improvements.
- Increasing the number of layers increased the flexural strength improvement, however, not in a directly proportional manner to the increase in layers.
- The uni-directional carbon material reached higher strength improvements than the bi-directional alternative. This is mainly attributed to the area difference in the longitudinal direction.
- Beams with U-wrapped configuration had higher strength improvements than that of the soffit only application. However, neither arrangement debonded; therefore, the additional strength is due to the additional fibres applied in the tension zone on the beam's sides.
- Pseudo-ductility could not be calculated for group R20 specimens. However, for Group R8 it was noted that no substantial change in this metric versus the control. On the other hand, energy absorption increased for all but one beam.

The results of this test matrix are very promising. However, the author acknowledges that these conclusions are based on the parameters and practices carried out in this particular initiative.

Further validation, in flexural strengthening and other applications, is required to extend these conclusions to the FRCM system as a whole.

5.2 Research Contribution

This research initiative constitutes a significant contribution to the research community and towards the implementation of FRCM as a structural system in Canada. The test matrix was the first experimental work completed in Canada of flexural strengthening with FRCM. Completion with local materials, practice and design values is the basis for development of Canadian design guideslines and codes. This then will transition into the use of FRCM in the civil engineering industry. Further, these results are the first on full-scale specimen with a length of 4 meters. This contributed to the fact that no debonding failure occurred with the FRCM. Only once elsewhere had rupture been achieved in the literature, and only on prestressed specimens.

5.3 Limitations

Although a strong success, there are a few reservations with this study that should be acknowledged. The first reservation is based on the concrete delivery being under the design strength and its impact on the balanced reinforcement ratio. This unfortunately changed the dynamic of half of the test matrix. Although some conclusions and interesting points were brought about, proper design strength concrete could have garnered better conclusions from Group R20. Another FRCM fabric material type, and associated mortar matrix, would have added an interesting comparison point, both for strength results and application differences. With more resources, beams upgraded with FRP could have been added to the test matrix for a direct comparison as well. From a data perspective, the results could have been improved without loss of a few strain gauges. Finally, this test matrix looks at FRCM from a purely technical

improvement angle. To ensure its use in the industry, a cost analysis and life cycle cost assessment would be vital.

5.4 Future Research Scope

The current research work contributed to the short list of promising results of this innovative composite. The results helped fill voids in the literature such as results from Canadian construction methods and materials, full-scale beam tests, and debonding issues. To ensure adequate implementation of FRCM the following is further research recommended:

- Verification of these experimental results with a numerical model
- Explore lack of pre-yielding stiffness contribution from adding fabric
- Increase number of layers further to determine limit on strength improvement
- Determine if beams with more than one soffit layer will debond without anchorage
- Establish the effect of surface preparation, namely roughening of substrate surface, on strength improvements and bonding
- Further experimental results such as long term performance, shear strengthening and improvement of concrete/steel rebar bond that would contribute to the development of Canadian design guides
- Analyze the life cycle cost of FRCM as a method of extending the service life of an existing structure

REFERENCES

ACI 440.1R. (2007). *Report on Fiber-Reinforced Polymer (FRP) Reinforcement*. *American Concrete Institute (ACI) Committee 440*. Farmington Hills, MI.

ACI 440.2R. (2008). *Guide for the Design and Construction of Externally Bonded FRP Systems*. *American Concrete Institute (ACI) Committee 440*. Farmington Hills, MI.

ACI 544.1R. (2002). *State-of-the-Art Report on Fiber Reinforced Concrete*. *American Concrete Institute (ACI) Committee 544*. Farmington Hills, MI.

ACI 544.5R. (2010). *Report on the Physical Properties and Durability of Fiber-Reinforced Concrete*. *American Concrete Institute (ACI) Committee 544*. Farmington Hills, MI.

ACI 546.1R. (2014). *Guide to Concrete Repair*. *American Concrete Institute (ACI) Committee 546*. Farmington Hills, MI.

ACI 549.4R. (2013). *Design and construction of externally bonded Fabric-Reinforced Cementitious Matrix (FRCM) systems for repair and strengthening concrete and masonry Structures*. *American Concrete Institute (ACI) Committee 549*. Farmington Hills, MI.

ACSE. (2013). *Report Card for America's Infrastructure*. *American Society for Civil Engineers (ASCE)*. Reston, VA. Retrieved from www.infrastructurereportcard.org/ on September 20, 2014

Al-Kamaki, Y. S. S., Al-Mahaidi, R., & Bennetts, I. (2015). Strength model for heat-damaged reinforced concrete circular columns confined with carbon fibre reinforced polymer fabrics. *Journal of Reinforced Plastics and Composites*, *34*(22), 1833–1855. http://doi.org/10.1177/0731684415601901

Al-Salloum, Y. A., Almusallam, T. H., Elsanadedy, H. M., & Iqbal, R. A. (2016). Effect of elevated temperature environments on the residual axial capacity of RC columns strengthened with different techniques. *Construction and Building Materials*, *115*, 345–361. http://doi.org/10.1016/j.conbuildmat.2016.04.041

Al-Salloum, Y. A., Siddiqui, N. A., Elsanadedy, H. M., Abadel, A. A., & Aqel, M. A. (2011). Textile-Reinforced Mortar versus FRP as Strengthening Material for Seismically Deficient RC Beam-Column Joints. *Journal of Composites for Construction*, *15*(6), 920–933. http://doi.org/10.1061/(ASCE)CC.1943-5614.0000222

Al-Salloum, Y. A., Siddiqui, N. A., Elsanadedy, H. M., Abadel, A. A., & Aqel, M. A. (2012). Experimental and Numerical Study for the Shear Strengthening of Reinforced Concrete Beams Using Textile-Reinforced Mortar. *Journal of Composites for Construction*, *16*(1), 74–90. http://doi.org/10.1061/(ASCE)CC.1943-5614.0000239.

Alecci, V., Misseri, G., Rovero, L., Stipo, G., De Stefano, M., Feo, L., & Luciano, R. (2016). Experimental investigation on masonry arches strengthened with PBO-FRCM composite. *Composites Part B: Engineering*, *100*, 228–239. http://doi.org/10.1016/j.compositesb.2016.05.063

Alhaddad, M. S., Siddiqui, N. A., Abadel, A. A., Alsayed, S. H., & Al-Salloum, Y. A. (2012). Seismic Behavior of Trm and Gfrp Upgraded Rc Exterior Beam-Column Joints. *Journal of Composites for Construction*, *16*(3), 308–321. http://doi.org/10.1061/(ASCE)CC.1943-5614.0000265.

Aljazaeri, Z. R., & Myers, J. J. (2015). Fatigue and Flexural Behavior of Reinforced Concrete Beams Strengthened With a Fiber Reinforced Cementitious Matrix. *Journal of Composites for Construction*, (October), 1–7. http://doi.org/10.1061/(ASCE)CC.1943-5614.0000726.

APA - The Engineered Wood Association. (2012). *Concrete Forming: Design/Construction Guide*. Tacoma, WA.

Arboleda, D. (2014). *Fabric Reinforced Cementitious Matrix (FRCM) Composites for Infrastructure Strengthening and Rehabilitation: Characterization Methods*. Open Access Dissertations. University of Miami. Paper 1282. Retrieved from http://scholarlyrepository.miami.edu/oa_dissertations/1282 on June 8, 2016

Arboleda, D., Carozzi, F. G., Nanni, A., & Poggi, C. (2015). Testing procedures for the uniaxial tensile characterization of fabric-reinforced cementitious matrix composites. *Journal of*

Composites for Construction. http://doi.org/10.1061/(ASCE)CC.1943-5614.0000626.

ASTM. (2010). *Standard Test Method for Flexural Strength of Concrete (Using Simple Beam with Third-Point Loading). ASTM C78/C78M*. West Conshohocken, PA. http://doi.org/10.1520/C0078

ASTM. (2011). *Standard Test Method for Splitting Tensile Strength of Cylindrical Concrete Specimens*. *ASTM C496/C496M*. West Conshohocken, PA. http://doi.org/10.1520/C0496

ASTM. (2012). *Standard Test Method for Compressive Strength of Hydraulic Cement Mortars (Using 2-in or [50-mm] Cube Specimens). ASTM C109*. West Conshohocken, PA. http://doi.org/10.1520/C0109

ASTM. (2014). *Standard Test Method for Air Content of Freshly Mixed Concrete by the Pressure Method*. *ASTM C231/C231M* (Vol. i). West Conshohocken, PA. http://doi.org/10.1520/C0231

ASTM. (2015a). *Standard Specification for Compressible-Washer-Type Direct Tension Indicators for Use With Structural Fasteners [Metric]*. *ASTM F959*. West Conshohocken, PA. http://doi.org/10.1520/F0959-15.

ASTM. (2015b). *Standard Specification for High Strength Structural Bolts, Steel and Alloy Steel, Heat Treated, 120 ksi (830 MPa) and 150 ksi (1040 MPa) Minimum Tensile Strength , Inch and Metric Dimensions*. *ASTM F3125/F3125M*. West Conshohocken, PA. http://doi.org/10.1520/F3125

ASTM. (2015c). *Standard Specification for Packaged, Dry, Combined Materials for Mortar and High Strength Mortar*. *ASTM C387/C387M*. West Conshohocken, PA. http://doi.org/10.1520/C0887-13.2

ASTM. (2015d). *Standard Test Method for Slump of Hydraulic-Cement Concrete*. *ASTM C143/C143M*. West Conshohocken, PA. http://doi.org/10.1520/C0143

Attari, N., Amziane, S., & Chemrouk, M. (2012). Flexural strengthening of concrete beams using

CFRP, GFRP and hybrid FRP sheets. *Construction and Building Materials*, *37*, 746–757. http://doi.org/10.1016/j.conbuildmat.2012.07.052

Awani, O., El-Maaddawy, T., & Refai, A. El. (2015). Numerical Simulation and Experimental Testing of Concrete Beams Strengthened in Shear with Fabric-Reinforced Cementitious Matrix. *Journal of Composites for Construction*, 1–11. http://doi.org/10.1061/(ASCE)CC.1943-5614.0000711.

Awani, O., Refai, A. El, & El-Maaddawy, T. (2015). Bond characteristics of carbon fabric-reinforced cementitious matrix in double shear tests. *Construction and Building Materials*, *101*, 39–49. http://doi.org/10.1016/j.conbuildmat.2015.10.017

Aykac, S., Kalkan, I., Asce, A. M., Aykac, B., Karahan, S., & Kayar, S. (2013). Strengthening and Repair of Reinforced Concrete Beams Using External Steel Plates. *Journal of Structural Engineering*, *139*, 929–939. http://doi.org/10.1061/(ASCE)ST.1943-541X.0000714.

Babaeidarabad, S., Loreto, G., & Nanni, A. (2014). Flexural strengthening of RC beams with an externally bonded fabric-reinforced cementitious matrix. *Journal of Composites for Construction*, *18*(5), 1–12. http://doi.org/10.1061/(ASCE)CC.1943-5614.0000473.

Bandelt, M. J., & Billington, S. L. (2015). Impact of reinforcement ratio on on deformation capacity of reinforced high-performance fiber-reinforced cementitious composites. *Journal of Structural Engineering*, 457–463. http://doi.org/10.1061/(ASCE)ST.1943-541X.0001562.

Bernat-Maso, E., Gil, L., & Roca, P. (2015). Numerical analysis of the load-bearing capacity of brick masonry walls strengthened with textile reinforced mortar and subjected to eccentric compressive loading. *Engineering Structures*, *91*, 96–111. http://doi.org/10.1016/j.engstruct.2015.02.032

Bournas, D. A., & Triantafillou, T. C. (2011). Bond Strength of Lap-Spliced Bars in Concrete Confined with Composite Jackets. *Journal of Composites for Construction*, *15*(2), 156–167. http://doi.org/10.1061/(ASCE)CC.1943-5614.0000078

Bournas, D. A., Triantafillou, T. C., Zygouris, K., & Stavropoulos, F. (2009). Textile-Reinforced

Mortar versus FRP Jacketing in Seismic Retrofitting of RC Columns with Continuous or Lap-Spliced Deformed Bars. *Journal of Composites for Construction*, *13*(October), 360–371. http://doi.org/10.1061/(ASCE)CC.1943-5614.0000028

CAC. (2016). *Concrete: The Sustainable Construction Material*. *Cement Association of Canada (CAC)*. Retrieved from http://www.cement.ca/en/Concrete-Applications.html on August 20, 2016

Carozzi, F. G., Colombi, P., Fava, G., & Poggi, C. (2016). A cohesive interface crack model for the matrix-textile debonding in FRCM composites. *Composite Structures*, *143*, 230–241. http://doi.org/10.1016/j.compstruct.2016.02.019

CNR-DT 200. (2004). *Guide for the design and construction of externally bonded FRP systems for strengthening concrete structures - materials, RC and PC structures, masonry structures*. *Italian National Research Council (CNR)* (Vol. 24). Rome, Italy. http://doi.org/10.1061/40753(171)159

Colajanni, P., Fossetti, M., & MacAluso, G. (2014). Effects of confinement level, cross-section shape and corner radius on the cyclic behavior of CFRCM confined concrete columns. *Construction and Building Materials*, *55*, 379–389. http://doi.org/10.1016/j.conbuildmat.2014.01.035

Colombo, I., Colombo, M., Magri, A., Zani, G., & di Prisco, M. (2011). Textile Reinforced Mortar at High Temperatures. *Applied Mechanics and Materials*, *82*, 202–207. http://doi.org/10.4028/www.scientific.net/AMM.82.202

Crow, J. M. (2008). The concrete conundrum. *Chemistry World*, (March), 62–66. Retrieved from http://www.rsc.org/images/Construction_tcm18-114530.pdf on September 20, 2014

CSA A23.1/A23.2. (2014). *Concrete materials and methods of concrete construction / Methods of test and standard practices for concrete. Canadian Standards Association (CSA) Standard A23.1-14/A23.2-14*. Mississuaga, Ontario.

CSA A3000. (2013). *Cementitious materials compendium. Canadian Standards Association*

(CSA) Standard CAN/CSA-A3000-13. Mississauga, Ontario.

CSA S16. (2014). *Design of steel structures. Canadian Standards Association (CSA) Standard S16-14*. Toronto, Ontario.

CSA S6. (2014). *Canadian Highway Bridge Design Code. Canadian Standards Association (CSA) Standard S6-14*. Mississauga, Ontario.

CSA S806. (2012). *Design and construction of building structures with fibre-reinforced polymers. Canadian Standards Association (CSA) Standard S806-12*. Mississauga, Ontario.

CSA S807. (2010). *Specification for fibre-reinforced polymers. Canadian Standards Association (CSA) Standard S807-10*. Mississauga, Ontario.

D'Ambrisi, A., & Focacci, F. (2011). Flexural Strengthening of RC Beams with Cement-Based Composites. *Journal of Composites for Construction*, *15*(5), 707–720. http://doi.org/10.1061/(ASCE)CC.1943-5614.0000218.

D'Antino, T., Sneed, L. H., Carloni, C., & Pellegrino, C. (2015). Influence of the substrate characteristics on the bond behavior of PBO FRCM-concrete joints. *Construction and Building Materials*, *101*, 838–850. http://doi.org/10.1016/j.conbuildmat.2015.10.045

D'Antino, T., Sneed, L. H., Carloni, C., & Pellegrino, C. (2016). Effect of the inherent eccentricity in single-lap direct-shear tests of PBO FRCM-concrete joints. *Composite Structures*, *Article in*, 1–13. http://doi.org/10.1016/j.compstruct.2016.01.076

De Santis, S., & de Felice, G. (2015). Tensile behaviour of mortar-based composites for externally bonded reinforcement systems. *Composites Part B: Engineering*, *68*, 401–413. http://doi.org/10.1016/j.compositesb.2014.09.011

Ebead, U., & Saeed, H. (2014). Flexural and Interfacial Behavior of Externally Bonded / Mechanically Fastened Fiber-Reinforced Polymer- Strengthened Reinforced Concrete Beams. *ACI Structural Journal*, *111*(4), 741–751. http://doi.org/10.14359/51686628

Ebead, U., Shrestha, K. C., Afzal, M. S., Refai, A. El, & Nanni, A. (2015). Effectiveness of Fabric-

Reinforced Cementitious Matrix in Strengthening Reinforced Concrete Beams. *Journal of Composites for Construction*, *1*, 1–14. http://doi.org/10.1061/(ASCE)CC.1943-5614.0000741.

El Maaddawy, T., & Sherif, S. (2009). FRP composites for shear strengthening of reinforced concrete deep beams with openings. *Composite Structures*, *89*(1), 60–69. http://doi.org/10.1016/j.compstruct.2008.06.022

Elsanadedy, H. M., Almusallam, T. H., Alsayed, S. H., & Al-Salloum, Y. A. (2013). Flexural strengthening of RC beams using textile reinforced mortar - Experimental and numerical study. *Composite Structures*, *97*, 40–55. http://doi.org/10.1016/j.compstruct.2012.09.053

Escrig, C., Gil, L., Bernat-Maso, E., & Puigvert, F. (2015). Experimental and analytical study of reinforced concrete beams shear strengthened with different types of textile-reinforced mortar. *Construction and Building Materials*, *83*, 248–260. http://doi.org/10.1016/j.conbuildmat.2015.03.013

FIB TG 9.3. (2001). *Externally bonded FRP reinforcement for RC structures*. *International Federation for Structural Concrete (FIB) Task Group (TG) 9.3* (Vol. Bulletin 1). Lausanne, Switzerland. Retrieved from http://scholar.google.com/scholar?hl=en&btnG=Search&q=intitle:Externally+bonded+FRP+reinforcement+for+RC+structures#0 on May 31, 2016

Gadve, S., Mukherjee, A., & Malhotra, S. N. (2009). Corrosion of steel reinforcements embedded in FRP wrapped concrete. *Construction and Building Materials*, *23*(1), 153–161. http://doi.org/10.1016/j.conbuildmat.2008.01.008

GangaRao, H. V. S., & Vijay, P. V. (2010). *Feasibility Review Of FRP Materials For Structural Applications*. *Engeering Research & Development Center - US Army Corps of Engineers*. Vicksburg, MS.

Gil, L., Escrig, C., & Bernat, E. (2014). Bending performance of concrete beams strengthened with textile reinforced mortar TRM. *Key Engineering Materials*, *601*, 203–206. http://doi.org/10.4028/www.scientific.net/KEM.601.203

Gopinath, S., Murthy, A. R., Iyer, N. R., & Prabha, M. (2014). Behaviour of reinforced concrete beams strengthened with basalt textile reinforced concrete. *Journal of Industrial Textiles*, *44*(6), 924–933. http://doi.org/10.1177/1528083714521068

Hag-Elsafi, O., Lund, R., & Alampalli, S. (2001). Strengthening of a Bridge Capbeam Using Bonded FRP Composite Plates. In *Structures 2001: A Structural Engineering Odyssey* (pp. 1–6). Washington, D.C. http://doi.org/10.1061/40558(2001)2

Hamad, B. S., & Rteil, A. A. (2006). Comparison of Roles of FRP Sheets, Stirrups, and Steel Fibers in Confining Bond Critical Regions. *Journal of Composites for Construction*, *10*(4), 330–336. http://doi.org/10.1061/(ASCE)1090-0268(2006)10:4(330)

Hollaway, L. C., & Head, P. R. (2001). *Advanced Polymer Composites and Polymers in the Civil Infrastructure*. *Advanced Polymer Composites and Polymers in the Civil Infrastructure*. http://doi.org/10.1016/B978-008043661-6/50006-1

ICC Evaluation Service. (2013). *AC434 - Acceptance Criteria for Masonry and Concrete Strengthening Using Fiber-reinforced Cementitious Matrix (FRCM) Composite Systems*. *Journal of Chemical Information and Modeling* (Vol. 53). Birmingham, AL. http://doi.org/10.1017/CBO9781107415324.004

ICRI. (2013). *Selecting and Specifying Concrete Surface Preparation for Sealers, Coatings, and Polymer Overlays*. *Internation Concrete Repair Institute (ICRI) Guideline 310.2R-2013*. Rosemont, Illinois.

Júlio, E. N. B. S., & Branco, F. A. B. (2008). Reinforced concrete jacketing - Interface influence on cyclic loading response. *ACI Structural Journal*, *105*(4), 471–477.

Jung, K. S., Hong, K. N., & Han, S. H. (2015). Flexural Behaviour of Reinforced Concrete Beams Strengthened With a FRP- FRCM System. In *Fifth International Conference on Construction Materials (CONMAT'15)*. Whistler, B.C. Canada.

Kassem, C., Farghaly, A. S., & Benmokrane, B. (2011). Evaluation of Flexural Behavior and Serviceability Performance of Concrete Beams Reinforced with FRP Bars. *Journal of*

Composites for Construction, *15*(5), 682–695. http://doi.org/10.1061/(ASCE)CC.1943-5614.0000216

Korany, Y., & Drysdale, R. (2006). Rehabilitation of masonry walls using unobtrusive FRP techniques for enhanced out-of-plane seismic resistance. *Journal of Composites for Construction*, *10*(3), 213–222. http://doi.org/10.1061/(ASCE)1090-0268(2006)10:3(213)

Li, B., & Chua, H. Y. G. (2009). Seismic Performance of Strengthened Reinforced Concrete Beam-Column Joints Using FRP Composites. *Journal of Structural Engineering*, *135*(10), 1177–1190. http://doi.org/10.1061/(ASCE)0733-9445(2009)135:10(1177)

Li, Q., Gao, X., Xu, S., Peng, Y., & Fu, Y. (2016). Microstructure and Mechanical Properties of High-toughness Fiber-Reinforced Cementitious Compositres after Exposure to Elevated Temperatures. *Journal of Materials in Civil Engineering*. http://doi.org/10.1061/(ASCE)MT

Loreto, G., Leardini, L., Arboleda, D., & Nanni, A. (2013). Performance of RC slab-type elements strengthened with fabric-reinforced cementitious-matrix composites. *Journal of Composites for Construction*, *18*(3), A4013003 (1-9). http://doi.org/10.1061/(ASCE)CC.1943-5614.0000415.

Mackenzie, H. (2013). *Canada's Infastructure Gap: Where It Came From and Why it Will Cost So Much to Close*. *Canadian Centre for Policy Alternatives (CCPA)*. Ottawa, Ontario.

Michels, J., Zwicky, D., Scherer, J., Harmanci, Y. E., & Motavalli, M. (2014). Structural Strengthening of Concrete with Fiber Reinforced Cementitious Matrix (FRCM) at Ambient and Elevated Temperature – Recent Investigations in Switzerland. *Advances in Structural Engineering*, *17*(12), 1785–1800. http://doi.org/10.1260/1369-4332.17.12.1785

Micro-Measurements. (2014). SURFACE PREPARATION FOR STRAIN GAGE BONDING. Retrieved March 12, 2016, from http://ww2.bse.vt.edu/kumar/Instrumentation/Straingauge/Strain Gauge Surface Preparation.pdf

Micro-Measurements. (2015). Strain Gage Installations on Concrete Structures. Retrieved March

12, 2016, from http://www.vishaypg.com/docs/11091/tt611.pdf

Mobasher, B. (2011). *Mechanics of Fiber and Textile Reinforced Cement Composites*. Boca Rotan, FL: CRC Press.

Mostofinejad, D., & Mahmoudabadi, E. (2010). Grooving as Alternative Method of Surface Preparation to Postpone Debonding of FRP Laminates in Concrete Beams. *Journal of Composites for Construction*, *14*(6), 804–811. http://doi.org/10.1061/(ASCE)CC.1943-5614.0000117

Mufti, A. A. (2003). FRPs and FOSs lead to innovation in Canadian civil engineering structures. *Construction and Building Materials*, *17*(6–7), 379–387. http://doi.org/10.1016/S0950-0618(03)00039-4

Nanni, A. (2014). Guide to Design and Construction of Externally Bonded Fabric-Reinforced Cementitous Matrix (FRCM) Systems for Repair and Strengthening Concrete Structures. *ACI Webinar Notes*, 1–18.

Ombres, L. (2011). Flexural analysis of reinforced concrete beams strengthened with a cement based high strength composite material. *Composite Structures*, *94*(1), 143–155. http://doi.org/10.1016/j.compstruct.2011.07.008

Ombres, L. (2015). Structural performances of reinforced concrete beams strengthened in shear with a cement based fiber composite material. *Composite Structures*, *122*, 316–329. http://doi.org/10.1016/j.compstruct.2014.11.059

Ombres, L., & Verre, S. (2015). Structural behaviour of fabric reinforced cementitious matrix (FRCM) strengthened concrete columns under eccentric loading. *Composites Part B: Engineering*, *75*, 235–249. http://doi.org/10.1016/j.compositesb.2015.01.042

Papanicolaou, C. G., Triantafillou, T. C., Papathanasiou, M., & Karlos, K. (2007a). Textile reinforced mortar (TRM) versus FRP as strengthening material of URM walls: in-plane cyclic loading. *Materials and Structures*, *41*(1), 143–157. http://doi.org/10.1617/s11527-007-9226-0

Papanicolaou, C. G., Triantafillou, T. C., Papathanasiou, M., & Karlos, K. (2007b). Textile reinforced mortar (TRM) versus FRP as strengthening material of URM walls: out-of-plane cyclic loading. *Materials and Structures*, *41*(1), 143–157. http://doi.org/10.1617/s11527-007-9226-0

Papanicolaou, C., Triantafillou, T., & Lekka, M. (2011). Externally bonded grids as strengthening and seismic retrofitting materials of masonry panels. *Construction and Building Materials*, *25*(2), 504–514. http://doi.org/10.1016/j.conbuildmat.2010.07.018

Pellegrino, C., & D'Antino, T. (2013). Experimental behaviour of existing precast prestressed reinforced concrete elements strengthened with cementitious composites. *Composites Part B: Engineering*, *55*, 31–40. http://doi.org/10.1016/j.compositesb.2013.05.053

Pohoryles, D. A., Melo, J., Rossetto, T., Fabian, M., Mccague, C., Stavrianaki, K., … Sargeant, B. (2016). Use of DIC and AE for Monitoring Effective Strain and Debonding in FRP and FRCM-Retrofitted RC Beams. *Journal of Composites for Construction*. http://doi.org/10.1061/(ASCE)CC.1943-5614.0000715.

PSC. (2016). Canadian Infrastructure Report Card (CIRC): Informing the Future. *Project Steering Committee (PSC)*, 1–164. Retrieved from www.canadainfrastructure.ca on August 1, 2016

Ramaglia, G., Lignola, G. P., Balsamo, A., Prota, A., & Manfredi, G. (2015). Seismic Strengthening of Masonry Vaults with Abutments Using Textile-Reinforced Mortar. *Journal of Composites for Constructionou*, 1–16. http://doi.org/10.1061/(ASCE)CC.1943-5614.0000733.

RILEM Technical Committee 201. (2006). *Textile Reinforced Concrete - State-of-the-Art Report of RILEM Technical Comittee 201 -TRC*. (W. Brameshuber, Ed.). Bagneuz, France: RILEM Publications S.A.R.L.

Ruredil. (2008). *Instructions for the Planning of Static Consolidation Interventions through the use of Fibre Reinforced Cementitious Matrix -FRCM. Di. Te. R - Ruredil's Technical Department*. Retrieved from http://english.ruredil.it/Planning.pdf on August 20, 2014

Sezen, H. (2012). Effectiveness of Repair and Strengthening Methods for Reinforced Concrete Columns and Beam-Column Joints. In *Structures Congress* (Vol. 10, pp. 2015–2024). Chicago, IL. http://doi.org/10.1061/9780784412367.177

Si Larbi, A., Agbossou, A., & Hamelin, P. (2013). Experimental and numerical investigations about textile-reinforced concrete and hybrid solutions for repairing and/or strengthening reinforced concrete beams. *Composite Structures*, *99*, 152–162. http://doi.org/10.1016/j.compstruct.2012.12.005

Silfwerbrand, J. L. (2009). *Failure, Distress and Repair of Concrete Structures*. (N. Delatte, Ed.), *Failure, Distress and Repair of Concrete Structures*. Boca Rotan, FL: CRC Press. http://doi.org/10.1533/9781845697037.2.208

Tan, K. H. (2016). Beam strengthening by external post-tensioning: Design recommendations. *The IES Journal Part A: Civil & Structural Engineering*, *7*(4), 219–228. http://doi.org/10.1080/19373260.2014.947086

Trapko, T. (2013). The effect of high temperature on the performance of CFRP and FRCM confined concrete elements. *Composites Part B: Engineering*, *54*(1), 138–145. http://doi.org/10.1016/j.compositesb.2013.05.016

Trapko, T. (2014). Behaviour of fibre reinforced cementitious matrix strengthened concrete columns under eccentric compression loading. *Materials and Design*, *54*, 947–954. http://doi.org/10.1016/j.matdes.2013.09.008

Triantafillou, T. C., & Papanicolaou, C. G. (2005). Textile Reinforced Mortars (TRM) versus Fibre Reinforced Polymers (FRP) as strengthening materials of concrete structures. In *Seventh International Symposium of the Fiber-Reinforced Polymer Reinforcement for Reinforced Concrete Structures (FRPRCS)* (pp. 99–118).

Triantafillou, T., & Papanicolaou, C. (2013). Innovative Applications of Textile-Based Composites in Strengthening and Seismic Retrofitting as Well as in the Prefabrication of New Structures. *Advanced Materials Research*, *639–640*(1), 26–41. http://doi.org/10.4028/www.scientific.net/AMR.639-640.26

Wallace, I. W. (2013). Direct Tension Multi-Color Indicating Washers. US8382409. United States Patent Office. http://doi.org/10.1021/n10602701.

Williams Portal, N., Lundgren, K., Wallbaum, H., & Malaga, K. (2014). Sustainable Potential of Textile-Reinforced Concrete. *Journal of Materials in Civil Engineering*, *27*(7). http://doi.org/10.1061/(ASCE)MT.1943-5533.0001160.

Xu, S., Shen, L., & Wang, J. (2016). The high-temperature resistance performance of TRC thin-plates with different cementitious materials : Experimental study. *Construction and Building Materials*, *115*, 506–519. http://doi.org/10.1016/j.conbuildmat.2016.04.070

Yao, Y., Zhu, D., Zhang, H., Li, G., Mobasher, B., & Asce, M. (2016). Tensile Behaviors of Basalt, Carbon, Glass, and Aramid Fabrics under Various Strain Rates, *28*(9), 1–10. http://doi.org/10.1061/(ASCE)MT.1943-5533.0001587.

Yin, S., Sheng, J., Ph, D., Wang, X., & Li, S. (2014). Experimental Investigations of the Bending Fatigue Performance of TRC-Strengthened RC Beams in Conventional and Aggressive Chlorate Environments. *Journal of Composites for Construction*, *20*. http://doi.org/10.1061/(ASCE)CC.1943-5614.0000617.

Zhu, Y., Zhang, Z., Yao, Y., Guan, X., & Yang, Y. (2016). Effect of Water-Curing Time on the Mechanical Properties of Engineered Cementitious Composites. *Journal of Materials in Civil Engineering*. http://doi.org/10.1061/(ASCE)MT.1943-5533.0001636.

APPENDICES

Appendix A: FRP Material Properties

Table 0.1: Typical properties of the fibres used in FRP [(ACI 440.1R, 2007) © with permission from ACI]

Fiber	Typical diameter, microns	Density, g/cm^3 (lb/in.^{3})	Tensile modulus, GPa (10^6 psi)	Tensile strength, MPa (ksi)	Strain to failure, %	Coefficient of thermal expansion, 10^{-6}/°C	Poisson's ratio
Commercial composite reinforcing fibers (constructed from Mallick [1988])							
Glass							
E-glass	10	2.54 (0.092)	72.4 (10.5)	3450 (500.0)	4.8	5.0	0.2
S-glass	10	2.49 (0.090)	86.9 (12.6)	4300 (625.0)	5.0	2.9	0.22
Carbon PAN-carbon							
T-300	7	1.76 (0.064)	231 (34)	3650 (530)	1.4	–0.1 to –0.5 (longitudinal), 7 to 12 (radial)	–0.2
AS	7	1.77 (0.064)	220 (32)	3100 (450)	1.2	–0.5 to –1.2 (longitudinal), 7 to 12 (radial)	—
t-40	6	1.81 (0.065)	276 (40)	5650 (820)	2.0	—	—
HSB	7	1.85 (0.067)	345 (50)	2340 (340)	0.58	—	—
Fortafil 3™	7	1.80 (0.065)	227 (33)	3800 (550)	1.7	–0.1	—
Fortafil 5™	7	1.80 (0.065)	345 (50)	2760 (400)	0.8	—	—
Toray M40J	—	1.77 (0.064)	377 (55)	4410 (640)	1.2	—	—
Zoltek (2006)	7	1.81 (0.065)	242 (35)	3800 (550)	—	—	—
Pitch-carbon							
P-555	10	2.00 (0.072)	380 (55)	1900 (275)	0.5	–0.9 (longitudinal)	—
P-100	10	2.16 (0.078)	758 (110)	2410 (350)	0.32	–1.6 (longitudinal)	—
Aramid							
Kevlar™ 49	12	1.45 (0.052)	131 (19)	3620 (525)	2.8	–2.0 (longitudinal), +59 (radial)	0.35
Twaron™ 1055*	12	1.45 (0.052)	127 (18)	3600 (533)	2.5	–2.0 (longitudinal), +59 (radial)	0.35

*Mechanical properties: single filament at 22 °C (72 °F) per ASTM D 2101.

Table 0.2: Approximate properties of thermosetting polymer resins [(Mobasher, 2011) © adapted with permission from publisher]

	Density [g/cm^3 (lb/in^3)]	**Tensile Modulus [GPa (Msi)]**	**Tensile Strength [MPa (ksi)]**	**Max Elongation (%)**
Polyester	1.2 (0.043)	4.0 (0.58)	65 (9.4)	2.5
Epoxy	1.2 (0.043)	3.0 (0.44)	90 (13.1)	8.0
Vinylester	1.12 (0.041)	3.5 (0.51)	82 (11.9)	6.0
Phenolic	1.24 (0.045)	2.5 (0.36)	40 (5.8)	1.8
Polyurethane	varies	2.9 (0.42)	71 (10.3)	5.9

Table 0.3: Typical properties of commercially available FRP strengthening strips [(CSA S806, 2012) © with permission from publisher]

	Standard modulus CFRP epoxy	High modulus CFRP epoxy	GFRP epoxy	CFRP vinylester
Fibre volume (%)	65-70	65-70	65-70	60
Fibre architecture	Unidirectional	Unidirectional	Unidirectional	Unidirectional
Nominal thickness (mm)	1.2-2.9	1.2	1.4-1.9	2.0
Width (mm)	50-100	50-100	50-100	16
Tensile strength, longitudinal (MPa)	2690-2800	1290	900	2070
Tensile strain (max), longitudinal (%)	1.8	--	2.2	1.7
Tensile modulus, longitudinal (MPa)	155-165	300	41	131

Table 0.4: Selected properties of typcial available FRP strengthening systems as reported by the manufacturer [(ACI 440.1R, 2007) © with permission from ACI]

FRP system	Fiber type	Weight, g/m^2 (lb/ft^2)	Design thickness, mm (in.)	Tensile strength, MPa (ksi)	Tensile elastic modulus, GPa (ksi)	ACI 440.3R test reporting method
Fyfe Co. LLC (2005)						
Tyfo SEH51 sheet	Glass	915 (0.19)	1.3 (0.052)	575 (83.4)	26.1 (3785)	Method 1
Tyfo SCH41 sheet	Carbon	644 (0.14)	1.0 (0.040)	985 (143)	95.8 (13,900)	Method 1
Sika Corp. (2007)						
SikaWrap Hex 100G sheet	Glass	913 (0.19)	1.0 (0.040)	531 (77)	23.6 (3430)	Method 1
SikaWrap Hex 103C sheet	Carbon	618 (0.13)	1.0 (0.040)	717 (104)	65.1 (9450)	Method 1
CarboDur S plate	Carbon	1800 (0.37)	1.2 to 1.4 (0.048 to 0.055)	2800 (406)	165 (23,900)	Method 1
CarboDur M plate	Carbon	1900 (0.39)	1.2 (0.048)	2400 (348)	210 (30,500)	Method 1
CarboDur H plate	Carbon	1900 (0.39)	1.2 (0.048)	1300 (189)	300 (43,500)	Method 1
BASF (2006)						
MBrace EG 900 sheet	Glass	900 (0.19)	0.37 (0.015)	1517 (220)	72.4 (10,500)	Method 2
MBrace AK 60 sheet	Aramid	600 (0.12)	0.28 (0.011)	2000 (290)	120 (17,400)	Method 2
MBrace CF 130	Carbon	300 (0.062)	0.17 (0.007)	3800 (550)	227 (33,000)	Method 2
MBrace CF 160	Carbon	600 (0.124)	0.33 (0.013)	3800 (550)	227 (33,000)	Method 2
S&P 100/1.4	Carbon	—	1.4 (0.055)	2700 (390)	159 (23,000)	Method 1
Hughes Brothers (2005)						
Aslan 400 plate	Carbon	—	1.4 (0.055)	2400 (350)	131 (19,000)	Method 1
Aslan 500 tape	Carbon	—	2.0 (0.079)	2068 (300)	124 (18,000)	Method 1
Aslan 500 tape	Carbon	—	4.5 (0.177)	1965 (285)	124 (18,000)	Method 1

Appendix B: FRCM Material Properties

Table 0.5: Constituent materials properties of available FRCM products [(ACI 549.4R, 2013) © with permission from ACI]

Constituent Characteristics	US Cust.	SI	US Cust.	SI	US Cust.	SI	US Cust.	SI	US Cust.	SI	US Cust.	SI	US Cust.	SI
FIBER FILAMENT PROPERTIES			**AR-GLASS**		**BASALT**		**BASALT**		**CARBON**		**CARBON**		**PBO**	
Density	lb/cu.ft	(g/cm^3)	156	2.50	169	2.70	172	2.75	109	1.74	113	1.81	97	1.56
Tensile strength	ksi	(GPa)	188	1.28	382	2.60	705	4.80	557	3.79	720	4.90	852	5.80
Modulus of elasticity	ksi	(GPa)	10,581	72	12,492	85	13,079	89	33,801	230	37,475	255	39,679	270
Ultimate deformation	-	-	0.018	0.018	0.031	0.031	0.030	0.030	0.016	0.016	0.019	0.019	0.025	0.025
Breakdown temperature	°F	(°C)			2,462	1350	2,372	1,300	4,532	2500	1,202	650	1,202	650
Coefficient of thermal dilation	10^{-6} °F^{-1}	(10^{-6} °C^{-1})			0.31	0.55			-0.01	-0.01	0.28	0.50	-3.33	-6.00
MESH PROPERTIES														
Weight of the mesh	oz/sq.ft.	(g/m^2)	0.74	225	0.72	220	0.82	250	0.88	270	0.66	202	0.36	111
Weight of fibers in the mesh	oz/sq.ft.	(g/m^2)	0.57	175	0.56	170	0.70	214	0.72	220	0.56	172	0.23	70
Equivalent dry fabric thickness in the direction of the wa	in	(mm)	0.0014	0.035	0.0012	0.032	0.0015	0.039	0.0025	0.063	0.0019	0.048	0.0018	0.046
Equivalent dry fabric thickness in the direction of the we	in	(mm)	0.0014	0.035	0.0012	0.032	0.0015	0.039	0.0025	0.063	0.0019	0.048	0.0005	0.012
Ultimate tensile strength of the warp by width unit	kip/ft	(kN/m)	3.1	45	5.6	82	4.1	60	16.4	240	17.2	252	18.9	276
Ultimate tensile strength of the weft by width unit	kip/ft	(kN/m)	3.1	45	5.6	82	4.1	60	16.4	240	17.2	252	5.1	75
Ultimate tensile strain of the warp by width unit	-	-	0.018	0.018	0.031	0.031	0.018	0.018	0.016	0.016	0.019	0.019	0.081	0.081
Ultimate tensile strain of the weft by width unit	-	-	0.018	0.018	0.031	0.031	0.018	0.018	0.016	0.016	0.019	0.019	0.081	0.081
Axial Stiffness of the warp by width unit	kip/ft	(kN/m)	174	2,539	183	2,678	228	3,333	996	14,536	898	13,100	234	3,421
Axial Stiffness of the weft by width unit	kip/ft	(kN/m)	174	2,539	183	2,678	228	3,333	996	14,536	898	13,100	64	932
Area of the warp by width unit	sq.in/in	(mm^2/m)	0.0014	35.27	0.0012	31.50	0.0015	38.91	0.0025	63.20	0.0020	51.37	0.0019	47.52
Area of the weft by width unit	sq.in/in	(mm^2/m)	0.0014	35.27	0.0012	31.50	0.0015	38.91	0.0025	63.20	0.0020	51.37	0.0005	12.95
MORTAR PROPERTIES			**Powder & liquid**		**Single component**		**Single component**		**Single component**		**Single component**		**Single component**	
Consistency (single component)	in	(mm)									6.5	165	6.9	175
Specific weight (component A)	lb/cu.ft	(g/cm^3)	68	1.10			87	1.40						
Specific weight (component B)	lb/cu.ft	(g/cm^3)	63	1.02			-	-						
Specific weight (green mortar)	lb/cu.ft	(g/cm^3)	112	1.8	100 ± 2	1.60 ± 0.04	124	2.0	96±2	1.54 ± 0.04	94±3	1.50 ± 0.05	112 ± 3	1.80 ± 0.05
Dry solids content (component A)	%	%	100	100			100	100						
Dry solids content (component B)	%	%	23	23			-	-						
Mixing ratio (comp. A to comp. B)	-	-	3 to 7	3 to 7			-	-						
Water/Mortar mix ratio by weight	%	(%)			14 - 16.6	14 - 16.6	16	16	14.8 - 18	14.8 - 18	25 - 27	25 - 27	25 - 27	25 - 27
Tensile strength (at 28 days)	psi	(MPa)	882	6.0			294	2.0						
Compressive strength (at 28 days)	psi	(MPa)	2,645	18.0	3,674	25.0	2,204	>15	3,674	25.0	2,903	>20.0	4,354	>30.0
Bending strength (28 days)	psi	(MPa)	1,176	8.0	882	6.0	882	6.0	1,029	7.0	508	>3.5	581	> 4.0
Secant modulus of elasticity (28 days)	ksi	(MPa)	1,161	8,000			1,451	10,000			1,016	7,000	1,016	7,000
Adhesion to concrete substrate (at 28 days)	psi	(MPa)	>367	>2.5			>103	>0.7						
Adhesion to masonry substrate (at 28 days)	psi	(MPa)	>294	>2			>103	>0.7						
Legend and notes														
Manufacturer A														
Manufacturer B														
Manufacturer C														
Blank cell means value not available														

Table 0.6: Textile mechanical properties considered for testing [(Gil et al., 2014) © with permission from publisher]

Material	*Tensile Strength* f_{fk} *(MPa)*	*Failure Strain* ε_{fu} *(%)*	*Young's Modulus* E_{fu} *(GPa)*	*Equivalent Thickness* t_f *(mm)*
Glass	2600	3,00	90	0,0042
PBO	5800	2,15	270	0,0455
LD-Steel	3070	1,60	190	0,0750
HD-Steel	3070	1,60	190	0,2270
Carbon	3400	1,80	240	0,0470

Table 0.7: Mechanical properties of mortars analyzed [(Gil et al., 2014) © with permission from publisher]

Type of Mortar	*Compressive Strength (MPa)*	*Flexural Strength (MPa)*
Bicomponent mortar with high strength cement	34,84	8,63
Hydraulic mortar with fibers and additives	30,02	10,65
Hydraulic puzzolanic mortar	24,70	7,87
Hydraulic mortar with polymeric additives (PCC)	24,46	8,13

Appendix C: Concrete Formwork Construction

The details of the wood formwork construction are outlined in this Appendix. The design implemented a post-tension wall system to allow for future use of the formwork. Wall panels were reinforced with sets of two 2x4's that allowed threaded rods to slot between them. These rods then threaded into winged T-nuts that were placed in the base plywood as anchors. Washers spread the tension load when rods were tightened for casting. The plan dimensions of each base are 1220 x 4238mm and height of 440mm from bottom dunnage to top of the walls as shown in Figure 0.1 to Figure 0.3.

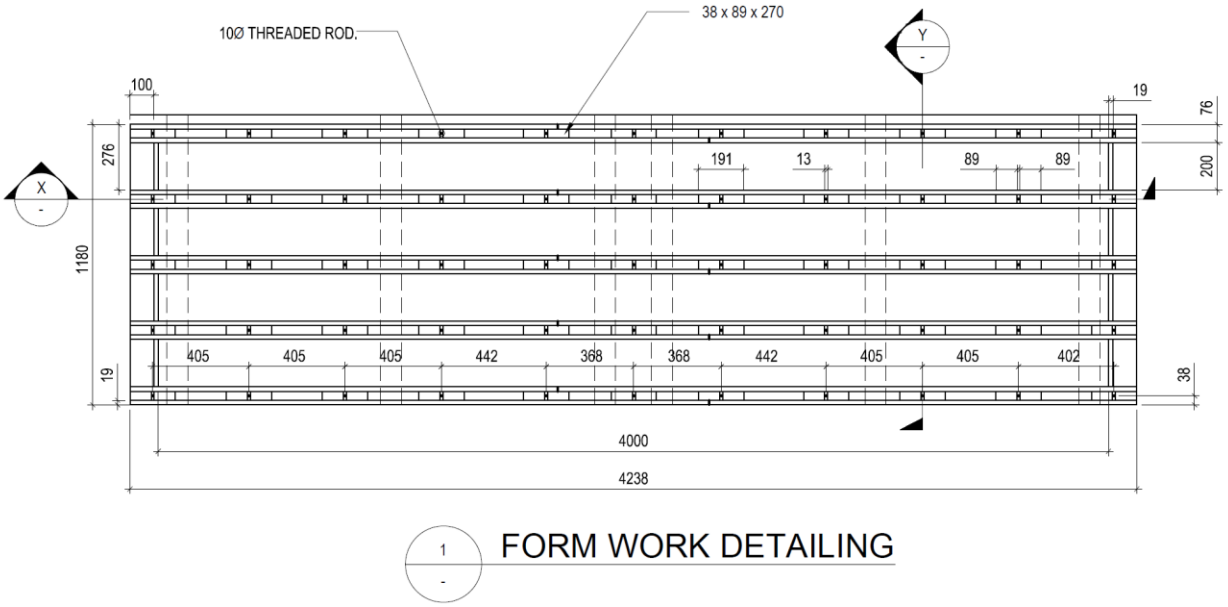

Figure 0.1: Plan drawing

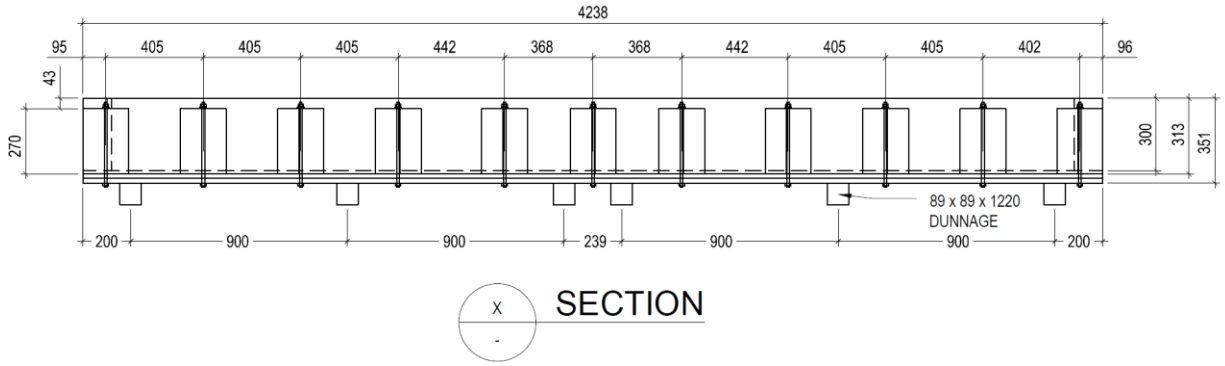

Figure 0.2: Side elevation drawing

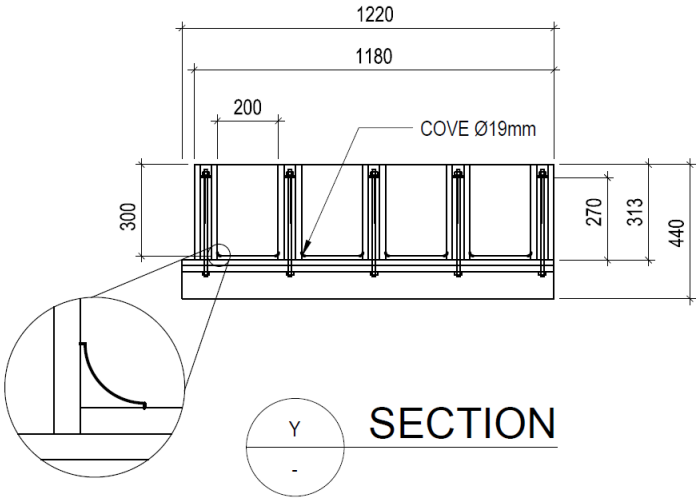

Figure 0.3: End elevation

Standard plywood panels available in sections of 4 x 8 feet (1220 x 2438 mm) were used to simplify the design and reduce cost. A base with thickness of 38 mm was created with two 6 feet long and two 8 feet long panels by gluing two 3/4 inch thick panels on top of one another with offsetting seams. A 4 x 4 inch treated lumber with length of 1220 mm was nailed to the bottom at the spacing shown in Figure 0.2 to allow for easy transportation with a forklift. Holes were drilled in the base where the threaded rods would slot through the walls (Figure 0.1).

Form walls (15 in total), made from one-side form ply, were created first by gluing and nailing 2x4 pieces with a length of 270mm back to back between 3/4 inch one-side plyform as per form guidelines (APA - The Engineered Wood Association, 2012). This construction process served beneficial in both removing bends in single panels and adding structural stability. All faces exposed to concrete were painted with exterior paint to seal wood surface and coated with form oil before casting to ensure the durability of the surface and therefore the formwork sets. Figure 0.4a shows 200mm wide bottom panels with the painted surface, where the walls fit between each bottom. Winged T-nuts were hammered into predrilled holes in the bottom of the base as shown in Figure 0.4b. Stainless steel nuts were welded to the end of 3/8 inch threaded rod, then threaded into winged T-nuts installed in the base. This allowed a tensile force to be applied to the walls when torque is applied to the threaded rod. Two stainless steel washers were used to distribute tension force to the top of 2 x 4 pieces as shown in Figure 0.4c. Pre-constructed wall panels were placed between the painted base plywood sheets (Figure 0.4a) such that threaded rods aligned with the T-nuts. Once all threaded rods aligned, each was tightened to anchor the wall to the base. Before use for casting, wood shims the thickness of the wall openings were placed over the rods to keep concrete out of the form openings. Figure 0.5 shows a complete formwork set ready for casting.

a) b) c)

Figure 0.4: Components of formwork construction: a) wood bases with bottom panels before walls, b) winged T-nuts in bottom of bases, and c) threaded rod top and washer used to distribute force

Figure 0.5: A complete formwork set with shims and cages ready for casting

Appendix D: Steel Frame Construction

The major design parameters for this test frame were as follows 1) carry a vertical load of 500kN, 2) cyclic and fatigue loading of 150kN, 3) clear width for beams, one way or two way slabs, 4) adjustable height for taller specimen, 4) small displacements and 5) mobile in the structures lab. A portal steel frame with bolted connections was designed with the aid of SAP2000. The design consisted of two W310x86 columns, two MC460x77.2 crossheads, a welded U-shaped actuator connection bracket, and 40-1.25 inch grade A490M bolts and nuts as per ASTM F3125M (ASTM, 2015b). Further pieces for design included W200x22 pedestals, and a W310x97 spreader bar. Due to load reversal on the frame and need for small deflections, the bolted connections were required to be designed as slip-critical connections. These connections utilize a precise tensile force on each bolt, using friction to resist loads as compared to typical bearing connections. Frame sections and actuator connector were sandblasted to achieve a Class B roughened surface, therefore improving the structural capacity. All steel sections and bolted connections were designed following CSA S16 code (CSA S16, 2014). The design utilized the structure lab's strong floor to anchor the frame to the ground with post-tension anchor bolts. Figure 0.6 shows the AutoCAD drawing of the final frame design. In Figure 0.9 and Figure 0.10 details of the design in SAP2000 are presented. Meanwhile all individual steel components, including drill holes, are detailed in Figure 0.11 to Figure 0.16

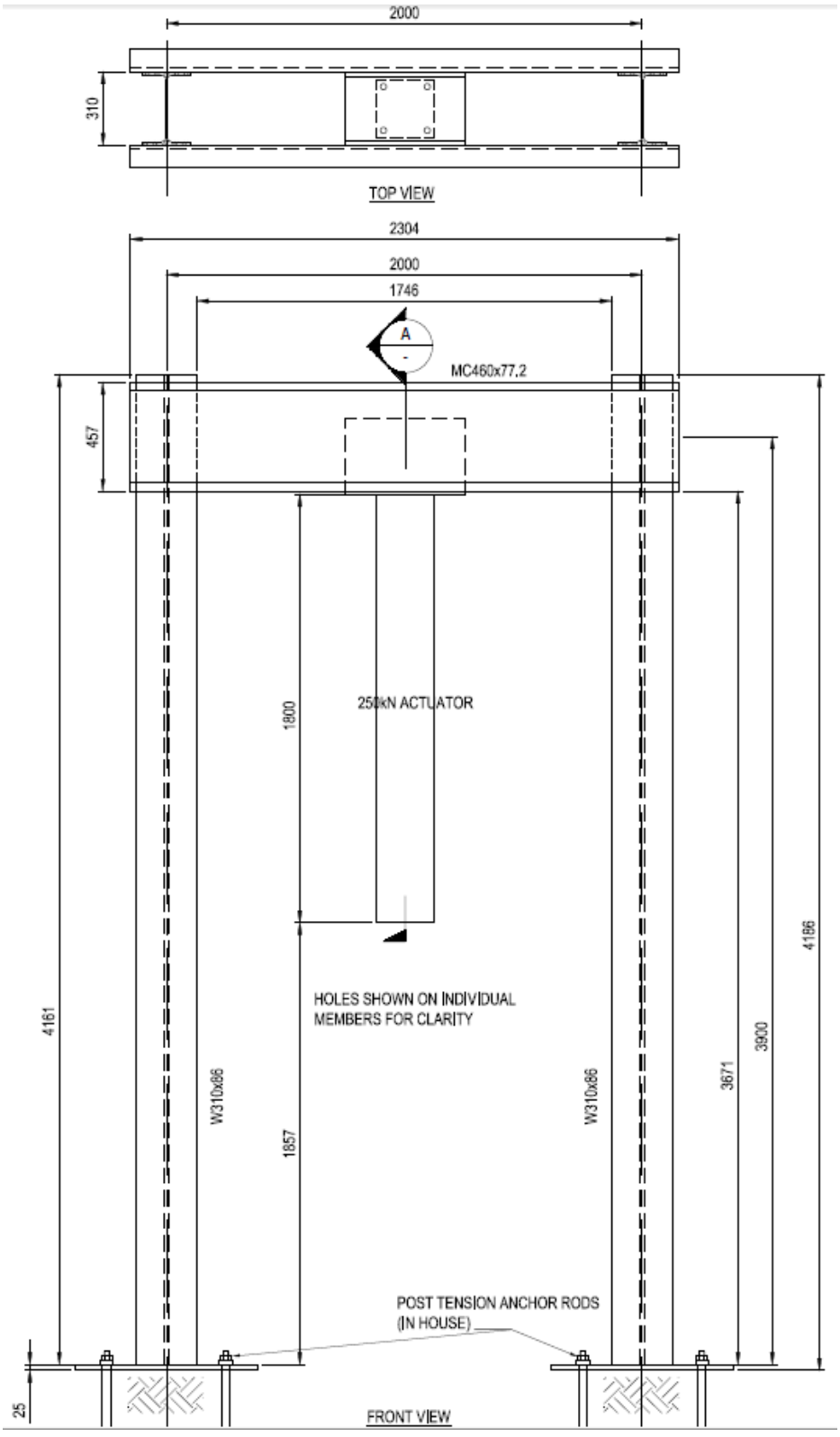

Figure 0.6: Sketch of final frame design

The research group worked closely with a local steel fabricator in Kelowna, BC to procure and manufacture the required steel components for the portal frame. The fabricators were responsible for drilling holes in the sections and plates, welding the actuator connecting bracket together, and welding column base plates. All welds were run through non-destructive testing (NDT) before being delivered to the lab.

The frame was constructed by a team of engineering technicians led by the author. An overhead crane was used to position members on floor and alignment pins ensure slotted holes lined up for bolts. Connections were completed on one side of the frame, before flipping longitudinally to place bolts on alternate side. Once bolted, the frame was tilted up again using the overhead crane and tie wires. Constructed on the strong floor, the base plats on both columns were posttensioned down using anchor rods with a diameter of 36 mm. Figure 0.7 shows the frame during construction process.

a) b)

Figure 0.7: Erection process of steel frame a) members aligned on floor and b) tilting frame up after all bolts tensioned and actuator connected

Bolted connections were pretensioned by hand with a 600 ft-lb torque wrench and a 4-1 torque multiplier to achieve slip critical connections; a vital component of the design requirements. Bolts were lubricated for improved tensioning. Torque applied was roughly 2200 ft-lb to achieve a tension force equal to 70% of the specified tensile strength. Direct Tension Indicators (DTIs) that squirted gel were utilized as washers to indicate when the proper tension had been reached in the bolt (Wallace, 2013). These washers are constructed as per ASTM F959 (ASTM, 2015a). Figure 0.8 below shows the tightening setup as well as the gel indicator from the DTI washers.

a) b)

Figure 0.8: Construction of frame showing a) torque wrench and multiplier set up, and b) bolts with DTIs and orange indicator gel showing

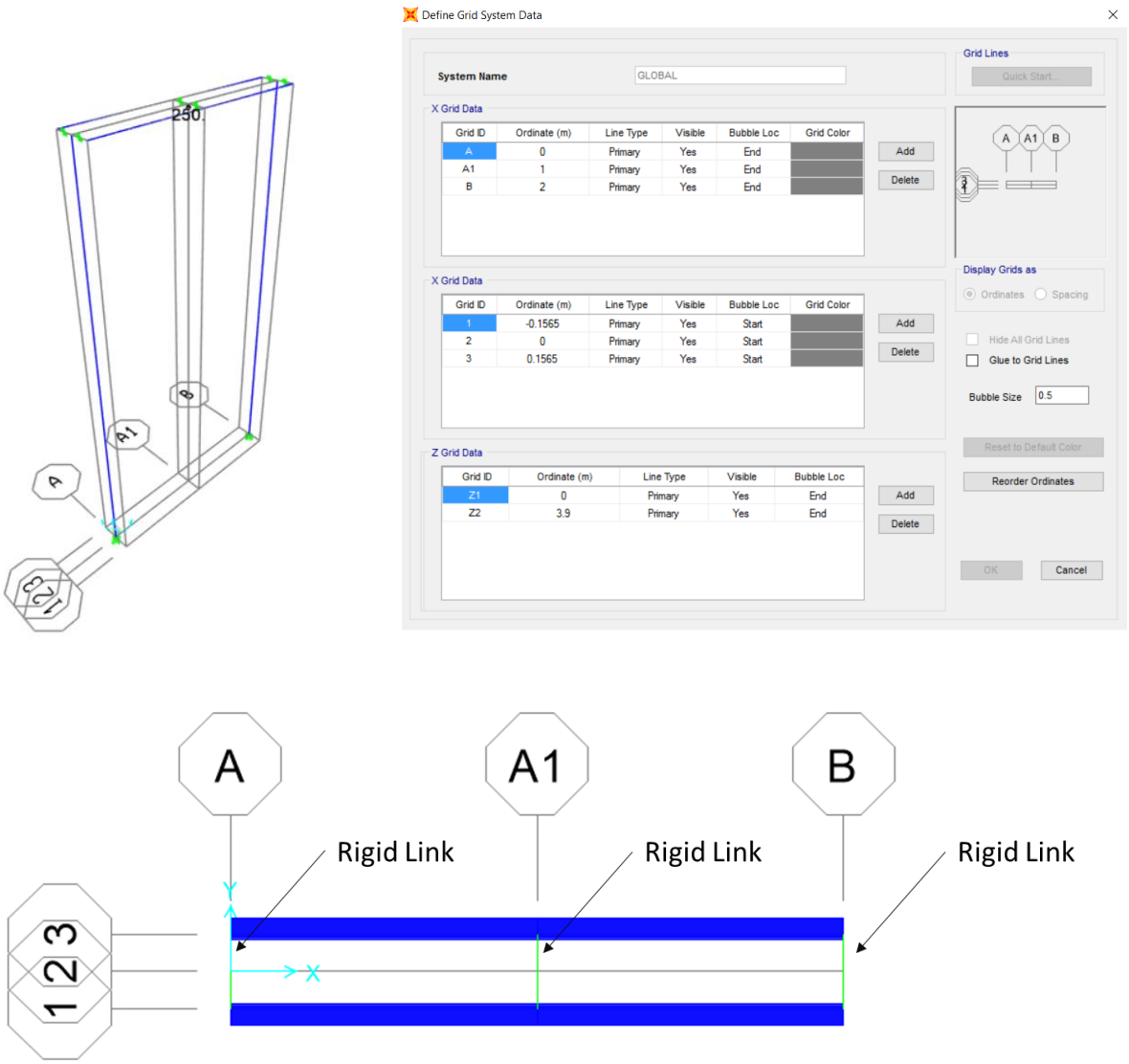

Figure 0.9: Details of the SAP2000 model used to design the steel frame sections

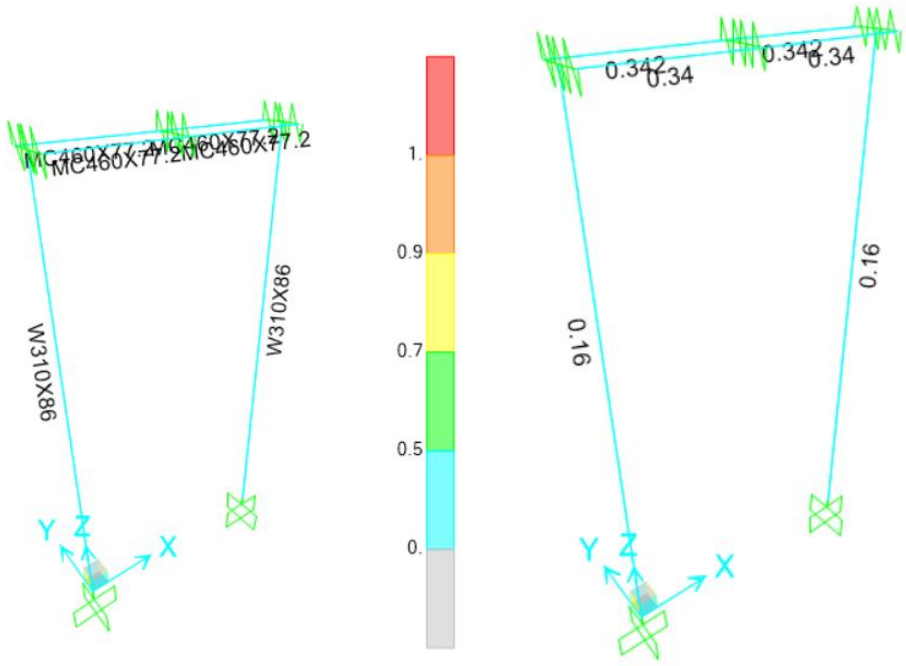

Figure 0.10: Force-moment interaction diagrams

1. Model geometry

This section provides model geometry information, including items such as joint coordinates, joint restraints, and element connectivity.

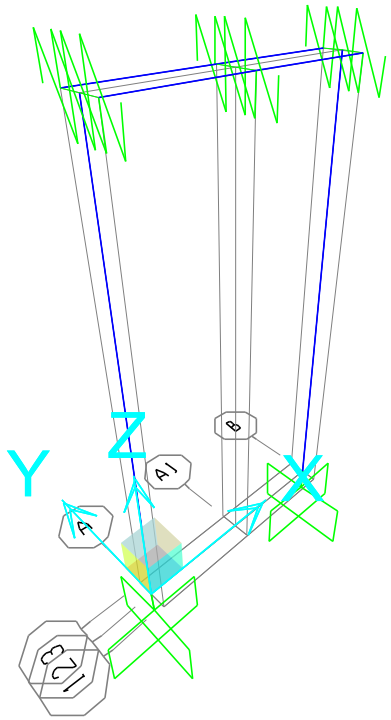

Figure 1: Finite element model

1.1. Joint coordinates

Table 1: Joint Coordinates

Table 1: Joint Coordinates

Joint	CoordSys	CoordType	GlobalX	GlobalY	GlobalZ
			m	m	m
6	GLOBAL	Cartesian	0.	0.1565	3.9
7	GLOBAL	Cartesian	0.	-0.1565	3.9
8	GLOBAL	Cartesian	2.	0.1565	3.9
9	GLOBAL	Cartesian	2.	-0.1565	3.9
10	GLOBAL	Cartesian	1.	0.1565	3.9
11	GLOBAL	Cartesian	1.	-0.1565	3.9
13	GLOBAL	Cartesian	0.	0.	0.
14	GLOBAL	Cartesian	0.	0.	3.9
15	GLOBAL	Cartesian	2.	0.	0.
16	GLOBAL	Cartesian	2.	0.	3.9
17	GLOBAL	Cartesian	1.	0.	3.9

1.2. Joint restraints

Table 2: Joint Restraint Assignments

Table 2: Joint Restraint Assignments

Joint	U1	U2	U3	R1	R2	R3
13	Yes	Yes	Yes	Yes	Yes	Yes
15	Yes	Yes	Yes	Yes	Yes	Yes

1.3. Element connectivity

Table 3: Connectivity - Frame

Table 3: Connectivity - Frame

Frame	JointI	JointJ	Length m
3	6	10	1.
6	10	8	1.
7	11	9	1.
8	7	11	1.
9	13	14	3.9
10	15	16	3.9

Table 4: Frame Section Assignments

Table 4: Frame Section Assignments

Frame	AnalSect	DesignSect	MatProp
3	MC460X77.2	MC460X77.2	Default
6	MC460X77.2	MC460X77.2	Default
7	MC460X77.2	MC460X77.2	Default
8	MC460X77.2	MC460X77.2	Default
9	W310X86	W310X86	Default
10	W310X86	W310X86	Default

2. Material properties

This section provides material property information for materials used in the model.

Table 5: Material Properties 02 - Basic Mechanical Properties

Table 5: Material Properties 02 - Basic Mechanical Properties

Material	UnitWeight KN/m3	UnitMass KN-s2/m4	E1 KN/m2	G12 KN/m2	U12	A1 1/C
4000Psi	2.3563E+01	2.4028E+00	24855578.06	10356490.86	0.2	9.9000E-06
A416Gr270	7.6973E+01	7.8490E+00	196500599.9			1.1700E-05
A615Gr60	7.6973E+01	7.8490E+00	199947978.8			1.1700E-05

Table 5: Material Properties 02 - Basic Mechanical Properties

Material	UnitWeight	UnitMass	E1	G12	U12	A1
	KN/m3	KN-s2/m4	KN/m2	KN/m2		1/C
A992Fy50	7.6973E+01	7.8490E+00	199947978.8	76903068.77	0.3	1.1700E-05

Table 6: Material Properties 03a - Steel Data

Table 6: Material Properties 03a - Steel Data

Material	Fy	Fu	FinalSlope
	KN/m2	KN/m2	
A992Fy50	344737.89	448159.26	-0.1

Table 7: Material Properties 03b - Concrete Data

Table 7: Material Properties 03b - Concrete Data

Material	Fc	FinalSlope
	KN/m2	
4000Psi	27579.03	-0.1

Table 8: Material Properties 03e - Rebar Data

Table 8: Material Properties 03e - Rebar Data

Material	Fy	Fu	FinalSlope
	KN/m2	KN/m2	
A615Gr60	413685.47	620528.21	-0.1

Table 9: Material Properties 03f - Tendon Data

Table 9: Material Properties 03f - Tendon Data

Material	Fy	Fu	FinalSlope
	KN/m2	KN/m2	
A416Gr270	1689905.16	1861584.63	-0.1

3. Section properties

This section provides section property information for objects used in the model.

3.1. Frames

Table 10: Frame Section Properties 01 - General, Part 1 of 5

Table 10: Frame Section Properties 01 - General, Part 1 of 5

SectionName	Material	Shape	t3	t2	tf	tw	t2b	tfb
			m	m	m	m	m	m
MC460X77.2	A992Fy50	Channel	0.457	0.104	0.0159	0.0152		
Plate_686x50	A992Fy50	Rectangular	0.05	0.686				
W310X86	A992Fy50	I/Wide Flange	0.31	0.254	0.0163	0.0091	0.254	0.0163

Table 10: Frame Section Properties 01 - General, Part 2 of 5

Table 10: Frame Section Properties 01 - General, Part 2 of 5

SectionName	Area	TorsConst	I33	I22	I23	AS2	AS3
	m2	m4	m4	m4	m4	m2	m2
MC460X77.2	0.00984	8.420E-07	0.000261	6.810E-06	0.	0.006946	0.003307
Plate_686x50	0.0343	0.000027	7.146E-06	0.001345	0.	0.028583	0.028583
W310X86	0.011	8.770E-07	0.000199	0.000045	0.	0.002821	0.0069

Table 10: Frame Section Properties 01 - General, Part 3 of 5

Table 10: Frame Section Properties 01 - General, Part 3 of 5

SectionName	S33	S22	Z33	Z22	R33	R22
	m3	m3	m3	m3	m	m
MC460X77.2	0.001142	0.000083	0.00114	0.000083	0.162863	0.026307
Plate_686x50	0.000286	0.003922	0.000429	0.005882	0.014434	0.198031
W310X86	0.001284	0.00035	0.00142	0.000533	0.134502	0.063604

Table 10: Frame Section Properties 01 - General, Part 4 of 5

Table 10: Frame Section Properties 01 - General, Part 4 of 5

SectionName	EccV2	AMod	A2Mod	A3Mod	JMod	I2Mod	I3Mod	MMod
	m							
MC460X77.2	0.041566	1.	1.	1.	1.	1.	1.	1.
Plate_686x50		1.	1.	1.	1.	1.	1.	1.
W310X86		1.	1.	1.	1.	1.	1.	1.

Table 10: Frame Section Properties 01 - General, Part 5 of 5

Table 10: Frame Section Properties 01 - General, Part 5 of 5

SectionName	WMod
MC460X77.2	1.
Plate_686x50	1.
W310X86	1.

Table 11: Frame Property Modifiers

Table 11: Frame Property Modifiers

Frame	AMod	AS2Mod	AS3Mod	JMod	I22Mod	I33Mod	MassMod	WeightMod
3	0.9	0.9	0.9	0.9	0.9	0.9	1.	1.
6	0.9	0.9	0.9	0.9	0.9	0.9	1.	1.
7	0.9	0.9	0.9	0.9	0.9	0.9	1.	1.
8	0.9	0.9	0.9	0.9	0.9	0.9	1.	1.
9	0.9	0.9	0.9	0.9	0.9	0.9	1.	1.
10	0.9	0.9	0.9	0.9	0.9	0.9	1.	1.

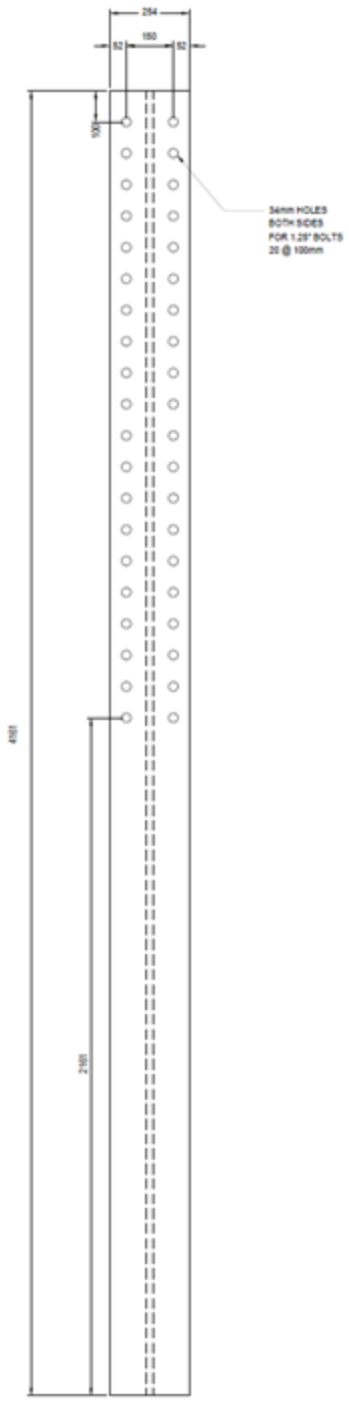

Figure 0.11: Wide flange column details

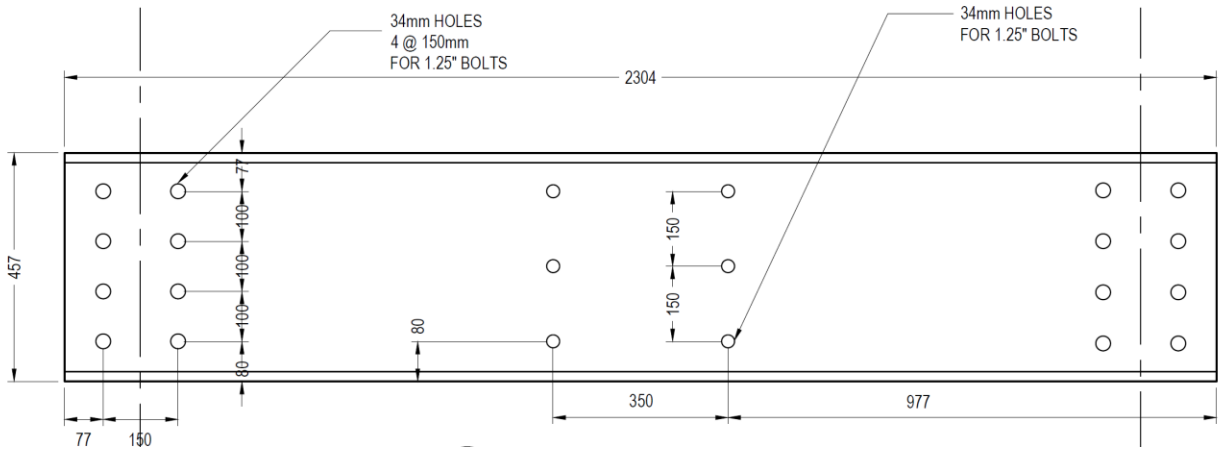

Figure 0.12: Crosshead beam details

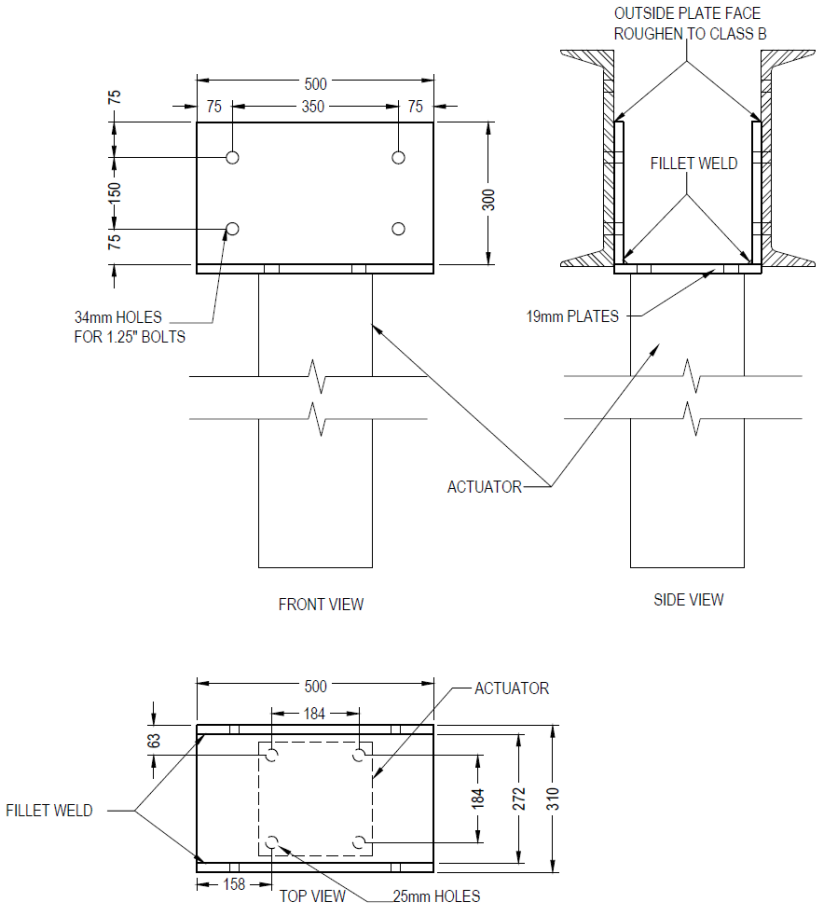

Figure 0.13: Actuator connection details

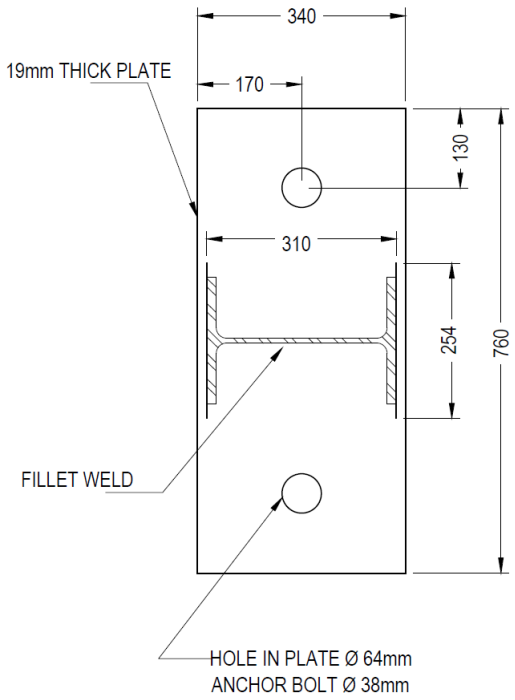

Figure 0.14: Column base plate detail

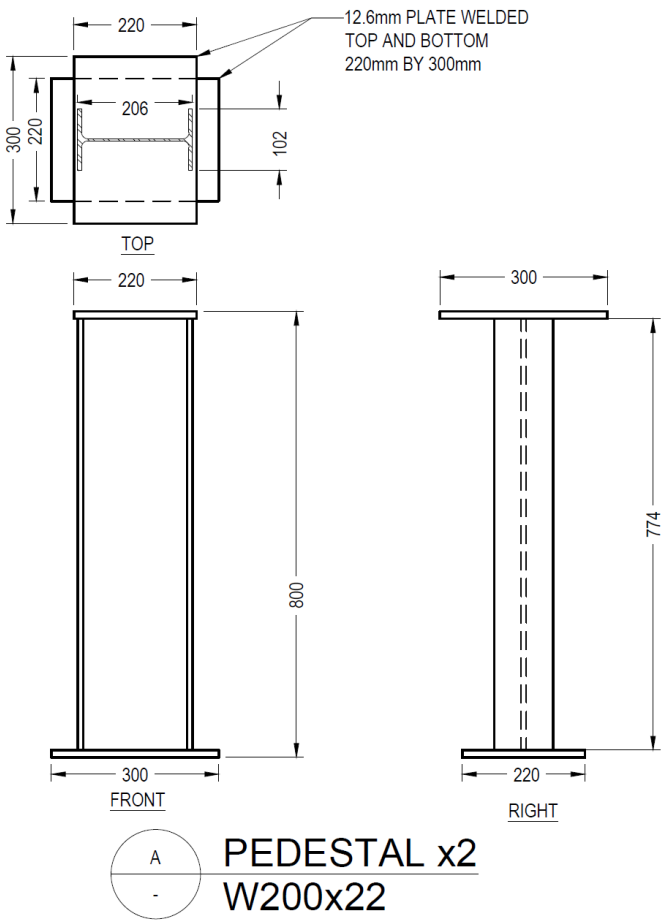

Figure 0.15: Beam support pedestal detail

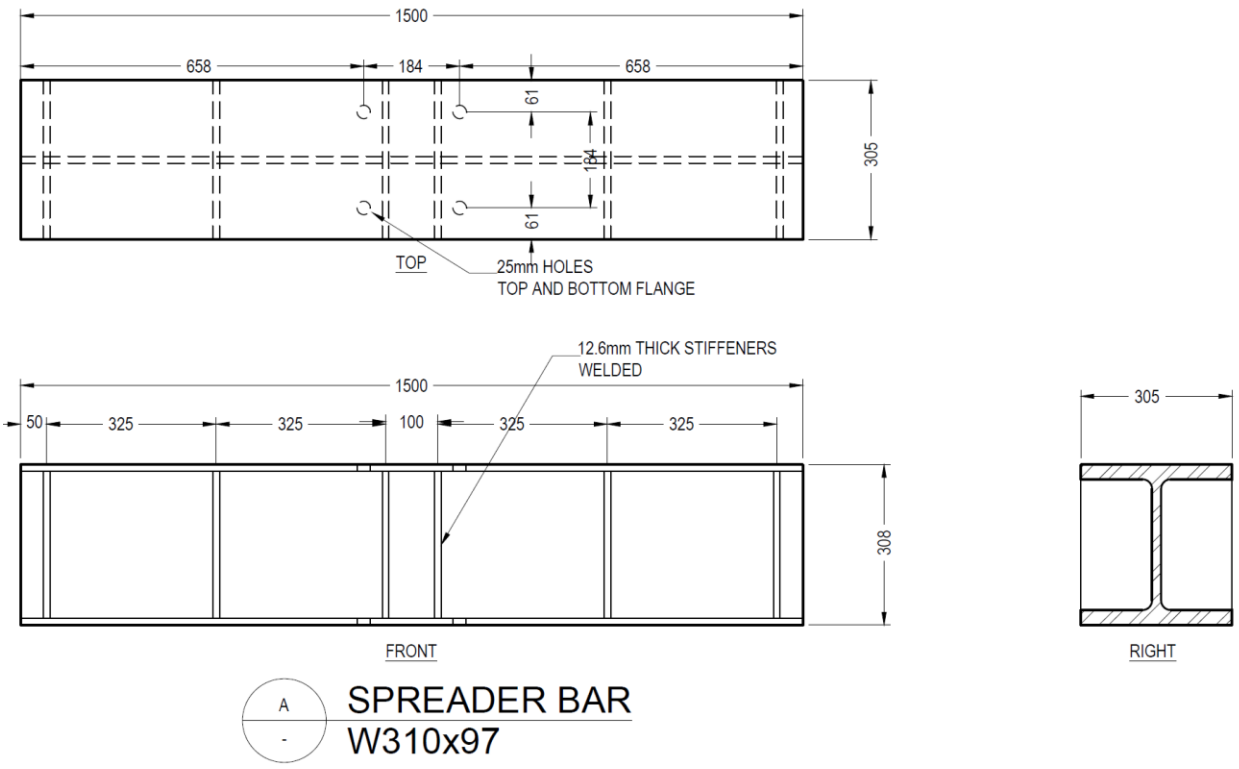

Figure 0.16: Four-point load spreader bar

Appendix E: Load Deflection Curves

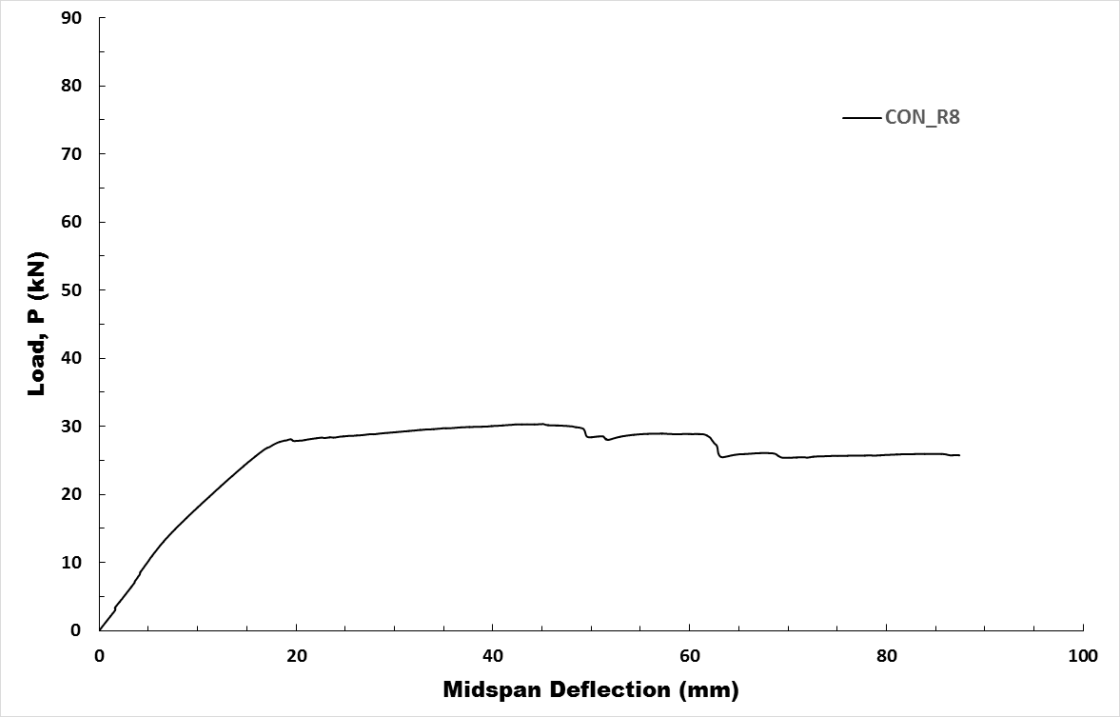

Figure 0.17: Load versus deflection plot for CON_R8 specimen

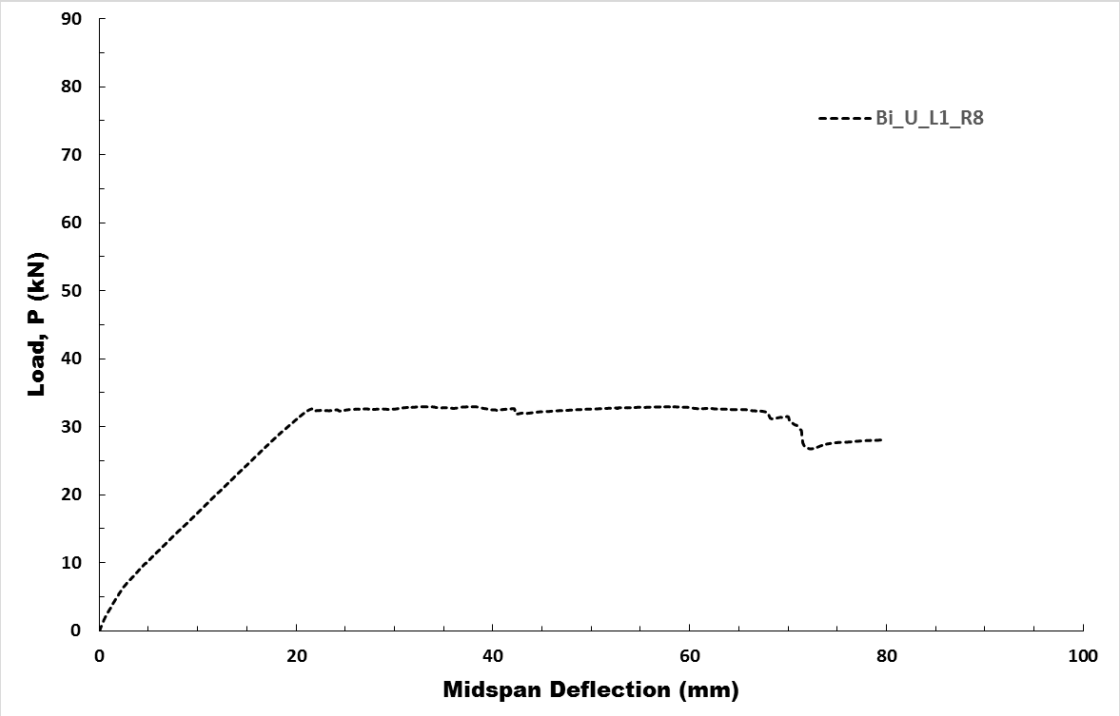

Figure 0.18: Load versus deflection plot for Bi_U_L1_R8 specimen

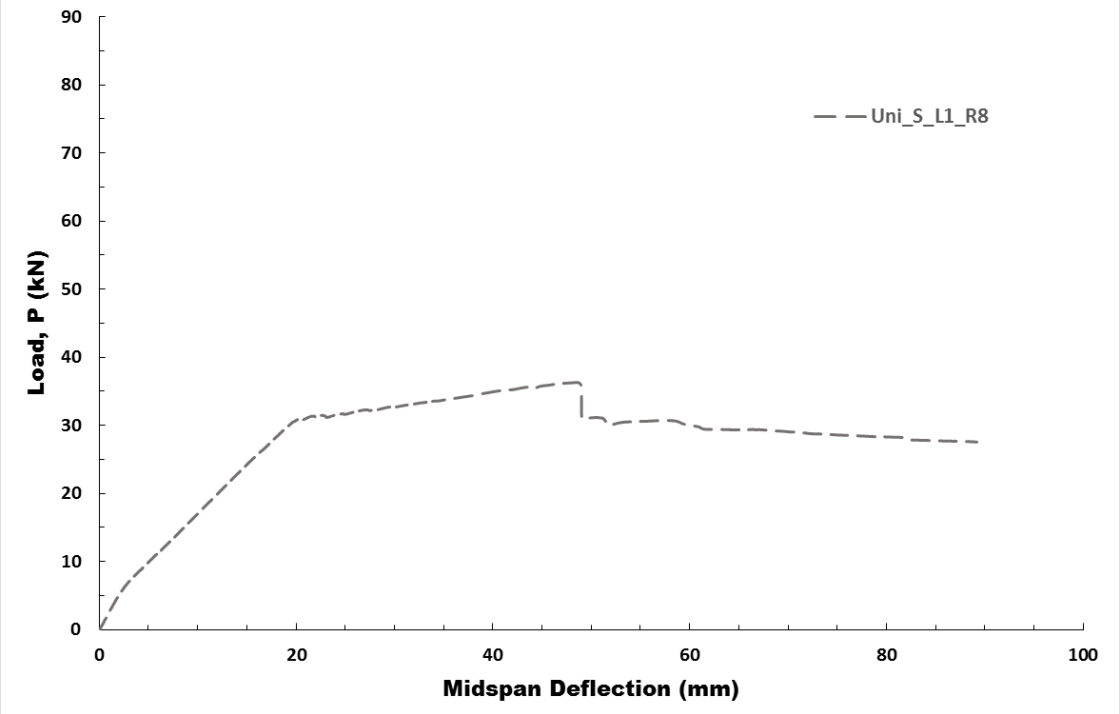

Figure 0.19: Load versus deflection plot for Uni_S_L1_R8 specimen

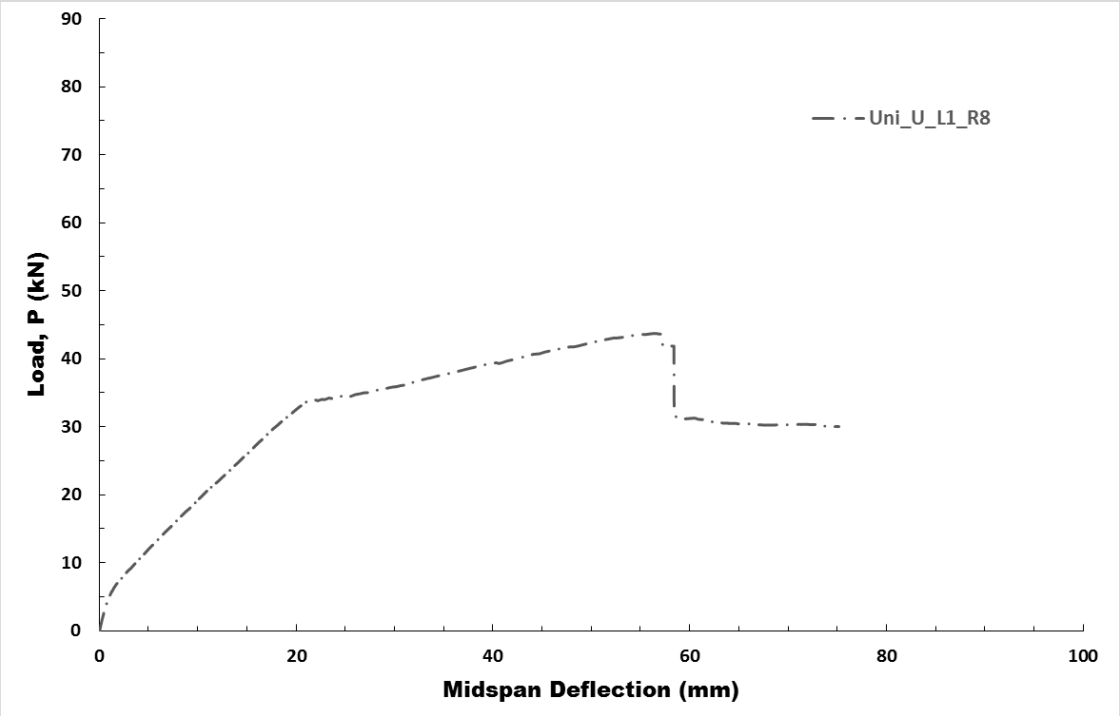

Figure 0.20: Load versus deflection plot for Uni_U_L1_R8 specimen

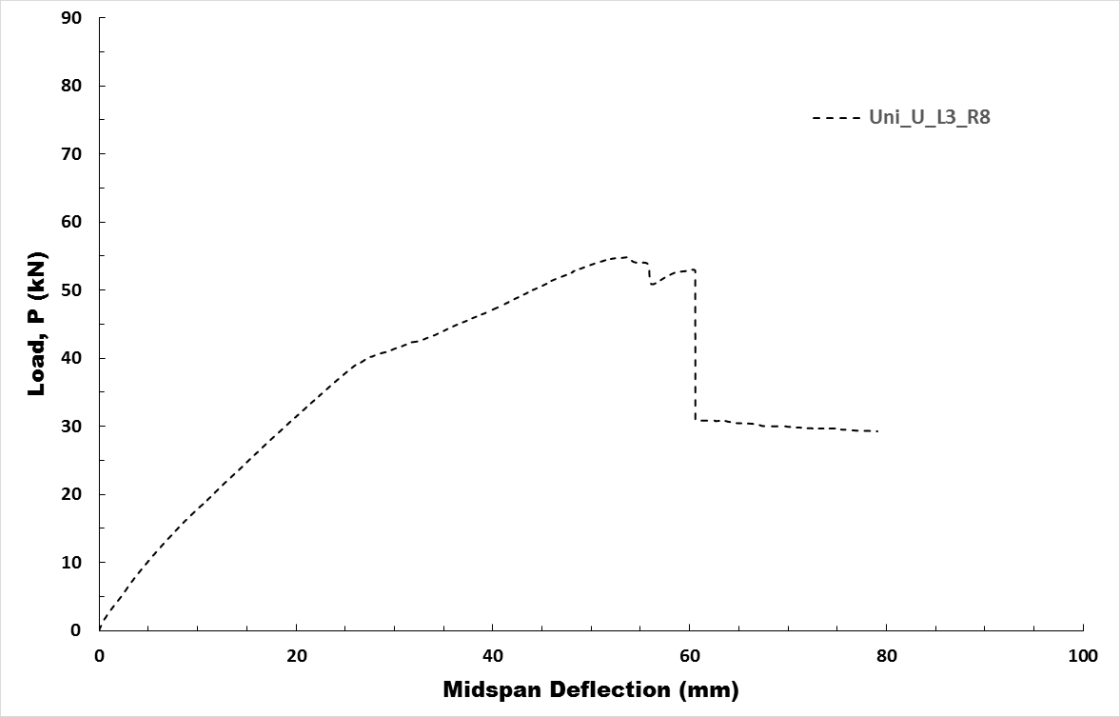

Figure 0.21: Load versus deflection plot for Uni_U_L3_R8 specimen

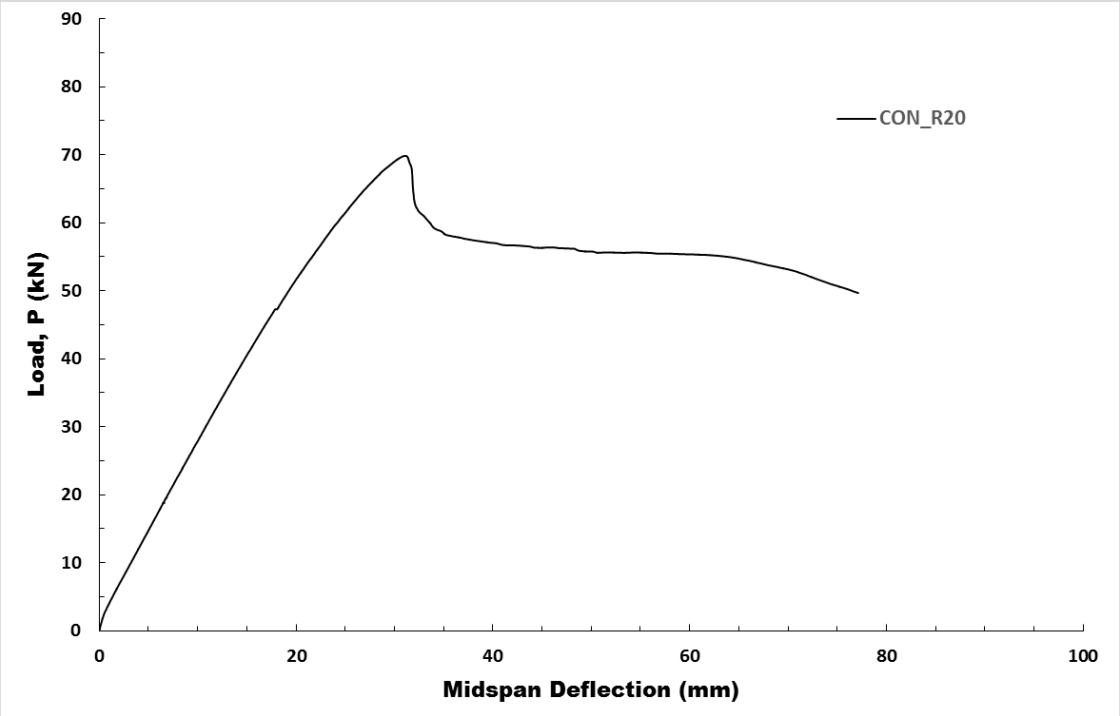

Figure 0.22: Load versus deflection plot for CON_R20 specimen

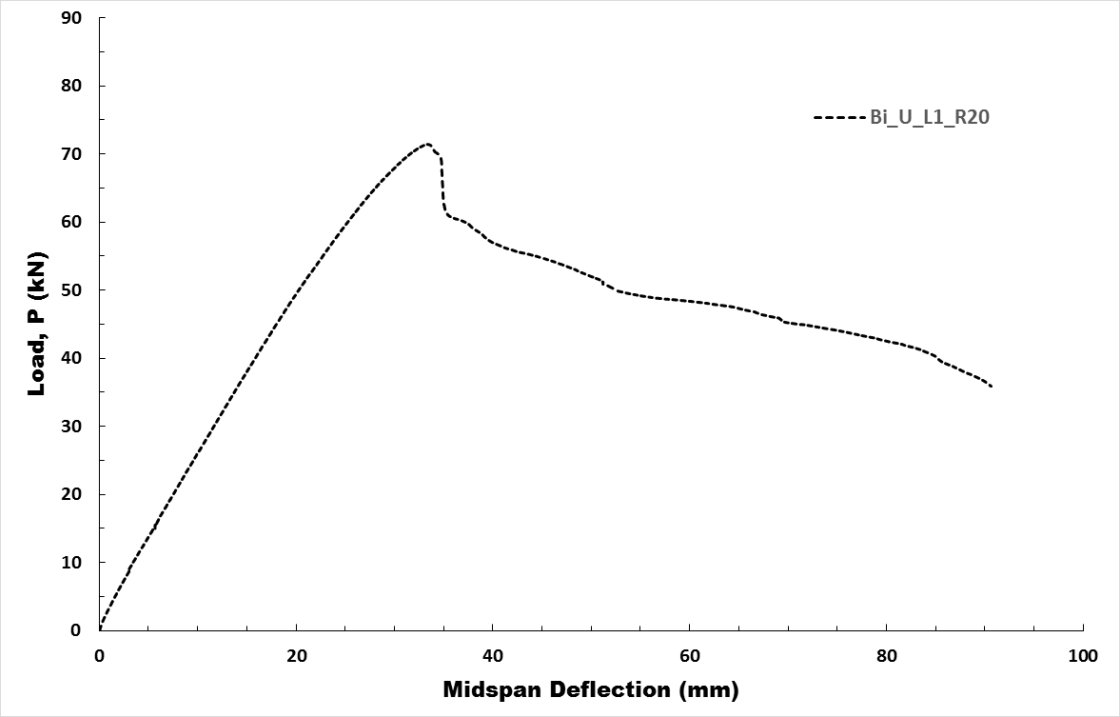

Figure 0.23: Load versus deflection plot for Bi_U_L1_R20 specimen

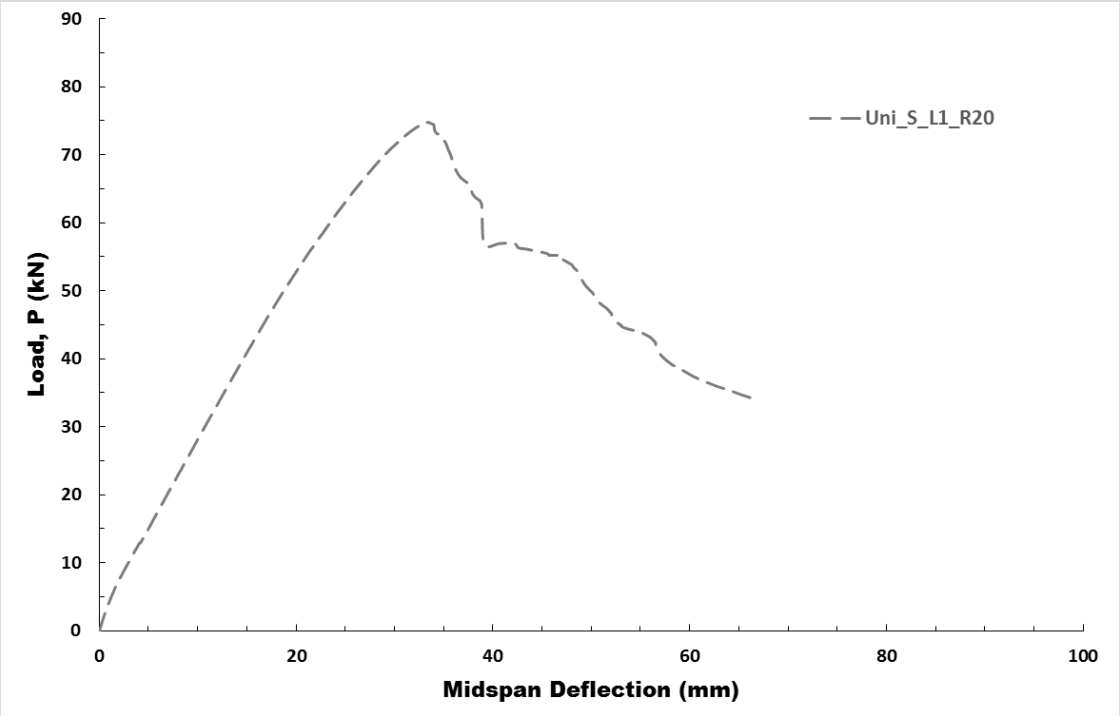

Figure 0.24: Load versus deflection plot for Uni_S_L1_R20 specimen

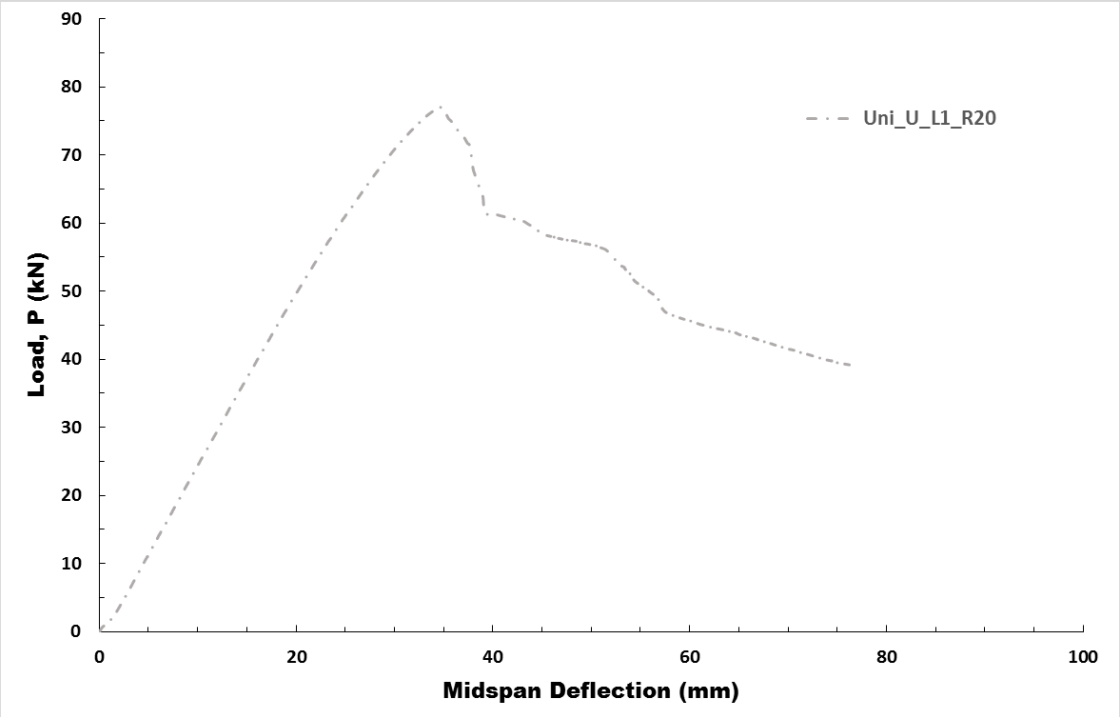

Figure 0.25: Load versus deflection plot for Uni_U_L1_R20 specimen

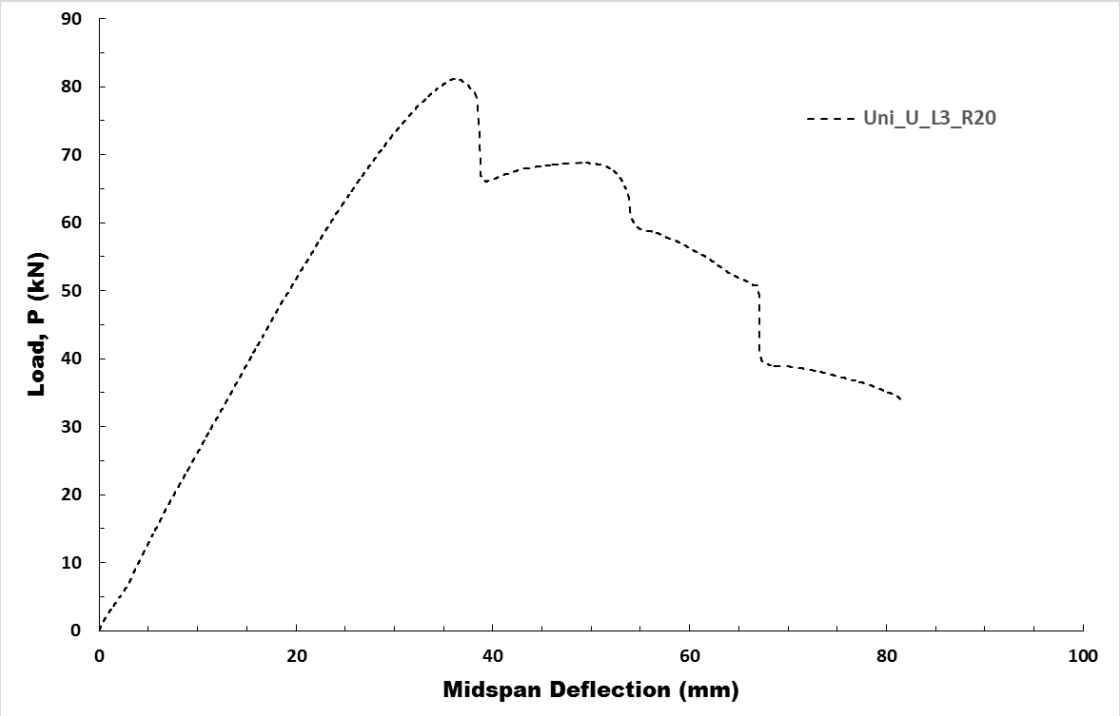

Figure 0.26: Load versus deflection plot for Uni_U_L3_R20 specimen

Appendix F: Strain Plots

The following figures show the strain distribution with concrete strain defined as negative. As a clarification the following acronyms are used, MID refers to midspan steel strain, SUPP refers to support steel strain, FAB refers to fabric strain, and CONC refers to concrete strain.

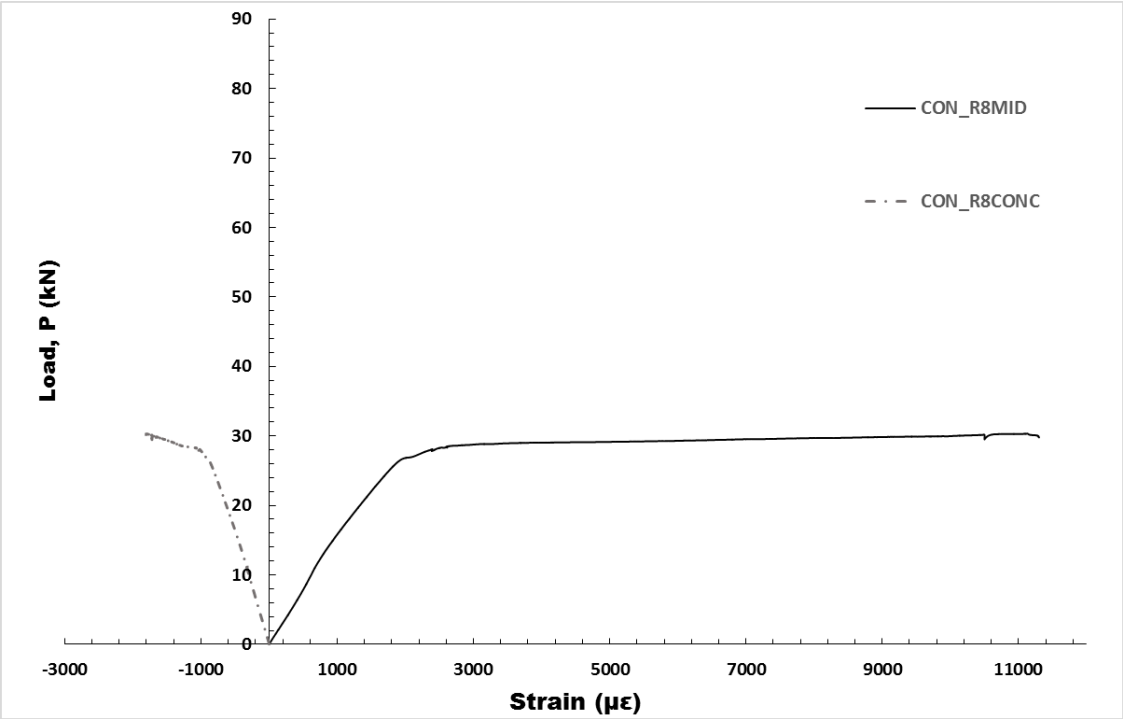

Figure 0.27: Load versus strain plot for CON_R8 specimen

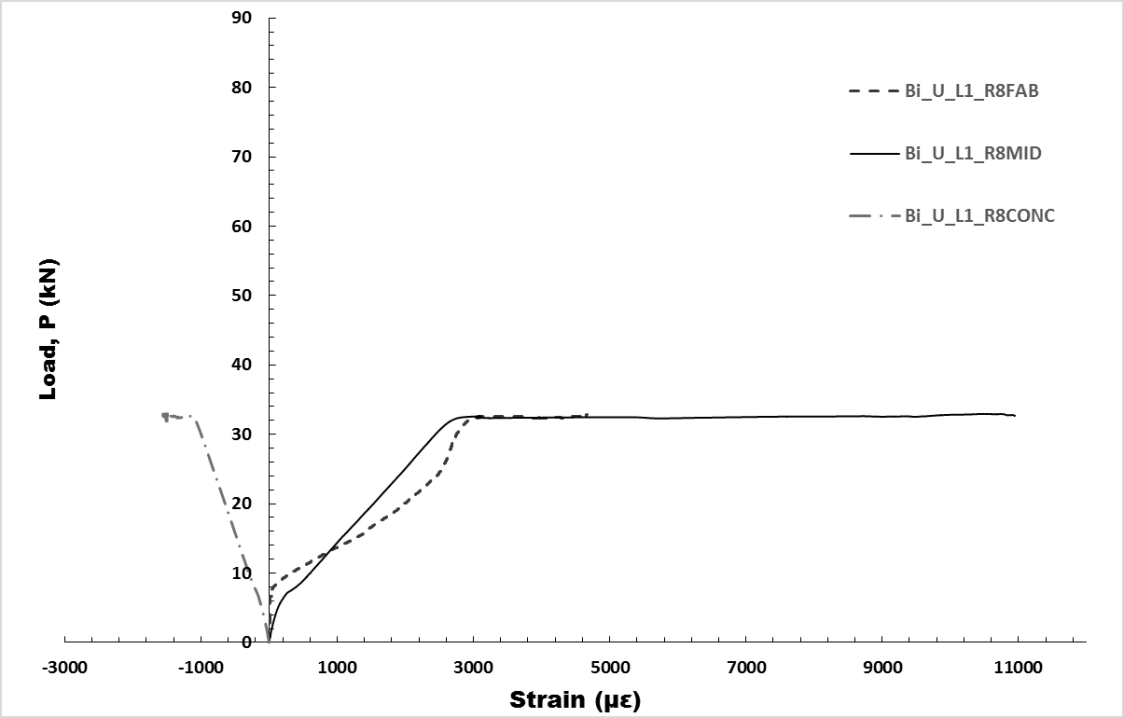

Figure 0.28: Load versus strain plot for Bi_U_L1_R8 specimen

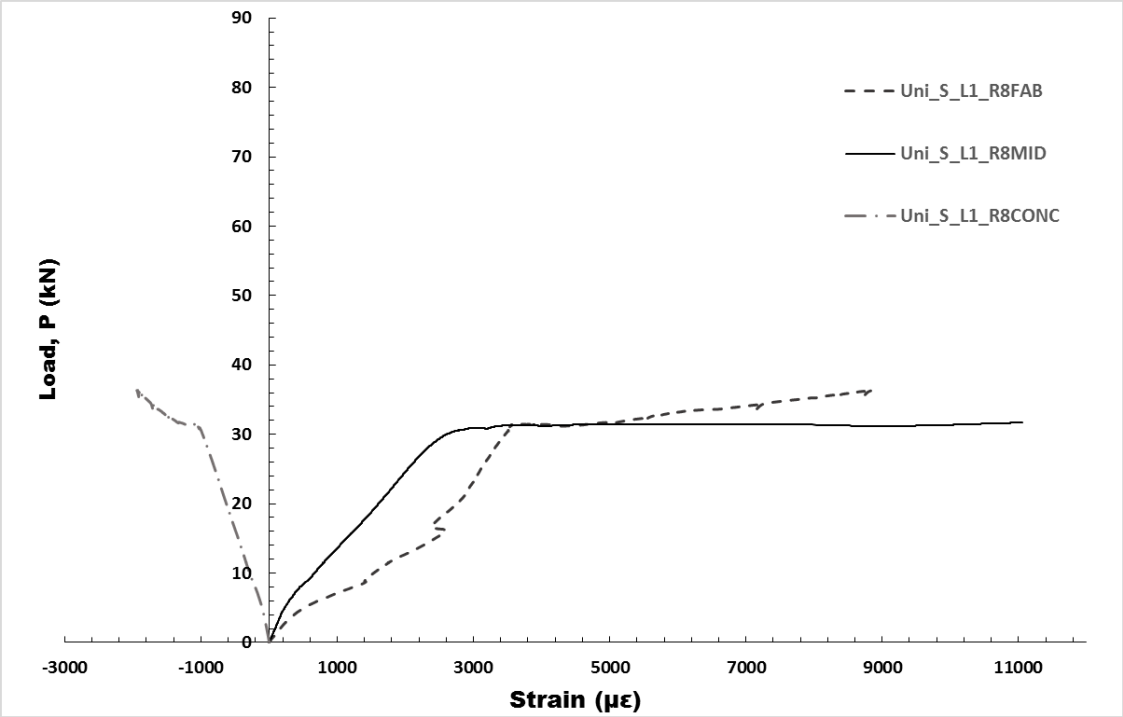

Figure 0.29: Load versus strain plot for Uni_S_L1_R8 specimen

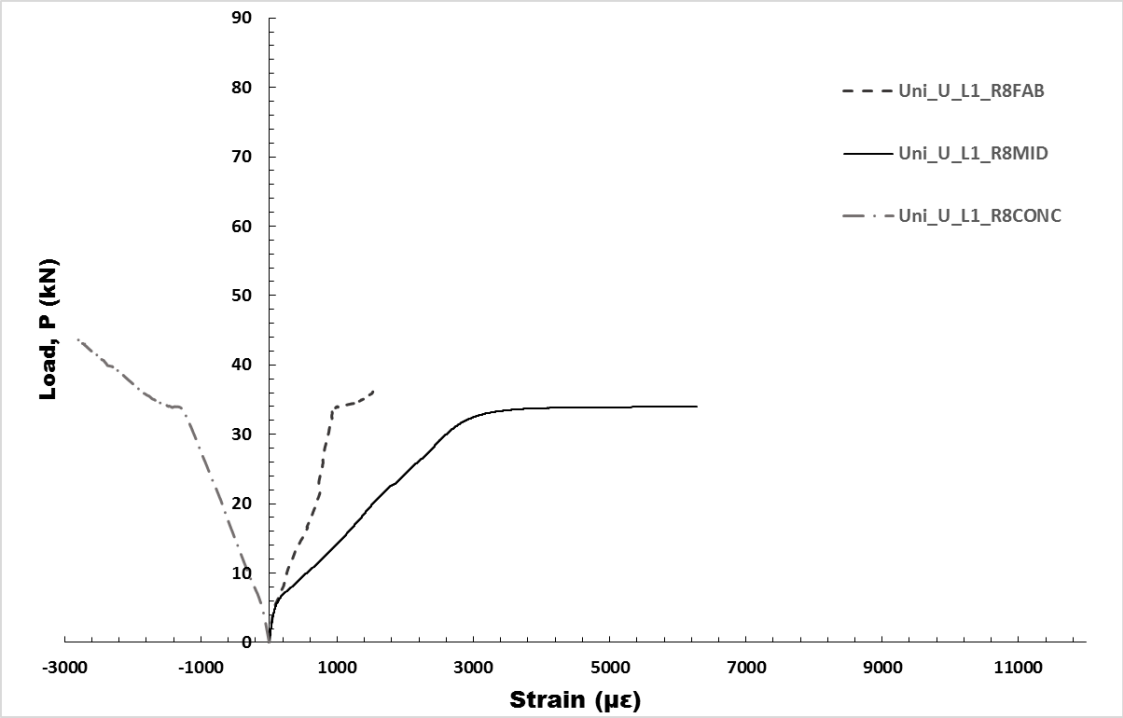

Figure 0.30: Load versus strain plot for Uni_U_L1_R8 specimen

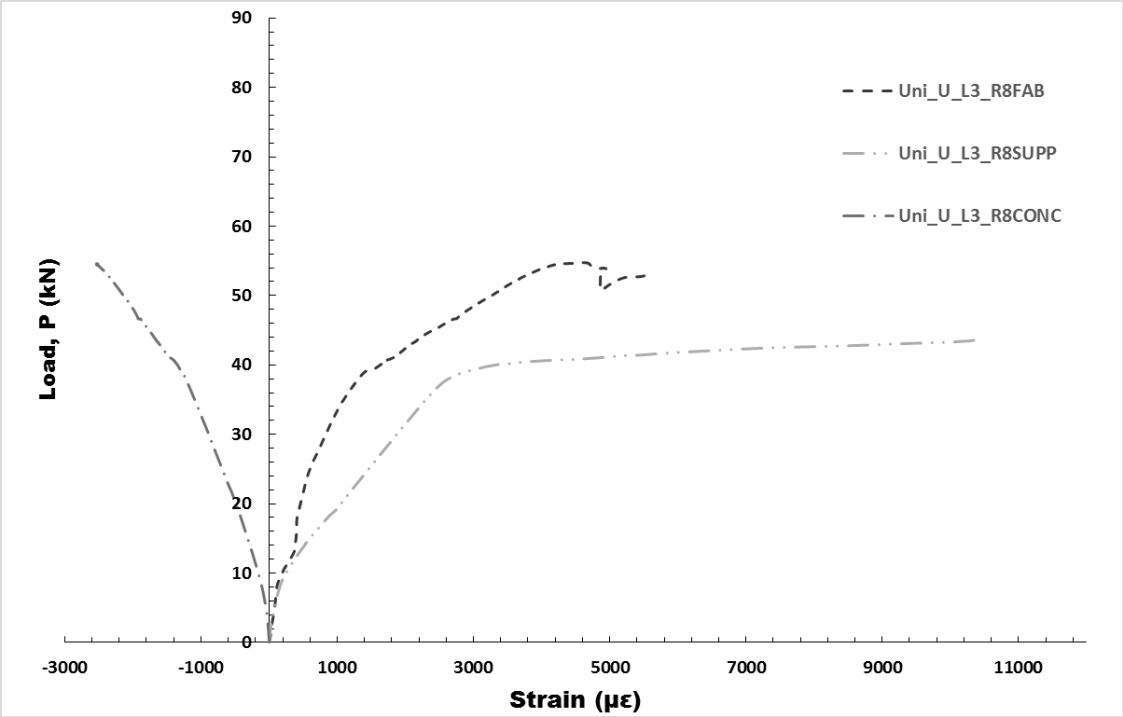

Figure 0.31: Load versus strain plot for Uni_U_L3_R8 specimen

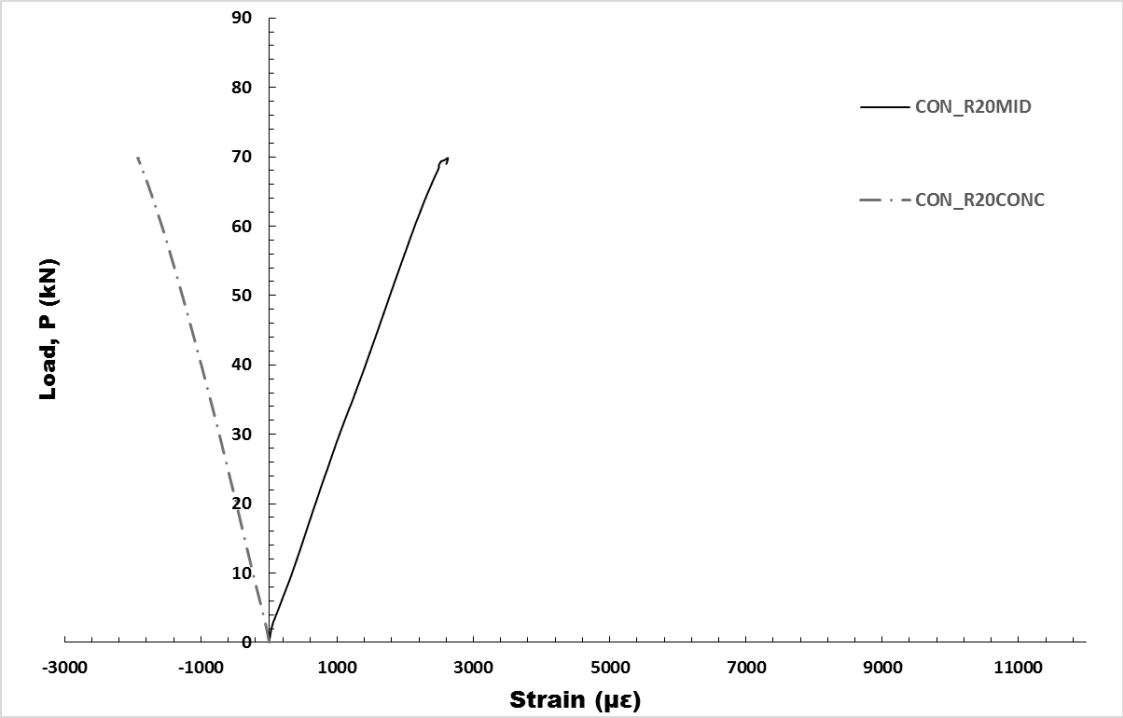

Figure 0.32: Load versus strain plot for CON_R20 specimen

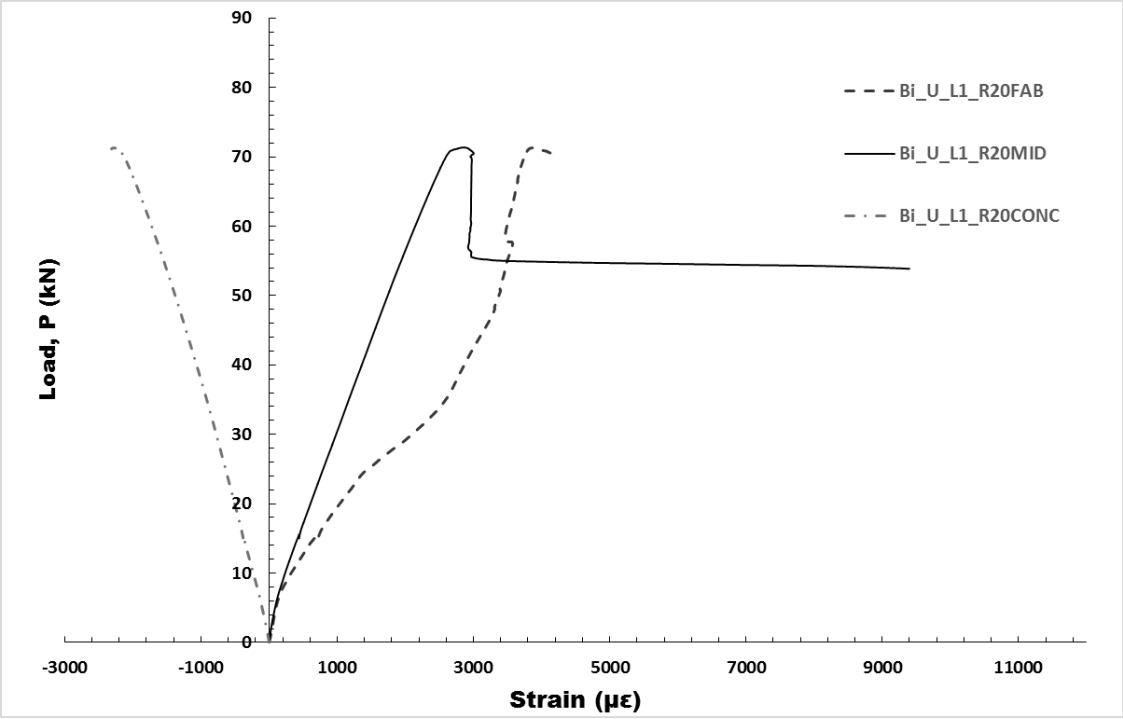

Figure 0.33: Load versus strain plot for Bi_U_L1_R20 specimen

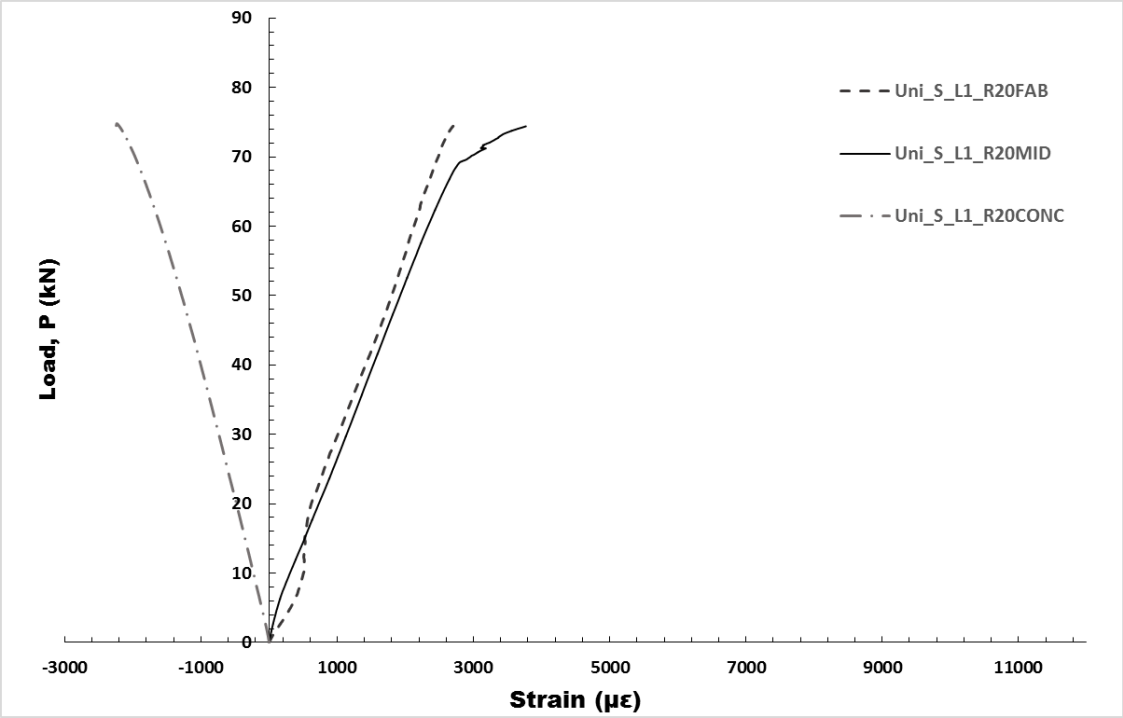

Figure 0.34: Load versus strain plot for Uni_S_L1_R20 specimen

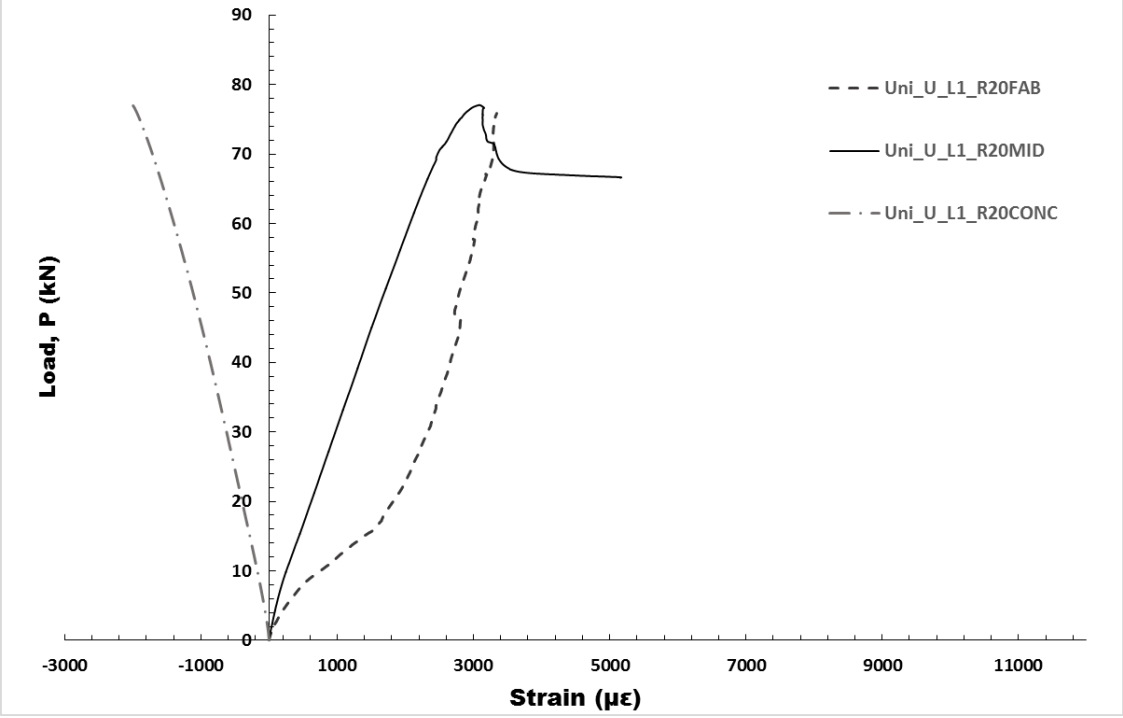

Figure 0.35: Load versus strain plot for Uni_U_L1_R20 specimen

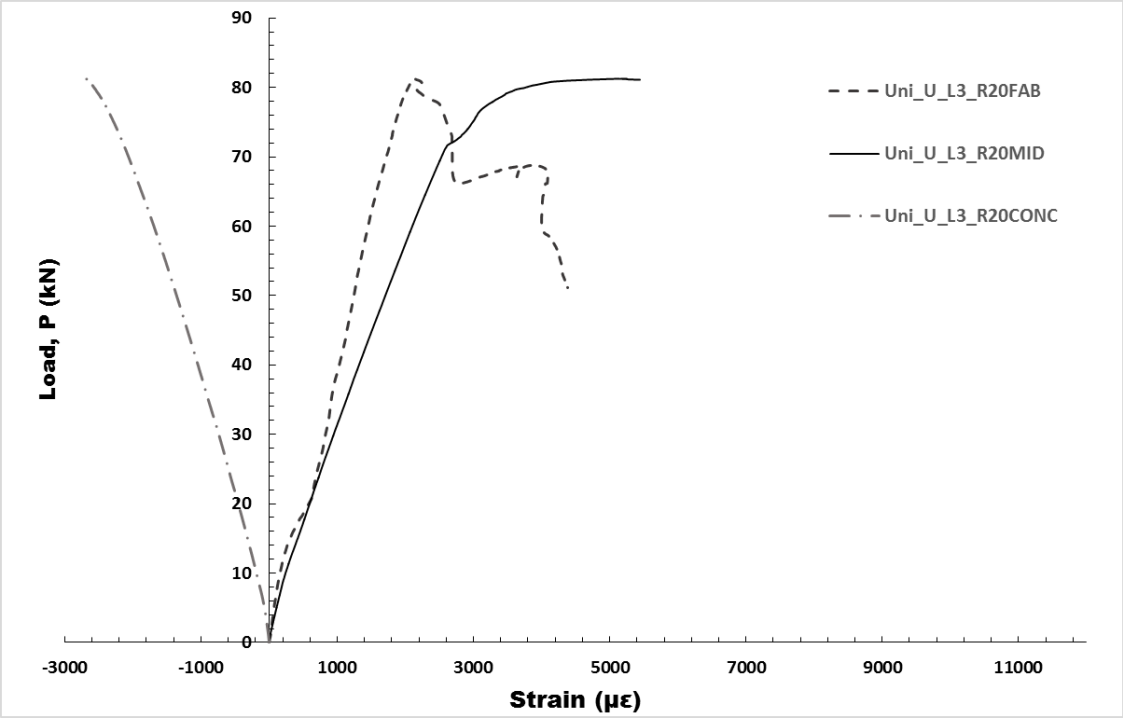

Figure 0.36: Load versus strain plot for Uni_U_L3_R20 specimen